The TRAPP complex mediates secretion arrest induced by stress granule assembly

Francesca Zappa[1], Cathal Wilson[1], Giuseppe Di Tullio[1], Michele Santoro[1], Piero Pucci[2], Maria Monti[2], Davide D'Amico[1], Sandra Pisonero Vaquero[1], Rossella De Cegli[1], Alessia Romano[1], Moin A. Saleem[3], Elena Polishchuk[1], Mario Failli[1], Laura Giaquinto[1], Maria Antonietta De Matteis[1, 2]

1 Telethon Institute of Genetics and Medicine, Pozzuoli (Naples), Italy

2 Federico II University, Naples, Italy

3 Bristol Renal, Bristol Medical School, University of Bristol, UK

Correspondence to: f.zappa@tigem.it, dematteis@tigem.it

The TRAnsport Protein Particle (TRAPP) complex controls multiple steps along the secretory, endocytic and autophagic pathways and is thus strategically positioned to mediate the adaptation of membrane trafficking to diverse environmental conditions including acute stress. We identified TRAPP as a key component of a branch of the integrated stress response that impinges on the secretory pathway. We found that TRAPP associates with, and drives the recruitment of the inner components of the COPII coat to, SGs. The sequestration to SGs of COPII, required for the ER export of newly synthesized proteins, and of TRAPP, the exchange factor for Rab1, a GTPase controlling the architecture of the Golgi complex, leads to arrest of the secretory activity and to the disorganization of the Golgi complex. Interestingly, the relocation of TRAPP and COPII to SGs only occurs in actively proliferating cells and it does it in a CDK1/2 dependent manner. We show that CDK1/2 activity controls the membrane-cytosol cycle of COPII at ER exit sites (ERES) and that CDK1/2 inhibition/depletion prevents the relocation of COPII and TRAPP to SGs by stabilizing them at the ERES. Importantly, TRAPP is not just a passive constituent of SGs but controls their maturation. This includes the acquisition of signaling components, such as RACK1 and Raptor, whose sequestration to SGs is needed to mediate the pro-survival response. SGs that assemble in TRAPP-depleted cells are no longer able to sequester RACK1 and Raptor thus rendering the cells more prone to undergo apoptosis upon stress exposure.

Altogether, our findings reveal a new property of the integrated stress response that is acquired through the recruitment of TRAPP to SGs: a high grade of plasticity that tailors the secretory pathway to stress according to different cell growth states.

Introduction

The TRAPP (TRAnsport Protein Particle) complex is a conserved multimolecular complex intervening in multiple segments of membrane trafficking along the secretory, the endocytic and the autophagy pathways (Kim et al., 2016).

Originally identified in yeast as a tethering factor acting in ER-to-Golgi trafficking, it was subsequently discovered to act as a GEF for Ypt1 and Ypt31/32 in yeast and for Rab1 and possibly Rab11 in mammals (Westlake et al., 2011; Yamasaki et al., 2009; Zou et al., 2012). The TRAPP complex has a modular composition and is present as two forms in mammals: TRAPPII and TRAPPIII which share a common heptameric core (TRAPPC1, TRAPPC2, TRAPPC2L, TRAPPC3, TRAPPC4, TRAPPC5, TRAPPC6) and additional subunits specific for TRAPPII (TRAPPC9/ TRAPPC10) or for TRAPPIII (TRAPPC8, TRAPPC11, TRAPPC12, TRAPPC13) (Sacher et al., 2018). TRAPPII has been implicated in late Golgi trafficking while TRAPPIII has a conserved role in the early secretory pathway (ER-to-Golgi) and in autophagy (Scrivens et al., 2011; Yamasaki et al., 2009). Recent lines of evidence have expanded the range of activities of the TRAPP complex by showing that it takes part in a cell survival response triggered by agents that disrupt the Golgi complex (Ramírez-Peinado et al., 2017) and can drive the assembly of lipid droplets in response to lipid load (Li et al., 2017).

The importance of the TRAPP complex in humans is testified by the deleterious consequences caused by mutations in genes encoding distinct TRAPP subunits. Mutations in TRAPPC2L, TRAPPC6A, TRAPPC6B, TRAPPC9 and TRAPPC12 cause neurodevelopmental disorders leading to intellectual disability and dysmorphic syndromes (Harripaul et al., 2018; Khattak and Mir, 2014; Milev et al., 2018, 2017, p. 12; Mohamoud et al., 2018), mutations in TRAPPC11 lead to ataxia (Koehler et al., 2017), and mutations in TRAPPC2 lead to the spondyloepiphyseal dysplasia tarda (SEDT) (Gedeon et al., 1999).

SEDT is characterized by short stature, platyspondyly, barrel chest and premature osteoarthritis that manifest in late childhood/prepubertal age. We have shown that pathogenic mutations or deletion of TRAPPC2 alter the ER export of procollagen (both type I and type II) and that TRAPPC2 interacts with the procollagen escort protein TANGO1 and regulates the cycle of the GTPase Sar1 at the ER exit sites

71 (ERES) (Venditti et al., 2012)). The Sar1 cycle in turn drives the cycle of the COPII coat
72 complex, which mediates the formation of carriers containing neo-synthesized cargo
73 to be transported to the Golgi complex. While this role of TRAPPC2 in the ER export
74 of PC might explain the altered ECM deposition observed in patient's cartilage
75 (Venditti et al., 2012; Tiller et al., 2001), it leaves the late onset of the disease signs
76 unexplained. We hypothesized that the latter could be due to an inability to
77 maintain long-term cartilage tissue homeostasis, possibly due to an impaired
78 capacity of chondrocytes to face the physiological stresses that underlie and guide
79 their development and growth. These include mechanical stress that can induce
80 oxidative stress leading to apoptosis (Henrotin et al., 2003; Zuscik et al., 2008).
81 Here, by analyzing the cell response to different stresses, we show that the TRAPPC2
82 and the entire TRAPP complex, are components of stress granules (SGs), membrane-
83 less organelles that assemble in response to stress (Protter and Parker, 2016).
84 The recruitment of TRAPP to SGs has multiple impacts on the stress response as it
85 induces the sequestration of Sec23/Sec24 (the inner layer of the COPII complex)
86 onto SGs thus inhibiting trafficking along the early secretory pathway, leads to the
87 inactivation of the small GTPase Rab1 with a consequent disorganization of the Golgi
88 complex, and is required for the recruitment of signalling proteins, such as Raptor
89 and RACK1, to SGs thus contributing to the anti-apoptotic role of SGs. Interestingly,
90 TRAPP and COPII recruitment to SGs only occurs in actively proliferating cells and is
91 under control of cyclin-dependent-kinases (CDK 1 and 2).
92 The TRAPP complex thus emerges as a key element in conferring an unanticipated
93 plasticity to SGs, which adapt their composition and function to cell growth activity,
94 reflecting the ability of cells to adjust their stress response to their proliferation state
95 and energy demands.
96
97
98 **Results**
99
100 **TRAPP redistributes to SGs in response to different stress stimuli**
101 To investigate the involvement of TRAPPC2 in the stress response, we exposed
102 chondrocytes (Figure 1A) or HeLa cells (Figure 1B) to sodium arsenite (SA) treatment

103 that induces oxidative stress. We have shown previously that TRAPPC2 associate
104 with ERES under steady state conditions (Venditti et al., 2012). SA treatment led to
105 dissociation of TRAPPC2 from ERES and a complete relocation to roundish structures.
106 Oxidative stress is known to lead to the formation of stress granules (SGs; Anderson
107 and Kedersha, 2002), therefore, we considered the possibility that these TRAPPC2-
108 positive structures might be SGs. Indeed, co-labeling with an anti-eIF3 antibody, a
109 canonical SG marker (Aulas et al., 2017), showed the co-localization of TRAPPC2 with
110 eIF3 after SA treatment (Figure 1A,B). Other TRAPP components, such as TRAPPC1
111 and TRAPPC3, exhibited the same response to SA treatment (Figure 1C). TRAPP
112 recruitment to SGs also occurs in response to heat shock (Figure 1—figure
113 supplement 1A), and in different cell lines (Figure 1—figure supplement 1B,C). In
114 addition, TRAPP elements associate to SGs in yeast cells exposed to heat stress
115 (Figure 1—figure supplement 2, Figure 1—supplement video 1 and 2) thus
116 suggesting that this is a conserved process in evolution. Of note, the association of
117 TRAPP with SGs is fully reversible after stress removal (Figure 1—figure supplement
118 3).
119 We studied the kinetics of TRAPPC2 redistribution to SGs. The appearance of eIF3-
120 positive SGs occurred 7 min after SA treatment (Figure 1D), while TRAPPC2 re-
121 localization to SGs began 15 min after exposure to stress and gradually increased
122 over time, with massive recruitment occurring 60 min after treatment, thus lagging
123 behind the initial assembly of SGs (Figure 1D).
124 We observed that oxidative stress did not affect the overall integrity of the TRAPP
125 complexes (both TRAPPII and TRAPPIII), as analyzed by gel filtration. However, in
126 stressed cells TRAPPII and TRAPPIII components were also found in higher molecular
127 weight fractions (Figure 1E) containing the SG component TIAR-1 (Figure 1E),
128 possibly reflecting the SG-associated TRAPP.
129 To investigate the mechanisms that could mediate the recruitment of TRAPP to SGs,
130 we performed a proteomics analysis of the TRAPPC2 interactors (see Materials and
131 methods). This analysis (Figure 1F, Table S1), confirmed known TRAPPC2 interactors
132 (e.g. TRAPP complex components, Rab1, COPII and COPI) and revealed the presence
133 of many RNA binding proteins (RBPs), including those with a central role in the
134 assembly of SGs (Jain et al., 2016). This suggested that, as described for other

135 components of SGs, TRAPPC2 may be recruited to growing SGs by a piggyback
136 mechanism (Anderson and Kedersha, 2008), i.e. via the interaction with RBPs that
137 are components of SGs.
138 Altogether, these results led us to conclude that following stress the TRAPP complex,
139 through TRAPPC2 interaction with RBPs, becomes a SG component.
140
141
142 **TRAPPC2 is required for recruiting COPII to SGs**
143 The translocation of TRAPP to SGs prompted us to investigate whether other
144 components of membrane trafficking machineries behaved similarly. We screened
145 different coat complex components (COPI, COPII, clathrin adaptors, clathrin), and
146 other cytosolic proteins associated with the exocytic and endocytic pathways. Out of
147 the 15 proteins tested, only components of the inner layer of the COPII coat, Sec24
148 (Figure 2A, B) and Sec23 (Figure 2—figure supplement 1A), but none of the others
149 (Figure 2C, and Figure 2—figure supplement 1B-N, Figure 2—figure supplement 2)
150 associated with SGs. Notably, Sec24 was recruited to SGs with kinetics similar to
151 those of the TRAPP complex (Figure 2A).
152 Since TRAPP and COPII are known to interact and TRAPP is recruited to ERES in a
153 Sar1- and COPII-dependent manner (Lord et al., 2011; Venditti et al., 2012), we
154 asked whether COPII and TRAPP recruitment to SGs is interdependent. The depletion
155 of the COPII inner layer proteins Sec23 and Sec24 had no impact on the recruitment
156 of the TRAPP complex to SGs (Figure 2D,E, Figure 2—figure supplement 1A,B) while
157 the depletion of the entire TRAPP complex (by KD of TRAPPC3, which destabilizes the
158 entire complex) or of the TRAPPC2 subunit (by KD of TRAPPC2 that leaves unaltered
159 the rest of the TRAPP complex; Venditti et al., 2012) abrogated the recruitment of
160 COPII components to SGs (Figure 2F, Figure 2—figure supplement 1C). These results
161 indicated that the TRAPP complex, through its component TRAPPC2, drives the
162 recruitment of COPII to SGs.
163 It is worth mentioning that COPII components have been reported to associate, in
164 Drosophila S2 cells, with other membrane-less organelles: the “Sec bodies”
165 (Zacharogianni et al., 2014). However, Sec bodies are distinct from SGs since they do
166 not contain ribonucleoproteins and form in response to prolonged starvation, but

167 not to oxidative stress. In addition, the recruitment of COPII to Sec bodies in
168 Drosophila S2 cells depends of the ERES component Sec16. We found that in
169 mammalian cells Sec16 neither significantly associates with SGs (Figure 2—figure
170 supplement 2A,B) nor is it required for the recruitment of COPII to SGs (Figure 2—
171 figure supplement 2C). These results indicate that stress-induced COPII phase
172 separation diverges in Drosophila and mammalian cells for the inducing stresses
173 (starvation vs oxidative or heat stress), for the composition of the membrane-less
174 organelles (Sec bodies vs SGs) and for the underlying mechanisms (Sec16-dependent
175 vs TRAPP-dependent mechanism).
176 We then moved to investigate the nature of association of COPII to SGs since the
177 COPII coat cycles in a very dynamic fashion at ERES (D'Arcangelo et al., 2013). To this
178 end, we permeabilized living cells (Kapetanovich et al., 2005) at steady state and
179 upon stress induction. Treatment with digitonin forms pores at the plasma
180 membrane that allows the exit of the cytosolic content into the extracellular space.
181 Under these conditions, we found that the COPII pool recruited to SGs is less
182 dynamic than the pool cycling at the ERES, since COPII remained associated with SGs
183 in permeabilized cells exposed to stress while the COPII pool cycling at the ERES was
184 completely lost upon permeabilization of unstressed cells (Figure 3A). We then
185 assessed the possible interplay between the COPII fraction at ERES and the pool that
186 eventually relocates to SGs. We asked whether changes in the association of COPII at
187 the ERES could have an impact on the recruitment of COPII to SGs. To this end, we
188 stabilized COPII and TRAPP at ERES by expressing either a constitutively active GTP-
189 bound Sar1 mutant (Sar1-H79G) or decreasing the rate of GTP hydrolysis on Sar1 by
190 depleting Sec31, which is a co-GAP that potentiates by an order of magnitude the
191 Sar1 GAP activity of Sec23-24 (Bi et al., 2007). Under both conditions, COPII and
192 TRAPP were more tightly associated with ERES (Figure 3—figure supplement 1),
193 while their translocation to SGs upon exposure to stress was significantly reduced
194 (Figure 3B,C). Thus, COPII/TRAPP recruitment to SGs is commensurate with the rate
195 of their association at the ERES indicating that the cytosolic pool of COPII generated
196 through the fast cycling at ERES is the one available to be recruited to SGs upon
197 stress.
198

199 **The association of TRAPP is under the control of CDK1/2**

200 To dissect the regulation of TRAPP/COPII recruitment to SGs, we screened a library
201 of kinase inhibitors for their ability to affect the re-localization of COPII to SGs. HeLa
202 cells were pre-treated with kinase inhibitors for 150 min and then exposed to SA for
203 a further 30 min in the continuous presence of the inhibitors. Out of the 273
204 inhibitors tested, 194 had no effect on SG formation or on COPII recruitment, 13
205 were generally toxic (65% mortality) at the tested concentrations, one (AZD4547)
206 affected the formation of SGs, while the remaining 32 specifically inhibited (by at
207 least 35%) the association of Sec24C with SGs without affecting SG formation (Figure
208 4A). Enrichment analysis on this last group of inhibitors highlighted that CDK
209 inhibitors were the most represented class (Figure 4B). Western blot analysis
210 confirmed that CDK activity was impaired in cells treated with the CDK inhibitors
211 (Figure 4C). In addition, we observed that there is an increase in CDK activity in SA-
212 treated cells that was sensitive to CDK inhibitors (Figure 4C).

213 The CDK protein kinase family is composed of 21 members (Malumbres, 2014) and
214 available inhibitors have limited selectivity (Asghar et al., 2015). To identify which
215 specific CDK might be involved in Sec24C recruitment, we compared the potency of
216 selected CDK inhibitors (Flavopiridol hydrochloride, SNS-032, Dinaciclib, AT7519,
217 PHA-793887, ADZ5438, JNJ-7706621, PHA-767491, BMS-265246, PHA-848125,
218 Roscovitine, Palbociclib, BS-181HCl) in the Sec24C recruitment assay with their
219 ability to inhibit different CDK isoforms, as described by Selleckchem
220 (https://www.selleckchem.com/CDK.html). This analysis revealed that CDK1 and 2
221 were those commonly targeted by the inhibitors that most potently affected Sec24C
222 recruitment to SGs (Figure 4D), strongly suggesting that CDK1/2 are the most likely
223 CDKs controlling COPII recruitment to SGs. This was confirmed by the observation
224 that down-regulating the expression of CDK1 and CDK2 by siRNA inhibited COPII
225 recruitment to SGs (Figure 4E, Figure 4—figure supplement 1). The three best hits
226 (Flavopiridol, Dinaciclib, SNS032, Figure 4D,F) were assayed using a dose-response
227 analysis and were found to be effective at concentrations as low as 100 nM (Figure
228 4G). As a negative control, the specific CDK7 inhibitor (BS-181HCl) was ineffective,
229 even at the highest concentration tested (Figure 4G).

230 Since COPII recruitment to SGs is driven by TRAPP recruitment (Figure 2F), we
231 predicted that CDK1/2 inhibitors would also inhibit TRAPP recruitment. In line with
232 our expectations, TRAPP re-localization to SGs was reduced in cells treated with
233 CDK1/2 inhibitors (Figure 4H).
234 Altogether, these results indicate that a signaling pathway involving CDK1/2
235 regulates the redistribution of TRAPP and COPII from ERES to SGs and prompted us
236 to search for the process and possibly the substrates targeted by CDK1/2.
237 We excluded the possibility that CDK1/2 could directly target TRAPPC2 or Sec23/24
238 as none of them appeared to undergo CDK1/2 dependent phosphorylation (data not
239 shown). Thus, we hypothesized that CDK inhibition might indirectly inhibit the
240 recruitment of TRAPP/COPII to SGs by stabilizing their association with ER
241 membranes. Indeed, we found that CDK inhibitors stabilize TRAPP and COPII on ERES
242 membranes even in unstressed cells (Figure 5A). The analysis of the ERES associated
243 pool using a permeabilization assay confirmed that the CDK1/2 inhibitors strongly
244 stabilized COPII at the ERES, thus increasing the membrane associated pool and
245 decreasing the cytosolic one (Figure 5B,C).
246 To identify a possible target of CDK1/2 among the regulators of COPII cycle at the
247 ERES, we focused on Sec31 for three main considerations. First, Sec31 regulates Sar1
248 cycling at the ERES acting as co-GAP of Sec23-24 (Bi et al., 2007); second, we knew
249 that the regulation of Sar1 cycle by Sec31 is required for the relocation of
250 COPII/TRAPP from ERES to SGs (Figure 3C); finally, it has been shown that Sec31 is a
251 target of CDKs in yeast (Holt et al., 2009) and in *Trypanosoma brucei* (Hu et al., 2016).
252 In mammals, Sec31 activity is known to be modulated by post-translational
253 modifications and specifically by phosphorylation on multiple sites (Koreishi et al.,
254 2013) one of which (serine 799) is included in a consensus motif for CDK
255 phosphorylation. We tested whether Sec31 could be a substrate for CDK using an
256 antibody specific for phosphoSer CDK substrates. We found that Sec31 is indeed a
257 target for CDKs (Figure 5D), and that its CDK-dependent phosphorylation is increased
258 upon SA treatment and decreased by the CDK inhibitor Dinaciclib (Fig. 5D).
259 Altogether, the above results suggest that at least one of the mechanisms underlying
260 the regulation of TRAPP/COPII recruitment to SGs by CDK1/2 involves the ability of
261 CDK1/2 to control the rate of Sar1 and COPII cycling at the ERES. This control is likely

262 to be exerted through Sec31, which, acting as a co-GAP for Sar1, speeds up the COPII
263 cycle at the ERES, thus controlling the size of the COPII pool that can be mobilized to
264 SGs in response to stress.
265
266
267 **The recruitment of TRAPP and COPII to SGs occurs in actively proliferating cells**
268 The observation that the recruitment of TRAPP and COPII to SGs is under control of
269 CDK1/2 suggested that it could be linked to the cell proliferation. We explored this
270 possibility by decreasing the cell proliferation rate in diverse and independent ways.
271 First, cells were subjected to prolonged nutrient starvation (HBSS for 8 hr) and then
272 were exposed to SA for 30 min. Under these conditions, which inhibited cell
273 proliferation, TRAPP/COPII association with SGs was reduced (Figure 6A,B).
274 Second, HeLa cells were seeded at different confluency and then treated with SA for
275 30 min. Strikingly, the extent of confluency was inversely related to the extent of
276 TRAPP/COPII association with SGs and to the degree of proliferation (Figure 6C).
277 Third, we monitored the recruitment of TRAPP/COPII to SGs in podocyte cells
278 expressing a temperature sensitive LTA-SV40 that actively proliferate at the
279 permissive temperature of 33ºC but arrest proliferation and differentiate at the
280 restrictive temperature of 37ºC (Saleem et al., 2002) (Figure 6—figure supplement 1).
281 While TRAPP and COPII associate with SGs in undifferentiated podocytes in response
282 to stress, this association was reduced in differentiated podocytes (Figure 6D). Of
283 note, the proliferation to differentiation switch, as described (Saurus et al., 2016), is
284 also accompanied by a decline in CDK activity (Figure 6E,F). Interestingly, also the
285 extent of CDK-dependent phosphorylation of Sec31 is dampened in differentiated as
286 compared with proliferating podocytes (Figure 6G), thus reinforcing the correlation
287 between the phosphorylation of Sec31 and the recruitment of COPII and TRAPP to
288 SGs.
289 Altogether these data indicate that the association of COPII and TRAPP with SGs
290 occurs only in proliferating cells and requires active CDK1/2 signaling.
291
292 **The TRAPP complex imposes SG size, composition, and function**

293 The identification of TRAPP as a component of SGs led us to ask whether it could
294 play any role in the assembly and function of SGs themselves. Indeed, we observed
295 that depleting the entire TRAPP complex or only TRAPPC2 (through siRNA-mediated
296 depletion) decreased the size of SGs (Figure 2F and Figure 7A). Microinjection of a
297 TRAPPC3-blocking Ab (Yu et al., 2006; Venditti et al., 2012) had a similar effect
298 (Figure 7B). Moreover, a smaller size of SGs was also observed upon treatment with
299 CDK1/2 inhibitors, which prevents TRAPP translocation to SGs (Figure 4F,H). Under
300 all of the above conditions the size of the SGs recall that of "immature SGs"
301 (Wheeler et al., 2016).

302 In fact, the processes that lead to SG nucleation, i.e. shut-down of protein synthesis
303 or phosphorylation of eIF2alpha induced by oxidative stress, were not affected by
304 TRAPP depletion (Figure 7—figure supplement 1A,B). Instead, the successive
305 increase in size of the nucleated SGs (i.e. SG maturation) was impaired in TRAPP-
306 depleted cells, consistent with our observation that TRAPP is recruited after the
307 initial formation of SGs (Figure 1D) and occupies an outer position in the SGs (figure
308 7C). A feature of SG maturation is the acquisition of an array of signaling molecules
309 (which can be either hyperactivated or deactivated) to drive the pro-survival
310 program (Franzmann and Alberti, 2019). This is the case of the energy sensor
311 mTORC1 (through the sequestration of its partner Raptor) and the kinase RACK1
312 (Arimoto et al., 2008; Thedieck et al., 2013; Wippich et al., 2013). To evaluate
313 whether the absence of TRAPP could affect SG maturation and/or signaling function
314 by interfering with the recruitment of these proteins, we checked the localization of
315 Raptor (Figure 7D) and RACK1 (Figure 7E, Figure 7—figure supplement 2) in TRAPP-
316 and or TRAPPC2-depleted cells subjected to oxidative stress. We observed that the
317 amount of these signaling proteins sequestered to SGs was strongly reduced by
318 TRAPP depletion, thus indicating that the TRAPP complex is necessary to generate
319 "mature" SGs that can accomplish a fully functional stress response. Localization of
320 RACK1 and Raptor was also evaluated in a context of CDK inhibition. Again,
321 treatment with CDK inhibitors strongly reduced Raptor (Figure 7F) and RACK1 (Figure
322 7G) sequestration, further supporting that the TRAPP complex is needed for SG
323 maturation. Notably, the distribution of Raptor in response to oxidative stress was

324 also studied by transiently expressing a cMyc-tagged version of the protein in control
325 cells, in TRAPP KD and in cells treated with CDK inhibitors. While myc-Raptor readily
326 relocated to SGs in control cells exposed to stress, it failed to associate with SGs
327 under conditions that prevented TRAPP association with SGs (i.e. TRAPP depletion
328 and CDK inhibition; data not shown).

329 SGs are part of a pro-survival program that aims to save energy to cope with stress
330 insults. Interfering with this program by impairing SG formation sensitizes cells to
331 apoptosis (Takahashi et al., 2013). We thus assayed stress resistance in cells with an
332 impaired capability to recruit TRAPP to SGs, i.e. upon CDK inhibition. As shown in
333 Figure 7H, CDK inhibition significantly sensitized cells to cell death, suggesting that
334 the presence of TRAPP at SGs is required for their anti-apoptotic role and
335 highlighting the TRAPP complex as a novel player in the cell response to stress.

336

337 **The recruitment of TRAPP and COPII to SGs impairs ER export of newly synthesized**
338 **cargoes and induces the fragmentation of the Golgi complex**

339 We finally investigated the functional relevance of the recruitment of TRAPP/COPII
340 to SGs by analyzing its impact on the function and structure of the secretory pathway.
341 We first analysed the ER export of procollagen type I (PC-I), which is known to be
342 regulated by COPII and TRAPP (Gorur et al., 2017; Venditti et al., 2012). PC-I
343 transport can be synchronized by temperature, being unfolded and blocked in the ER
344 at 40°C while properly folded and assembled and able to be exported from the ER,
345 transported to the Golgi complex (GC) and secreted at 32°C (Mironov et al., 2001,
346 and Methods). Human fibroblasts were incubated at 40°C, left untreated or treated
347 with SA, which induces the recruitment of Sec24C to SGs (Figure 8A). PC-I was
348 blocked in the ER under both conditions (Figure 8A). Monitoring of PC-I transport
349 after the shift to 32°C showed that while PCI reaches the GC in untreated cells, it
350 remains blocked in the ER in SA-treated cells (Figure 8A).

351 We then investigated to what extent the inhibition of cargo export from the ER
352 induced by oxidative stress is dependent on COPII/TRAPP sequestering onto SGs. To
353 this end we compared the ER export of neosynthesised cargo in control cells and in
354 SA-treated cells either under conditions permissive for the formation of SGs (and of

355 the recruitment of COPII/TRAPP to SG) or under conditions that prevent SG
356 formation. For the latter, we took advantage of the use of ISRIB, a compound that
357 antagonises the effect of eIF2α phosphorylation on translation and impairs SG
358 assembly (Sidrauski et al., 2015). In preliminary experiments, we checked the ability
359 of ISRIB to impair SG formation under our experimental conditions and found that
360 ISRIB completely abrogates SG assembly after 15 min SA treatment, delaying their
361 appearance at later time points of treatment and thus significantly also impairing
362 COPII sequestering to SGs (Figure 8—figure supplement 1). To monitor the
363 synchronized export of neosynthesised cargo we followed a reporter cargo, VSVG-
364 UVR8, that exits the ER in a UV light-inducible manner (Chen et al., 2013). After UV
365 light induction, VSVG-UVR8 exited the ER and reached the Golgi in control cells,
366 while its ER export was severely impaired in cells treated with SA under conditions
367 permissive for SG formation where COPII was massively recruited to SGs (Figure 8B,
368 D). Interestingly, the inhibition of ER export of VSVG-UVR8 was largely prevented
369 when the cells were exposed to similar oxidative stress, but under conditions that
370 prevented SG formation (i.e. when cells were pretreated with ISRIB (Figure 8B, D)).

371 We next tested whether COPII and TRAPP maintain their functionality once released
372 from SGs upon stress removal (Figure 1—figure supplement 3). Cells were treated
373 with SA for 30 min, the SA was washed out, and cells were left to recover for 180 min
374 in the presence of cycloheximide to prevent *de novo* synthesis of TRAPP and COPII
375 components. Under these conditions SGs were resolved, COPII returned to its native
376 location (ERES/cytosol) and cells completely recovered their capability to transport
377 cargo to the Golgi apparatus (Figure 8C,D). These data indicate that sequestration of
378 COPII/TRAPP onto SGs halts ER-to-Golgi trafficking while removal of the stress
379 releases COPII/TRAPP and allows trafficking to resume.

380 COPII and TRAPP not only control ER export but are also needed to maintain the
381 organization of the GC. In particular, the TRAPP complex acts as GEF for Rab1, a
382 GTPase with a key role in the organization and function of the GC (Tisdale et al.,
383 1992; Wilson et al., 1994). We monitored Golgi complex morphology in response to
384 SA by following the distribution of the early Golgi marker GM130. Strikingly, the GC
385 starts to fragment after 30 min and completely redistributes throughout the

386 cytoplasm after 60 min of SA treatment (Figure 9A). This time window overlaps with
387 the progressive recruitment of the TRAPP complex onto SGs (Figure 1D). To assess
388 whether the Golgi fragmentation induced by oxidative stress was due to
389 sequestration of TRAPP/COPII onto SGs, we analyzed the morphology of the GC in
390 cells exposed to oxidative stress under conditions that prevent COPII/TRAPP
391 recruitment to SGs, i.e. treatment with CDK inhibitors, highly confluent cells or cells
392 treated with ISRIB. We found that CDK inhibitors prevented the fragmentation of the
393 GC in cells exposed to oxidative stress (Figure 9B,C) and that oxidative stress had no
394 impact on the organization of the Golgi complex in highly confluent cells (Figure 8C).
395 Finally, ISRIB was effective in preventing the fragmentation of the Golgi complex
396 induced by SA (Figure 8D).

397 These results indicated a causal link between TRAPP/COPII sequestration to SGs and
398 Golgi fragmentation. To gain insight into the nature of the fragmentation of the Golgi
399 complex, we performed ultrastructural analysis that revealed the presence of
400 residual swollen cisternae with the loss of stacked structures and extensive
401 vesiculation in SA-treated cells (Figure 9E), a situation that is reminiscent of the
402 effect of Rab1 inactivation (Wilson et al., 1994). We hypothesized that the
403 dismantling of the Golgi complex could have been due to impaired Rab1 activation as
404 a consequence of TRAPP (the Rab1 GEF) sequestering to SGs. We monitored Rab1
405 activity by using an antibody that specifically recognizes the GTP-bound Rab1 and
406 found, indeed, that the fraction of active Rab1 (i.e. the GTP-bound form) is
407 progressively reduced in cells exposed to SA (Figure 9F). Overexpression of wt Rab1
408 reduced fragmentation/vesiculation of the GC induced by oxidative stress without
409 affecting the capacity of TRAPP to migrate to SGs (Figure 9G, Figure 9—figure
410 supplement 1), establishing a causal a link between Rab1 inactivation and Golgi
411 fragmentation. It is worth mentioning that a further contribution to the
412 disorganization of the Golgi complex upon oxidative stress may derive from the
413 delocalization of the TGN-located PARP12 to SGs, which, however, affects mainly
414 late Golgi compartments (Catara et al., 2017).
415
416 **Discussion**

417

418 We described a branch of the integrated stress response that is dependent on the
419 assembly of SGs and that impinges on the early secretory pathway. A key player of
420 this branch is TRAPP, a multimolecular complex that intervenes in multiple
421 membrane trafficking steps.

422

423 We showed that TRAPP is massively recruited to SGs in response to different acute
424 stress stimuli and in turn recruits components of the inner layer of the COPII
425 complex Sec23-Sec24, the protein complex that drives the export of newly
426 synthesized proteins from the ER, to SGs. The functional consequences of the
427 recruitment of TRAPP/COPII to SGs are double-edged since on the one hand they
428 impact on the function and organization of the secretory pathway while on the other
429 they impact on the composition and function of the SGs (Figure 10).
430 We have shown that the sequestering to SGs of these two complexes, one, COPII,
431 with a pivotal role in ER export and another, TRAPP, acting as a GEF for Rab1, a
432 master GTPase orchestrating the organization of the Golgi complex, induces a slow-
433 down of the ER-to-Golgi transport of newly synthesized proteins and the
434 disorganization of the structure of the Golgi complex. This halt in secretory activity,
435 an energetically costly process, can be seen as a way to limit energy expenditure
436 upon acute stress but also to prevent the ER export of newly synthesized proteins
437 that might have been damaged/misfolded by the acute stress before an adequate
438 UPR is installed and becomes operative. Importantly, these changes are completely
439 reversible since ER export resumes and proper Golgi morphology is restored upon
440 stress removal and relocation of the two complexes to their natural sites.
441 An intriguing feature of this branch of the integrated stress response that involves
442 the secretory pathway is its strict dependence on the proliferation status of the cells.
443 Indeed, the sequestration of TRAPP and COPII to SGs occurs only when the acute
444 stress affects actively proliferating cells. Cells with a slow/halted proliferation rate
445 still form SGs in response to acute stress stimuli, but do not delocalize TRAPP/COPII
446 from their steady state sites, i.e., the ERES, to SGs. We have used multiple strategies
447 to slow down (or halt) proliferation: nutrient deprivation, a high cell density, or a
448 switch from a proliferation to a differentiation program. Under all circumstances, we

449 observed a very tight correlation between the extent of recruitment of TRAPP/COPII
450 to SGs and the proliferation rate, indicating that acquisition of components of the
451 secretory machinery does not occur by default as a consequence of the assembly of
452 the SGs but is an active process that is subject to specific regulation.
453 We found that this regulation involves the activity of CDK1&2, since CDK1&2
454 inhibitors and/or CDK1&2 downregulation prevented the relocation of TRAPP/COPII
455 to SGs by stabilizing their association with the ERES. Indeed, the function of the
456 ERES and some of the components of the COPII coat are known to be controlled by
457 CDKs. A member of the CDK family, PCTAIRE, is recruited to ERES via its interaction
458 with Sec23 and controls ER export (Palmer et al., 2005), while Sec31, a component
459 and a regulator of Sar1/COPII cycle, is a substrate for CDKs in yeast and in
460 Trypanosoma, and, as we have shown here, also in mammalian cells (Figure 7C,D).
461 Further, the phosphorylation of Sec31 in response to growth factor and mitogenic
462 signals has also been reported (Dephoure et al. 2008; Olsen et al., 2006). We have
463 shown here that, consistent with the described role of Sec31 as a co-GAP for Sar1,
464 Sec31 function is required to control the COPII cycle at the ERES, since Sec31
465 depletion induces a tighter association of Sec23-24 with ERES and prevents their
466 translocation to SGs.
467 In fact, our results indicate that the extent of translocation of COPII/TRAPP to SGs is
468 directly proportional to their cycling rate at the ERES membranes. We have shown
469 that this rate is diminished by CDK inhibitors, but also, importantly, in starved cells as
470 compared to actively proliferating cells. These observations are in line with previous
471 reports showing that the cycling rate of ERES components is under control of growth
472 factors and growth factor-dependent signaling (Farhan et al., 2010; Tillmann et al.,
473 2015). Thus, the activity of the ERES, as measured by their number and by the rate of
474 cycling of COPII and other ERES components, is stimulated under conditions that
475 demand maximal output efficiency from the ER (i.e. during cell proliferation) as they
476 involve cell size increase and organelle expansion. If cells experience an acute stress
477 under these conditions of active growth, then the fast cycling COPII components are
478 susceptible to being temporarily sequestered to the SGs to instantly slow down ER
479 output and reduce energy consumption. By contrast, conditions that are not
480 permissive for cell proliferation, such as nutrient starvation, stabilize the association

481 of COPII/TRAPP with ERES membranes and prevent their translocation to SGs.
482 Indeed, a profound remodeling of ERES is known to occur during nutrient starvation
483 and coincides with the rerouting of COPII and TRAPP from their role in mediating the
484 ER export of newly synthesized proteins to their role in autophagosome formation
485 (Ge et al., 2017; Imai et al., 2016; Kim et al., 2016; Lamb et al., 2016; Ramírez-
486 Peinado et al., 2017; van Leeuwen et al., 2018). The kinetics of the COPII cycling at
487 the sites of phagosome formation in the ER have not been specifically explored. It is
488 tempting to speculate that it might be slower than that at the "conventional" ERES
489 under feeding conditions and that this more stable association of COPII with the ER
490 during autophagosome formation may in turn prevent its sequestration to SGs upon
491 stress exposure. Preventing the sequestration of TRAPP/COPII in starved cells
492 exposed to stress would preserve the function of COPII and TRAPP in the autophagy
493 process, a process that leads to nutrient recycling and energy production, two
494 desirable events in cells exposed to stress.
495
496 Finally, we have shown that TRAPP is required for the proper maturation of SGs.
497 Impeding the recruitment of TRAPP to SGs or depleting TRAPP does not impair the
498 formation of SGs *per se* but hampers their maturation, as evaluated by their size
499 (smaller SGs in the absence of TRAPP) and composition. In particular, key signaling
500 components, such as RACK1 and Raptor, are no longer recruited to SGs in TRAPP-
501 depleted cells. The mechanisms underlying the TRAPP-dependent maturation of SGs
502 remain to be identified. Two possible non-exclusive scenarios are worthy of
503 consideration, the engagement of specific protein-protein interactions between
504 TRAPP components and signaling molecules or a central role of TRAPP, originally
505 identified as a tethering complex, in mediating tethering/coalescence of smaller SGs
506 into larger ones, which might be the only ones competent for recruiting signaling
507 molecules. Whatever the underlying mechanisms, the impaired recruitment to SGs
508 of RACK1 and Raptor in TRAPP-depleted cells leads to lower resistance to stress and
509 higher tendency to undergo apoptosis, as the association of these signaling elements
510 with SGs exerts an anti-apoptotic role (Arimoto et al., 2008; Thedieck et al., 2013;
511 Wippich et al., 2013).

512 Our finding that TRAPP, and in particular TRAPPC2, acts as a mediator of the
513 secretory arrest in response to stress and as a driver of SG maturation elicits the
514 question as to whether and how these unsuspected properties of TRAPPC2 may be
515 relevant for the pathogenesis of SEDT, which is caused by mutations in TRAPPC2
516 (Gedeon et al., 1999). This, as well as the more general question on the physiological
517 relevance of assembling SGs in response to stress (Protter and Parker, 2016), remain
518 outstanding questions for further investigation. For now, we can only speculatively
519 propose that, given the role of TRAPPC2 in mediating secretory arrest and SG
520 maturation in actively proliferating cells, the main target cells in SEDT are likely to be
521 proliferative chondrocytes. Derived from chondrocyte progenitor cells, rapidly
522 proliferating chondrocytes are key components of the epiphyseal growth plate and
523 undergo terminal differentiation into postmitotic hypertrophic chondrocytes, which
524 eventually transdifferentiate into osteoblasts or undergo apoptosis, being replaced
525 by osteoblasts and osteoclasts. It is established that the rate of proliferation,
526 together with the height of columnar hypertrophic chondrocytes, are major
527 determinant of growth plate function and thus of bone length (Lui et al., 2018). We
528 hypothesize that TRAPPC2-defective proliferative chondrocytes are less resistant to
529 repetitive stresses, including mechanical and oxidative stresses (Henrotin et al.,
530 2003; Zuscik et al., 2008), and are thus more prone to undergo apoptosis. The
531 accelerated loss of proliferative chondrocytes would thus lead to a premature
532 growth plate senescence that could manifest as progressive delayed growth.
533

534 **Supplementary Materials**

535

536 **Materials and methods**

537 **Reagents and antibodies**

538 Primary antibodies used in this study were: mouse monoclonal antibody anti-G3BP
539 (BD Transduction Laboratories cat. no. 611126), rabbit polyclonal antibody anti-G3BP
540 (Bethil, cat. no. A302-033), mouse monoclonal antibody anti-TRAPPC5 (Abnova cat.
541 no. H00126003-A01), goat polyclonal antibody anti-eIF3 (Santa Cruz cat. no. sc-
542 16377), rabbit polyclonal antibody anti-Sec24C (Sigma-Aldrich cat. no. HPA040196),
543 mouse monoclonal anti-TIAR (BD Transduction Laboratories cat. no. 610352), mouse
544 monoclonal TRAPPC12 (Abcam cat. no. 88751), mouse monoclonal TRAPPC10 (Sanza
545 Cruz cat. no. SC-101259) mouse monoclonal anti-flag (Sigma-Aldrich cat. no. F1804),
546 rabbit polyclonal antibody anti-phosphor-Ser CDK substrates motif (Cell signaling cat.
547 no. 9477), mouse monoclonal anti-GM130 (BD Transduction Laboratories cat. no.
548 610823), human monoclonal antibody anti-Rab1-GTP (Adipogen cat. no. AG-27B-
549 0006), mouse monoclonal anti-RACK1 (Sanza Cruz cat. no. 17754), rabbit polyclonal
550 anti-Raptor (Cell signaling cat.no. 2280), rabbit polyclonal Sec16A (Bethil, cat.no.
551 A300-648A), sheep polyclonal anti-TGN46 (Serotec cat. no. AHP500), rabbit
552 polyclonal antibody anti-Sec31A (Sigma-Aldrich cat. no. HPA005457), mouse
553 monoclonal antibody AP-II (Pierce, cat. no. MA1-064), mouse monoclonal ??adaptin
554 (Transduction cat. no. 618305), mouse monoclonal antibody anti-Retinoblastoma
555 (Cell Signaling cat. no. 9309), rabbit polyclonal antibody anti-phospho
556 Retinoblastoma (Cell Signaling cat. no. 9516), rabbit polyclonal antibody anti-eiF2α
557 (Cell Signaling cat. no. 9722), rabbit polyclonal antibody anti-phospho-eiF2α (ser51)
558 (Cell Signaling cat. no. 3597), mouse monoclonal antibody anti-puromycin (Millipore
559 cat.no. MABE343), rabbit polyclonal anti-ß-actin (Sigma-Aldrich cat. no. A2066),
560 mouse monoclonal antibody anti-GAPDH (Santa Cruz cat. no. sc-32233). Guinea pig
561 polyclonal antibody anti-Synaptopodin (Acris cat. no. AP33487SU-N). Polyclonal
562 antibodies against Arfaptin, p115, G-97, COPI, TRAPPC2 and TRAPPC3 were obtained
563 in our labs. Media, serum and reagents for tissue culture were purchased from
564 Thermo Fisher Scientific.

565 Sodium arsenite (cat. no. S7400), Puromycin (cat.no. A1113802) and cycloheximide
566 (cat.no. C7698) were purchased from Sigma-Aldrich, Flavopirodol hydrochloride (cat.
567 no. S2679), SNS-032 (BMS-387032) (cat. no. S1145) and Dinaciclib (SCH727965) (cat.
568 no. S2768) were purchased from Sellekchem.
569
570 **Plasmid construction**
571 TRAPPC3-GFP, Sec23A-GFP, Sar1GTP-GFP, Rab1-GFP, OCRL-GFP, Rab5-GFP and Rab7-
572 GFP were obtained as previously described (De Leo et al., 2016; Venditti et al., 2012;
573 Vicinanza et al., 2011). Construct encoding GFP-ARF1 has been described (Dubois et
574 al., 2005).
575
576 **Cell culture, transfection, and RNA interference**
577 HeLa cells were grown in high glucose (4,500 mg/L) DMEM supplemented with 10%
578 FCS. U2OS were grown in McCoy's supplemented with 20% FCS. Human fibroblasts
579 were grown in DMEM and M199 (1:4) supplemented with 10% FCS. Podocytes were
580 grown in RPMI-1640 supplemented with 10% Insulin-transferrin-Selenium (ITS) and
581 10% FCS.
582 For transfection of DNA plasmids, HeLa cells were transfected using either TransIT-
583 LT1 (Mirus Bio LLC, for BioID2 experiment) or JetPEI (Polyplus, for
584 immunofluorescence analysis) as transfection reagents, and the expression was
585 maintained for 16 hr before processing. Microinjection of TRAPPC3 antibody was
586 performed as described (Venditti et al., 2012).
587 siRNA sequences used in this study are listed in table S2. HeLa cells were treated for
588 72 hr with Oligofectamine (Life Technologies) for direct transfection.
589 Knock-down efficiency was evaluated by western blot for TRAPPC2, TRAPPC3 and
590 Sec31 (figure 2-Supplementary 3C and figure 3-Supplementary 1) and by q-PCR for
591 Sec16, Sec23 and sec24 isoforms, CDK1 and CDK2 (figure 2-Supplementary 2; figure
592 2-Supplementary 3A,B; figure 4 Supplementary 1).
593
594 **Stress stimuli**
595 Mammalian cells were treated with 300 µM SA for 30 min (unless otherwise stated)
596 in DMEM 10% FBS supplemented with 20mM Hepes. Temperature was maintained

597 at 37°C for the time of treatment in water bath. Heat treatment (44°C) was for 45
598 min in water bath.
599
600 **Immunofluorescence microscopy**

601 HeLa, human fibroblast, U2OS and rat chondrosarcoma cells were grown on
602 coverslips and fixed with 4% PFA for 10 min, washed three times with PBS, blocked
603 and permeabilized for 5 min in 0.1% Triton in PBS. Samples were washed three times
604 and blocked with blocking solution (0.05% saponin, 0.5% BSA, 50 mM NH_4Cl in PBS)
605 and incubated with primary antibodies diluted in blocking solution for 1 hr at
606 RT. Coverslips were washed with PBS and incubated with fluorochrome-conjugated
607 secondary antibodies (Alexa-Fluor-488, Alexa-Fluor-568 and Alexa-Fluor-633) for 1 hr
608 at RT. Fixed cells were mounted in Mowiol and imaged with Plan-Apochromat
609 63x/1.4 oil objective on a Zeiss LSM800 confocal system equipped with an ESID
610 detector and controlled by a Zen blue software. Fluorescence images presented are
611 representative of cells imaged in at least three independent experiments and were
612 processed with Fiji (ImageJ; National Institutes of Health) software. Sec24C and
613 TRAPPC2 quantification and Golgi particle analysis are described in the
614 corresponding figure legends. Differences among groups were performed using the
615 unpaired Student's *t* test calculated with the GraphPad Prism software. All data are
616 reported as mean ± s.e.m. as indicated in the figure legends. For Structured
617 Illumination Microscopy (SIM, Figure 7D, figure7-supplementary 1C), cells were
618 imaged with a Plan-Apochromat 63x/1.4 oil objective on a Zeiss LSM880 confocal
619 system. Image stacks of 0.88 µm thickness were acquired with 0.126 µm z-steps and
620 15 images (three angles and five phases per angle) per z-section. The field of view
621 (FOV) was ~ 75 x 75 µm at 0.065 µm/pixel, and a SIM grating of 34 µm was used.
622 Image stacks were processed and reconstructed with Zen software, using the SIM
623 tool in the Processing palette.

624
625
626 **Gel filtration**

627 The lysate used for gel filtration was prepared by cell cracker homogenizing 1.8X10^8
628 cells in 2 ml of buffer 20 mM HEPES, pH 7.2, 150 mM NaCl, 2 mM EDTA, 1 mM DTT
629 and Protease inhibitor (Roche). The sample was centrifuged at 100,000xg for 1 h. 10
630 mg of protein was concentrated in 350µL and loaded onto a Superose6 gel filtration
631 column (GE) and 400 µL of each fraction was collected. 50µL of fractions were
632 processed for SDS-PAGE analysis and proteins were detected by Western blot using
633 specific antibodies as described in Figure 1E.

634 **Yeast Methods**

635 The centromeric plasmid pUG23-Bet3-GFP (His selection) was described previously
636 (Mahfouz et al., 2012). A Pab1-mRFP expressing plasmid was constructed by PCR
637 amplification of the Pab1 gene plus 419 bp of the promoter region from yeast
638 genomic DNA and cloning into the vector backbone of the centromeric plasmid
639 pUG35 (Ura selection), removing the Met25 promoter and replacing GFP with mRFP,
640 using standard cloning techniques. Yeast cells (BY4743) were transformed with both
641 plasmids and grown in –Ura-His media with 2% Dextrose at 30°C to early log phase.
642 Stress granules were induced by incubating cells at 46°C for 10 min (Riback et al.,
643 2017) and observed immediately on an LSM800 microscope.
644

645 **Immunoprecipitation**

646 For the studies of TRAPPC2 interactors, HeLa cells were transfected with the
647 TRAPPC2-3XFLAG and 3XFLAG constructs. 16 hr post-transfection, cells were lysed
648 with lysis buffer (50 mM Tris-HCl pH 7.4, 100 mM NaCl, 1 mM EDTA, 0.5% Lauryl
649 Maltoside, protease and phosphatase inhibitors).
650 Cell extracts from control transfected HeLa cells or cells expressing TRAPPC2-3XFLAG
651 were immune-precipitated for 5 hr at 4°C using M2-flag agarose beads. Immune-
652 precipitates were analysed by Western blot or by LC-MS/MS (Central Proteomics
653 Facility, Sir William Dunn Pathology School, Oxford University).
654 HeLa cells or podocytes were used to analyse Sec31 phosphorylation status. IP of
655 HeLa cells: cells were plated in 15 mm plates. The day after, samples were treated
656 with Dinaciclib (10 µM in DMSO) for 150 min and with SA (300 µM, 10 min) alone or
657 in combination. Cells were then lysed with RIPA buffer (20mM Tris-HCl pH 7.5, 150

658 mM NaCl, 1 mM Na2EDTA, 1 mM EGTA, 1% NP-40, 1% sodium deoxycholate,
659 protease and phosphatase inhibitors). Cells extracts were immune-precipitated for
660 30 min at 4°C using the anti-Sec31A antibody. Finally, protein-A Sepharose beads
661 were added to the samples and left for 45 min at 4°C. Samples were analyzed by
662 Western blot using the antibodies indicated in the main text. IP of podocytes:
663 growing and differentiated podocytes were lysed and processed as described for
664 HeLa cells.
665
666 **Functional annotation of the TRAPPC2 interactors**
667 TRAPPC2-FLAG IP samples were compared with the proteins immunoprecipitated in
668 the control IP (Table S1): 427 proteins were specifically immunoprecipitated in
669 TRAPPC2-FLAG samples. Moreover, 113 were enriched in the TRAPPC2-FLAG IP
670 samples versus the control IP (ratio >2). Functional Annotation analysis (Dennis et al.,
671 2003; Huang et al., 2009) was used to group the putative TRAPPC2 protein partners
672 according to Molecular Function (MF). The DAVID online tool (DAVID Bioinformatics
673 Resources 6.7) was used restricting the output to all MF terms (MF_FAT). Of note,
674 we found that 251 out of the total 539 proteins were annotated as RNA-binding
675 proteins (GO:0003723) (Ashburner et al., 2000).
676
677 **Digitonin Assay**
678 HeLa cells were exposed to SA or treated with Dinaciclib (10 µM). After treatment,
679 cells were washed twice with permeabilization buffer (25mM HEPES, 125 mM
680 CH_3COOK, 2.5 mM $Mg(CH_3COO)_2$, 5 mM EGTA, 1mM DTT) and then permeabilized in
681 PB buffer supplemented with 30 µg/mL of digitonin plus the indicated antibody to
682 visualize permeabilized cells. To analyze Sec24C association with SGs, digitonin was
683 left for 6 min at room temperature. Cells were then washed three times with PB
684 buffer and left in PB buffer for 10 min at RT. Finally, samples were fixed with 4% PFA
685 and processed for IF. To analyse Sec24C association at ERES in the presence of
686 Dinaciclib, cells were fixed for 2 min after digitonin permeabilization.
687
688 **High content screening**

689 HeLa cells were plated in 384-well culture plates. The day after, a kinase inhibitor
690 library, purchased from Selleckchem, was dispensed using a liquid-handler system
691 (Hamilton) to give a final concentration of 10 µM. 150 minutes after drug
692 administration, cells were treated with sodium arsenite (300 µM) for 30 min at 37°C
693 in the presence of compounds. Finally, samples were fixed for 10 min at room
694 temperature by adding 1 volume of 4% PFA (paraformaldehyde in PBS) to the growth
695 medium and stained with the appropriate antibodies.
696 For image acquisition, at least 25 images per field were acquired per well of the 384-
697 well plate using confocal automated microscopy (Opera high content system; Perkin-
698 Elmer). A dedicated script was developed to perform the analysis of Sec24C
699 localization on the different images (Harmony and Acapella software; Perkin-Elmer).
700 The script calculated the co-localization value of Sec24C with the SG marker (G3BP).
701 The results were normalized using positive (mock cells exposed to SA) control
702 samples in the same plate.
703 P-values were calculated on the basis of mean values from three independent wells.
704 The data are represented as a percentage of Sec24C recruitment in the control cells
705 (100%) using Excel (Microsoft) and Prism software (GraphPad software).
706
707 **Cell cycle analysis by flow cytometry**
708 HeLa cells were harvested and resuspended in PBS. For the fixation, a 9-fold volume
709 of 70% ethanol was added and incubated a 4°C for at least 1hr. Next, cells were
710 centrifuged, washed in PBS and resuspended in PBS containing RNase A 0.1 mg/ml.
711 After incubation for 1hr at 37°C, propidium iodide was added to a final concentration
712 of 10 µg/ml and samples were analyzed in an Accuri C6 flow cytometer.
713
714 **Cell proliferation analysis by High Content Imaging**
715 Cell cycle analysis by high content imaging was performed using the Click-iT Plus EdU
716 Alexa Fluor 488 Imaging Kit (Life Technologies) according to the manufacturer's
717 instructions. Images were acquired with an automated confocal microscopy (Opera
718 System, Perkin-Elmer) and analyzed through Columbus Image Data Storage and
719 Analysis System (Perkin-Elmer). Nuclear intensity of EdU (5-ethynyl-2'-deoxyuridine,

720 a nucleoside analog of thymidine) in EdU-positive nuclei (S-phase cells) was used as a
721 measure of DNA replication rate.
722
723 **Cell death assay**
724 HeLa cells were pre-treated with CDK inhibitors (SNS-032, Flavopiridol and Dinaciclib)
725 for 150 min and exposed to SA (500 µM, 1 h). Subsequently, the stress stimulus was
726 washed out and cells left to recover for 16 h. To stain dead cells, a fluorophore dye
727 cocktail containing the cell-permeant nuclear dye Hoechst 33342 and the cell-
728 impermeant nuclear dye BOBO ™-3 that selectively labels dying cells (Invitrogen,
729 H3570, B3586), was added to the growth media and incubated for 45 min (37°C, 5%
730 CO_2). Cells were analyzed at automated microscopy (Operetta high content system;
731 Perkin-Elmer) using a customized script to calculate the ratio between BOBO ™-3
732 positive nuclei and total cells.
733
734 **Puromycin Assay**
735 The puromycin (PMY) assay was modified from David et al., JCB 2012 (David et al.,
736 2012). In brief, mock, TRAPPC2-KD or TRAPPC3-KD HeLa cells were exposed to SA
737 (500 µM, 30 min) in DMEM 10% FCS. Cells were washed three times in DMEM 1X
738 and incubated with 9 µM PMY in DMEM for 5 min at 37°C. Samples were lysed in
739 RIPA buffer and processed for Western blot analysis with the anti-puromycin
740 antibody.
741
742 **Transport assay**
743 VSVG-mEOS2-2XUVR8 was a gift from Matthew Kennedy (AddGene plasmid #49803).
744 HeLa cells were transfected with the plasmid for 16 h and treated with SA, CHX and
745 ISRIB for the indicated times. A UV-A lamp was used to illuminate samples (4 pulses,
746 15 sec each). After the light pulses, cells were left for 10 min at 37°C, then fixed with
747 a volume of 4% PFA and processed for immunofluorescence.
748 The PC-I transport assay was performed in human fibroblasts as previously described
749 (Venditti et al., 2012). For our purposes, cells were treated with SA (300 µM) for 120
750 min at 40°C and analyzed 10 min after the temperature switch (40 to 32°C). Cells
751 were then fixed and stained with appropriate antibodies.

752

753 **Electron microscopy**

754 EM samples were prepared as previously described (D'Angelo et al., 2007). Briefly,
755 cells were fixed by adding to the culture medium the same volume of a mixture of
756 PHEM buffer (10 mM EGTA, 2 mM $MgCl_2$, 60 mM PIPES, 25 mM HEPES, pH 6.9), 4%
757 paraformaldehyde, 2% glutaraldehyde for 2 h, and then stored in storage solution
758 (PHEM buffer, 0.5% paraformaldehyde) overnight. After washing with 0.15 M glycine
759 buffer in PBS, the cells were scraped and pelleted by centrifugation, embedded in
760 10% gelatin, cooled on ice, and cut into 0.5 mm blocks. The blocks were infused with
761 2.3 M sucrose and trimmed with an ultramicrotome (Leica Ultracut R) at –120°C
762 using a dry diamond knife.

763

764 **Quantitative real-time PCR**

765 Real-time quantitative PCR (qRT-PCR) was carried out with the LightCycler 480 SYBR
766 Green I mix (Roche) using the Light Cycler 480 II detection system (Roche) with the
767 following conditions: 95 °C, 10 min; (95 °C, 10 s; 60 °C, 10 s; 72 °C, 15 s) × 45 cycles.
768 For expression studies the qRT-PCR results were normalized against an internal
769 control (HPRT1).

770

771

References

Anderson P, Kedersha N. 2008. Stress granules: the Tao of RNA triage. *Trends Biochem Sci* 33:141–150. doi:10.1016/j.tibs.2007.12.003

Anderson P, Kedersha N. 2002. Stressful initiations. *J Cell Sci* 115:3227–3234.

Arimoto K, Fukuda H, Imajoh-Ohmi S, Saito H, Takekawa M. 2008. Formation of stress granules inhibits apoptosis by suppressing stress-responsive MAPK pathways. *Nat Cell Biol* 10:1324–1332. doi:10.1038/ncb1791

Asghar U, Witkiewicz AK, Turner NC, Knudsen ES. 2015. The history and future of targeting cyclin-dependent kinases in cancer therapy. *Nat Rev Drug Discov* 14:130–146. doi:10.1038/nrd4504

Ashburner M, Ball CA, Blake JA, Botstein D, Butler H, Cherry JM, Davis AP, Dolinski K, Dwight SS, Eppig JT, Harris MA, Hill DP, Issel-Tarver L, Kasarskis A, Lewis S, Matese JC, Richardson JE, Ringwald M, Rubin GM, Sherlock G. 2000. Gene ontology: tool for the unification of biology. The Gene Ontology Consortium. *Nat Genet* 25:25–29. doi:10.1038/75556

Aulas A, Fay MM, Szaflarski W, Kedersha N, Anderson P, Ivanov P. 2017. Methods to Classify Cytoplasmic Foci as Mammalian Stress Granules. *J Vis Exp JoVE*. doi:10.3791/55656

Ballock RT, O'keefe RJ. 2003. The Biology Of The Growth Plate. *J Bone Jt Surg-Am Vol* 85:715–726.

Bi X, Mancias JD, Goldberg J. 2007. Insights into COPII Coat Nucleation from the Structure of Sec23•Sar1 Complexed with the Active Fragment of Sec31. *Dev Cell* 13:635–645. doi:10.1016/j.devcel.2007.10.006

Catara G, Grimaldi G, Schembri L, Spano D, Turacchio G, Lo Monte M, Beccari AR, Valente C, Corda D. 2017. PARP1-produced poly-ADP-ribose causes the PARP12 translocation to stress granules and impairment of Golgi complex functions. *Sci Rep* 7:14035. doi:10.1038/s41598-017-14156-8

Chen D, Gibson ES, Kennedy MJ. 2013. A light-triggered protein secretion system. *J Cell Biol* 201:631–640. doi:10.1083/jcb.201210119

David A, Dolan BP, Hickman HD, Knowlton JJ, Clavarino G, Pierre P, Bennink JR, Yewdell JW. 2012. Nuclear translation visualized by ribosome-bound nascent chain puromycylation. *J Cell Biol* 197:45–57. doi:10.1083/jcb.201112145

D'Arcangelo JG, Stahmer KR, Miller EA. 2013. Vesicle-mediated export from the ER: COPII coat function and regulation. *Biochim Biophys Acta* 1833:2464–2472. doi:10.1016/j.bbamcr.2013.02.003

De Leo MG, Staiano L, Vicinanza M, Luciani A, Carissimo A, Mutarelli M, Di Campli A,

819 Polishchuk E, Di Tullio G, Morra V, Levtchenko E, Oltrabella F, Starborg T, Santoro M,
820 Di Bernardo D, Devuyst O, Lowe M, Medina DL, Ballabio A, De Matteis MA. 2016.
821 Autophagosome-lysosome fusion triggers a lysosomal response mediated by TLR9
822 and controlled by OCRL. *Nat Cell Biol* 18:839–850. doi:10.1038/ncb3386
823
824 Dennis G, Sherman BT, Hosack DA, Yang J, Gao W, Lane HC, Lempicki RA. 2003.
825 DAVID: Database for Annotation, Visualization, and Integrated Discovery. *Genome*
826 *Biol* 4:P3.
827
828 Dephoure N, Zhou C, Villén J, Beausoleil SA, Bakalarski CE, Elledge SJ, Gygi SP. 2008 A
829 quantitative atlas of mitotic phosphorylation. *Proc Natl Acad Sci U S A.*
830 105(31):10762-7
831
832 Dubois T, Paléotti O, Mironov AA, Fraisier V, Stradal TEB, De Matteis MA, Franco M,
833 Chavrier P. 2005. Golgi-localized GAP for Cdc42 functions downstream of ARF1 to
834 control Arp2/3 complex and F-actin dynamics. *Nat Cell Biol* 7:353–364.
835 doi:10.1038/ncb1244
836
837 Farhan H, Wendeler MW, Mitrovic S, Fava E, Silberberg Y, Sharan R, Zerial M, Hauri
838 H-P. 2010. MAPK signaling to the early secretory pathway revealed by
839 kinase/phosphatase functional screening. *J Cell Biol* 189:997–1011.
840 doi:10.1083/jcb.200912082
841
842 Franzmann TM, Alberti S. 2019. Protein Phase Separation as a Stress Survival
843 Strategy. *Cold Spring Harb Perspect Biol*. doi:10.1101/cshperspect.a034058
844
845 Ge L, Zhang M, Kenny SJ, Liu D, Maeda M, Saito K, Mathur A, Xu K, Schekman R. 2017.
846 Remodeling of ER-exit sites initiates a membrane supply pathway for
847 autophagosome biogenesis. *EMBO Rep* 18:1586–1603.
848 doi:10.15252/embr.201744559
849
850 Gedeon AK, Colley A, Jamieson R, Thompson EM, Rogers J, Sillence D, Tiller GE,
851 Mulley JC, Gécz J. 1999. Identification of the gene (SEDL) causing X-linked
852 spondyloepiphyseal dysplasia tarda. *Nat Genet* 22:400–404. doi:10.1038/11976
853
854 Gorur A, Yuan L, Kenny SJ, Baba S, Xu K, Schekman R. 2017. COPII-coated membranes
855 function as transport carriers of intracellular procollagen I. *J Cell Biol* 216:1745–1759.
856 doi:10.1083/jcb.201702135
857
858 Harripaul R, Vasli N, Mikhailov A, Rafiq MA, Mittal K, Windpassinger C, Sheikh TI,
859 Noor A, Mahmood H, Downey S, Johnson M, Vleuten K, Bell L, Ilyas M, Khan FS, Khan
860 V, Moradi M, Ayaz M, Naeem F, Heidari A, Ahmed I, Ghadami S, Agha Z, Zeinali S,
861 Qamar R, Mozhdehipanah H, John P, Mir A, Ansar M, French L, Ayub M, Vincent JB.
862 2018. Mapping autosomal recessive intellectual disability: combined microarray and
863 exome sequencing identifies 26 novel candidate genes in 192 consanguineous
864 families. *Mol Psychiatry* 23:973–984. doi:10.1038/mp.2017.60
865

866 Henrotin YE, Bruckner P, Pujol J-PL. 2003. The role of reactive oxygen species in
867 homeostasis and degradation of cartilage. *Osteoarthritis Cartilage* 11:747–755.
868
869 Holt LJ, Tuch BB, Villén J, Johnson AD, Gygi SP, Morgan DO. 2009. Global analysis of
870 Cdk1 substrate phosphorylation sites provides insights into evolution. *Science*
871 325:1682–1686. doi:10.1126/science.1172867
872
873 Hu H, Gourguechon S, Wang CC, Li Z. 2016. The G1 Cyclin-dependent Kinase CRK1 in
874 Trypanosoma brucei Regulates Anterograde Protein Transport by Phosphorylating
875 the COPII Subunit Sec31. *J Biol Chem* 291:15527–15539.
876 doi:10.1074/jbc.M116.715185
877
878 Huang DW, Sherman BT, Zheng X, Yang J, Imamichi T, Stephens R, Lempicki RA. 2009.
879 Extracting biological meaning from large gene lists with DAVID. *Curr Protoc*
880 *Bioinforma* Chapter 13:Unit 13.11. doi:10.1002/0471250953.bi1311s27
881
882 Imai K, Hao F, Fujita N, Tsuji Y, Oe Y, Araki Y, Hamasaki M, Noda T, Yoshimori T. 2016.
883 Atg9A trafficking through the recycling endosomes is required for autophagosome
884 formation. *J Cell Sci* 129:3781–3791. doi:10.1242/jcs.196196
885
886 Jain S, Wheeler JR, Walters RW, Agrawal A, Barsic A, Parker R. 2016. ATPase
887 modulated stress granules contain a diverse proteome and substructure. *Cell*
888 164:487–498. doi:10.1016/j.cell.2015.12.038
889
890 Kapetanovich L, Baughman C, Lee TH. 2005. Nm23H2 Facilitates Coat Protein
891 Complex II Assembly and Endoplasmic Reticulum Export in Mammalian Cells. *Mol*
892 *Biol Cell* 16:835–848. doi:10.1091/mbc.E04-09-0785
893
894 Khattak NA, Mir A. 2014. Computational analysis of TRAPPC9: candidate gene for
895 autosomal recessive non-syndromic mental retardation. *CNS Neurol Disord Drug*
896 *Targets* 13:699–711.
897
898 Kim JJ, Lipatova Z, Segev N. 2016. TRAPP Complexes in Secretion and Autophagy.
899 *Front Cell Dev Biol* 4:20. doi:10.3389/fcell.2016.00020
900
901 Koehler K, Milev MP, Prematilake K, Reschke F, Kutzner S, Jühlen R, Landgraf D, Utine
902 E, Hazan F, Diniz G, Schuelke M, Huebner A, Sacher M. 2017. A novel TRAPPC11
903 mutation in two Turkish families associated with cerebral atrophy, global retardation,
904 scoliosis, achalasia and alacrima. *J Med Genet* 54:176–185. doi:10.1136/jmedgenet-
905 2016-104108
906
907 Koreishi M, Yu S, Oda M, Honjo Y, Satoh A. 2013. CK2 Phosphorylates Sec31 and
908 Regulates ER-To-Golgi Trafficking. *PloS One* 8:e54382.
909 doi:10.1371/journal.pone.0054382
910
911 Lamb CA, Nühlen S, Judith D, Frith D, Snijders AP, Behrends C, Tooze SA. 2016.
912 TBC1D14 regulates autophagy via the TRAPP complex and ATG9 traffic. *EMBO J*

913 35:281–301. doi:10.15252/embj.201592695
914
915 Li C, Luo X, Zhao S, Siu GK, Liang Y, Chan HC, Satoh A, Yu SS. 2017. COPI-TRAPPII
916 activates Rab18 and regulates its lipid droplet association. *EMBO J* 36:441–457.
917 doi:10.15252/embj.201694866
918
919 Lord C, Bhandari D, Menon S, Ghassemian M, Nycz D, Hay J, Ghosh P, Ferro-Novick S.
920 2011. Sequential interactions with Sec23 control the direction of vesicle traffic.
921 *Nature* 473:181–186. doi:10.1038/nature09969
922
923 Lui JC, Jee YH, Garrison P, Iben JR, Yue S, Ad M, Nguyen Q, Kikani B, Wakabayashi Y,
924 Baron J. 2018. Differential aging of growth plate cartilage underlies differences in
925 bone length and thus helps determine skeletal proportions. *PLoS Biol* 16:e2005263.
926 doi:10.1371/journal.pbio.2005263
927
928 Malumbres M. 2014. Cyclin-dependent kinases. *Genome Biol* 15:122.
929 Milev MP, Graziano C, Karall D, Kuper WFE, Al-Deri N, Cordelli DM, Haack TB,
930 Danhauser K, Iuso A, Palombo F, Pippucci T, Prokisch H, Saint-Dic D, Seri M, Stanga D,
931 Cenacchi G, van Gassen KLI, Zschocke J, Fauth C, Mayr JA, Sacher M, van Hasselt PM.
932 2018. Bi-allelic mutations in TRAPPC2L result in a neurodevelopmental disorder and
933 have an impact on RAB11 in fibroblasts. *J Med Genet* 55:753–764.
934 doi:10.1136/jmedgenet-2018-105441
935
936 Milev MP, Grout ME, Saint-Dic D, Cheng Y-HH, Glass IA, Hale CJ, Hanna DS, Dorschner
937 MO, Prematilake K, Shaag A, Elpeleg O, Sacher M, Doherty D, Edvardson S. 2017.
938 Mutations in TRAPPC12 Manifest in Progressive Childhood Encephalopathy and Golgi
939 Dysfunction. *Am J Hum Genet* 101:291–299. doi:10.1016/j.ajhg.2017.07.006
940
941 Mironov AA, Beznoussenko GV, Nicoziani P, Martella O, Trucco A, Kweon H-S,
942 Giandomenico DD, Polishchuk RS, Fusella A, Lupetti P, Berger EG, Geerts WJC, Koster
943 AJ, Burger KNJ, Luini A. 2001. Small cargo proteins and large aggregates can traverse
944 the Golgi by a common mechanism without leaving the lumen of cisternae. *J Cell Biol*
945 155:1225–1238. doi:10.1083/jcb.200108073
946
947 Mohamoud HS, Ahmed S, Jelani M, Alrayes N, Childs K, Vadgama N, Almramhi MM,
948 Al-Aama JY, Goodbourn S, Nasir J. 2018. A missense mutation in TRAPPC6A leads to
949 build-up of the protein, in patients with a neurodevelopmental syndrome and
950 dysmorphic features. *Sci Rep* 8:2053. doi:10.1038/s41598-018-20658-w
951
952 Moujalled D, James JL, Yang S, Zhang K, Duncan C, Moujalled DM, Parker SJ,
953 Caragounis A, Lidgerwood G, Turner BJ, Atkin JD, Grubman A, Liddell JR,
954
955 Olsen JV[1], Blagoev B, Gnad F, Macek B, Kumar C, Mortensen P, Mann M 2006 Global,
956 in vivo, and site-specific phosphorylation dynamics in signaling networks
957 *Cell. 2006;127(3):635-48*
958
959 Proepper C, Boeckers TM, Kanninen KM, Blair I, Crouch PJ, White AR. 2015.

960 Phosphorylation of hnRNP K by cyclin-dependent kinase 2 controls cytosolic
961 accumulation of TDP-43. *Hum Mol Genet* 24:1655–1669. doi:10.1093/hmg/ddu578
962
963 Palmer KJ, Konkel JE, Stephens DJ. 2005. PCTAIRE protein kinases interact directly
964 with the COPII complex and modulate secretory cargo transport. *J Cell Sci* 118:3839–
965 3847. doi:10.1242/jcs.02496
966
967 Protter DSW, Parker R. 2016. Principles and Properties of Stress Granules. *Trends Cell*
968 *Biol* 26:668–679. doi:10.1016/j.tcb.2016.05.004
969
970 Ramírez-Peinado S, Ignashkova TI, van Raam BJ, Baumann J, Sennott EL, Gendarme
971 M, Lindemann RK, Starnbach MN, Reiling JH. 2017. TRAPPC13 modulates autophagy
972 and the response to Golgi stress. *J Cell Sci* 130:2251–2265. doi:10.1242/jcs.199521
973
974 Sacher M, Shahrzad N, Kamel H, Milev MP. 2018. TRAPPopathies: An emerging set of
975 disorders linked to variations in the genes encoding transport protein particle
976 (TRAPP)-associated proteins. *Traffic Cph Den*. doi:10.1111/tra.12615
977
978 Saleem MA, O'Hare MJ, Reiser J, Coward RJ, Inward CD, Farren T, Xing CY, Ni L,
979 Mathieson PW, Mundel P. 2002. A conditionally immortalized human podocyte cell
980 line demonstrating nephrin and podocin expression. *J Am Soc Nephrol JASN* 13:630–
981 638.
982
983 Saurus P, Kuusela S, Dumont V, Lehtonen E, Fogarty CL, Lassenius MI, Forsblom C,
984 Lehto M, Saleem MA, Groop P-H, Lehtonen S. 2016. Cyclin-dependent kinase 2
985 protects podocytes from apoptosis. *Sci Rep* 6:21664. doi:10.1038/srep21664
986
987 Scrivens PJ, Noueihed B, Shahrzad N, Hul S, Brunet S, Sacher M. 2011. C4orf41 and
988 TTC-15 are mammalian TRAPP components with a role at an early stage in ER-to-
989 Golgi trafficking. *Mol Biol Cell* 22:2083–2093. doi:10.1091/mbc.E10-11-0873
990
991 Sidrauski C, McGeachy AM, Ingolia NT, Walter P. 2015. The small molecule ISRIB
992 reverses the effects of eIF2α phosphorylation on translation and stress granule
993 assembly. *eLife* 4. doi:10.7554/eLife.05033
994
995 Takahashi M, Higuchi M, Matsuki H, Yoshita M, Ohsawa T, Oie M, Fujii M. 2013.
996 Stress Granules Inhibit Apoptosis by Reducing Reactive Oxygen Species Production.
997 *Mol Cell Biol* 33:815–829. doi:10.1128/MCB.00763-12
998
999 Thedieck K, Holzwarth B, Prentzell MT, Boehlke C, Kläsener K, Ruf S, Sonntag AG,
1000 Maerz L, Grellscheid S-N, Kremmer E, Nitschke R, Kuehn EW, Jonker JW, Groen AK,
1001 Reth M, Hall MN, Baumeister R. 2013. Inhibition of mTORC1 by Astrin and Stress
1002 Granules Prevents Apoptosis in Cancer Cells. *Cell* 154:859–874.
1003 doi:10.1016/j.cell.2013.07.031
1004
1005 Tiller GE, Hannig VL, Dozier D, Carrel L, Trevarthen KC, Wilcox WR, Mundlos S, Haines
1006 JL, Gedeon AK, Gecz J. 2001. A recurrent RNA-splicing mutation in the SEDL gene

1007 causes X-linked spondyloepiphyseal dysplasia tarda. *Am J Hum Genet* 68:1398–1407.
1008 doi:10.1086/320594
1009
1010 Tillmann KD, Reiterer V, Baschieri F, Hoffmann J, Millarte V, Hauser MA, Mazza A,
1011 Atias N, Legler DF, Sharan R, Weiss M, Farhan H. 2015. Regulation of Sec16 levels and
1012 dynamics links proliferation and secretion. *J Cell Sci* 128:670–682.
1013 doi:10.1242/jcs.157115
1014
1015 Tisdale EJ, Bourne JR, Khosravi-Far R, Der CJ, Balch WE. 1992. GTP-binding mutants
1016 of rab1 and rab2 are potent inhibitors of vesicular transport from the endoplasmic
1017 reticulum to the Golgi complex. *J Cell Biol* 119:749–761.
1018
1019 van Leeuwen W, van der Krift F, Rabouille C. 2018. Modulation of the secretory
1020 pathway by amino-acid starvation. *J Cell Biol* 217:2261–2271.
1021 doi:10.1083/jcb.201802003
1022
1023 Venditti R, Scanu T, Santoro M, Di Tullio G, Spaar A, Gaibisso R, Beznoussenko GV,
1024 Mironov AA, Mironov A, Zelante L, Piemontese MR, Notarangelo A, Malhotra V,
1025 Vertel BM, Wilson C, De Matteis MA. 2012. Sedlin controls the ER export of
1026 procollagen by regulating the Sar1 cycle. *Science* 337:1668–1672.
1027 doi:10.1126/science.1224947
1028
1029 Vicinanza M, Di Campli A, Polishchuk E, Santoro M, Di Tullio G, Godi A, Levtchenko E,
1030 De Leo MG, Polishchuk R, Sandoval L, Marzolo M-P, De Matteis MA. 2011. OCRL
1031 controls trafficking through early endosomes via PtdIns4,5P_2-dependent regulation
1032 of endosomal actin. *EMBO J* 30:4970–4985. doi:10.1038/emboj.2011.354
1033
1034 Westlake CJ, Baye LM, Nachury MV, Wright KJ, Ervin KE, Phu L, Chalouni C, Beck JS,
1035 Kirkpatrick DS, Slusarski DC, Sheffield VC, Scheller RH, Jackson PK. 2011. Primary cilia
1036 membrane assembly is initiated by Rab11 and transport protein particle II (TRAPPII)
1037 complex-dependent trafficking of Rabin8 to the centrosome. *Proc Natl Acad Sci U S A*
1038 108:2759–2764. doi:10.1073/pnas.1018823108
1039
1040 Wheeler JR, Matheny T, Jain S, Abrisch R, Parker R. n.d. Distinct stages in stress
1041 granule assembly and disassembly. *eLife* 5. doi:10.7554/eLife.18413
1042
1043 Wilson BS, Nuoffer C, Meinkoth JL, McCaffery M, Feramisco JR, Balch WE, Farquhar
1044 MG. 1994. A Rab1 mutant affecting guanine nucleotide exchange promotes
1045 disassembly of the Golgi apparatus. *J Cell Biol* 125:557–571.
1046
1047 Wippich F, Bodenmiller B, Trajkovska MG, Wanka S, Aebersold R, Pelkmans L. 2013.
1048 Dual specificity kinase DYRK3 couples stress granule condensation/dissolution to
1049 mTORC1 signaling. *Cell* 152:791–805. doi:10.1016/j.cell.2013.01.033
1050
1051 Yamasaki A, Menon S, Yu S, Barrowman J, Meerloo T, Oorschot V, Klumperman J,
1052 Satoh A, Ferro-Novick S. 2009. mTrs130 is a component of a mammalian TRAPPII
1053 complex, a Rab1 GEF that binds to COPI-coated vesicles. *Mol Biol Cell* 20:4205–4215.

1054 doi:10.1091/mbc.e09-05-0387
1055
1056 Yu S, Satoh A, Pypaert M, Mullen K, Hay JC, Ferro-Novick S. 2006. mBet3p is required
1057 for homotypic COPII vesicle tethering in mammalian cells. *J Cell Biol* 174:359–368.
1058 doi:10.1083/jcb.200603044
1059
1060 Zacharogianni M, Aguilera-Gomez A, Veenendaal T, Smout J, Rabouille C. n.d. A
1061 stress assembly that confers cell viability by preserving ERES components during
1062 amino-acid starvation. *eLife* 3. doi:10.7554/eLife.04132
1063
1064 Zou S, Liu Y, Zhang XQ, Chen Y, Ye M, Zhu X, Yang S, Lipatova Z, Liang Y, Segev N.
1065 2012. Modular TRAPP complexes regulate intracellular protein trafficking through
1066 multiple Ypt/Rab GTPases in Saccharomyces cerevisiae. *Genetics* 191:451–460.
1067 doi:10.1534/genetics.112.139378
1068
1069 Zuscik MJ, Hilton MJ, Zhang X, Chen D, O'Keefe RJ. 2008. Regulation of
1070 chondrogenesis and chondrocyte differentiation by stress. *J Clin Invest* 118:429–438.
1071 doi:10.1172/JCI34174
1072

1073

1074 **Acknowledgements**

1075 We thank Andrea Ballabio, Carmine Settembre, Leandro Raul Soria, Maria Chiara
1076 Masone, Rossella Venditti and Graciana Diez Roux for helpful discussion. MADM
1077 acknowledges the support of Telethon (grant TGM11CB1), the Italian Association for
1078 Cancer Research (AIRC, grant IG2013_14761), European Research Council Advanced
1079 Investigator grant no. 670881 (SYSMET).
1080

1081 **Author contributions**

1082 F.Z. and M.A.D.M. conceived the work. F.Z. planned and analyzed most of the
1083 experiments, C.W. performed experiments on yeast, G.D.T. performed gel filtration
1084 and Sec31-IP, M.S. provided technical support, P.P. and M.P. performed MS/MS
1085 analysis, D.D. helped with cell culture, S.P.V. performed cell proliferation and flow
1086 cytometry assays, R.D.C. and M.F. analyzed MS/MS data, A.R. helped in performing
1087 cell death assay, M.A.S. provided podocytes cell line, E.P. performed E.M. analyses,
1088 L.G. designed the script for high-content analysis, F.Z. and M.A.D.M. conceptualized
1089 the work and strategy and wrote the manuscript.
1090

1091 **Conflict of interest**

1092 The authors declare that they have no conflicts of interest with the contents of this
1093 article.

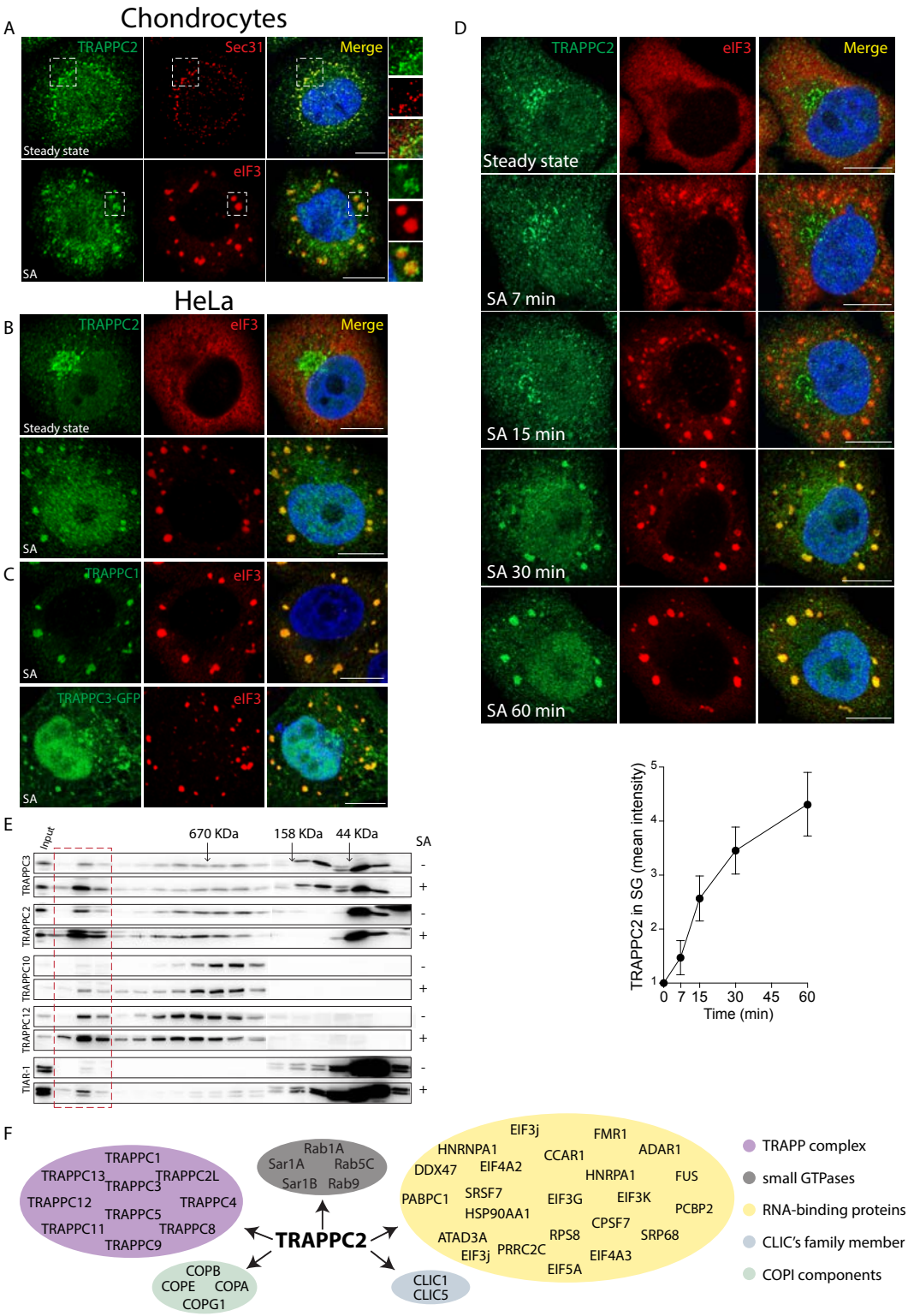

Figure 1. The TRAPP complex is recruited to stress granules. (A,B) Localization of endogenous TRAPPC2 under steady state conditions or after sodium arsenite (SA) treatment in (A) a rat chondrosarcoma cell line (300 µM, 1 hr) and (B) in HeLa cells (300 µM, 30 min). Fluorescence microscopy of fixed cells using antibodies against TRAPPC2, eIF3 (to label SGs), Sec31 (to label ERES). DAPI (blue). Small panels in (A) show details and merge of boxed areas. **(C)** Localization of endogenous TRAPPC1 and

1102 of GFP-TRAPPC3 to eIF3-labeled SGs in HeLa cells after SA treatment**. (D)**
1103 Representative images of a time course analysis of TRAPPC2 redistribution to SGs.
1104 Cells were treated as in (B). Graph, quantification of TRAPPC2 localization at SGs
1105 over time (the ratio between TRAPPC2 (mean fluorescence intensity) in SG puncta
1106 and cytosolic TRAPPC2). Mean ± s.e.m. n = 50 cells per experiment, N = 3. Scale bar,
1107 10 µm in (A-D) **(E)** Extracts from untreated and SA-treated HeLa cells were
1108 fractionated by size exclusion chromatography on a Superose6 column. Fractions
1109 were analyzed by Western blot using antibodies against TRAPPC2 and TRAPPC3
1110 (components of both TRAPPII and TRAPPIII complexes), TRAPPC10 (a component of
1111 the TRAPPII complex), TRAPPC12 (a component of the TRAPPIII complex), and
1112 against the SG marker TIAR-1. TRAPP components co-fractionated with a high
1113 molecular weight complex (red dashed box) containing TIAR-1 in SA-treated cells.
1114 Arrows indicate protein standards: thyroglobulin (670 kDa), γ-globulin (158 kDa),
1115 ovalbumin(44 kDa) **F)** Schematic representation of MS/MS analysis of TRAPPC2
1116 interactors. 251 out of 512 (46%) proteins are RNA-binding proteins, including
1117 several SG proteins (yellow ellipse).
1118 **Figure 1—figure supplement 1.** Re-localization of TRAPP to SGs is independent of
1119 stress stimulus and cell type.
1120 **Figure 1—figure supplement 2.** Stress-induced localization of Bet3 (TRAPPC3) to SGs
1121 in yeast cells.
1122 **Figure 1—supplement video 1.** Time lapse fluorescent microscopy of Bet3
1123 (TRAPPC3) and Pab1 at 30°C in yeast cells.
1124 **Figure 1—supplement video 2.** Time lapse fluorescent microscopy of Bet3
1125 (TRAPPC3) and Pab1 at 46°C in yeast cells.
1126 **Figure 1—figure supplement 3.** Association of TRAPP with SGs is reversible after SG
1127 disassembly.
1128

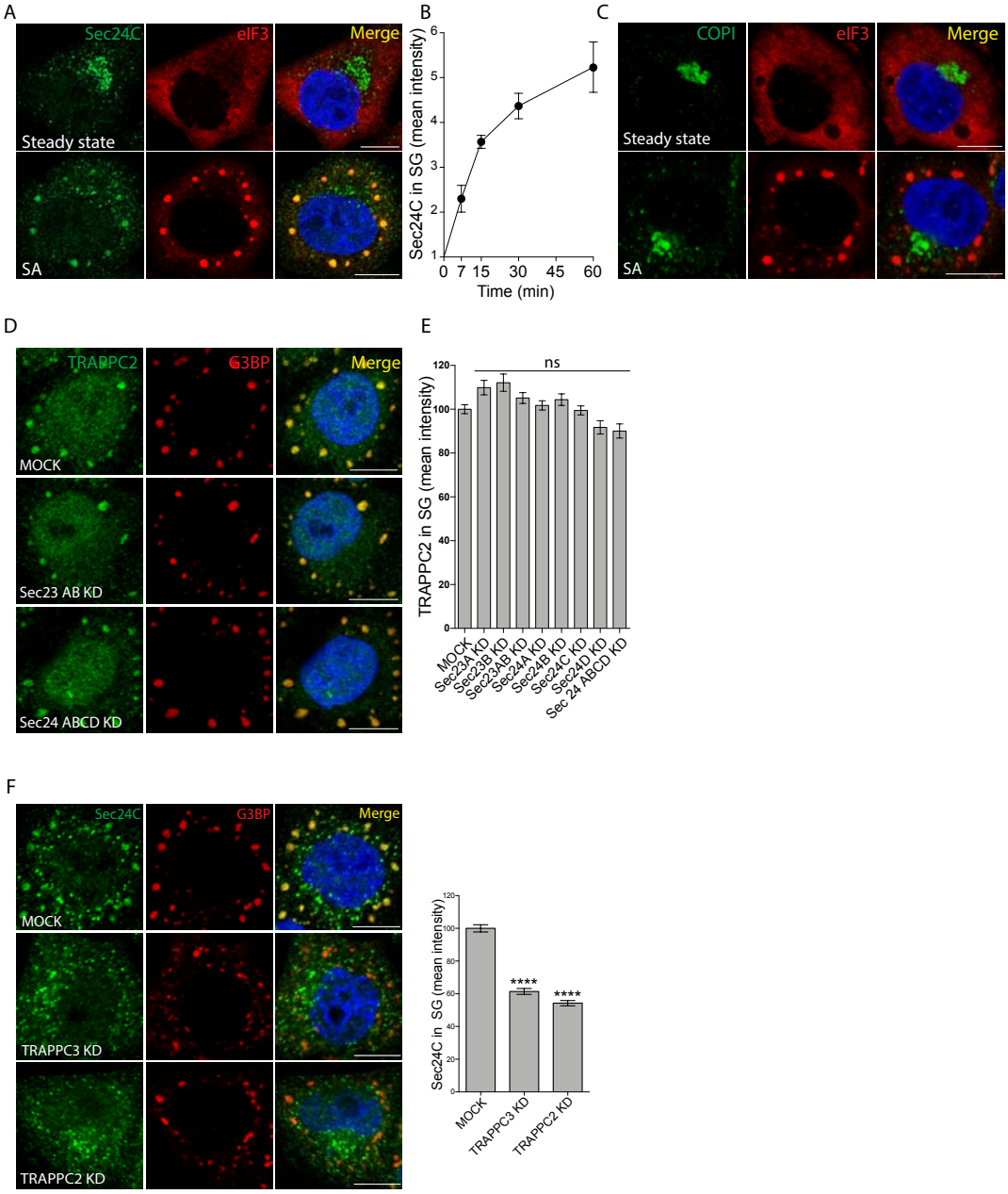

Figure 2. TRAPPC2 is required for Sec23/24 relocalization to SGs. (A) HeLa cells, untreated or treated with SA, were fixed and visualized by fluorescence microscopy using anti-Sec24C Ab, anti-eIF3 Ab, and DAPI (blue). **(B)** Quantification of Sec24C redistribution to SGs over time after SA treatment (the ratio between Sec24C (mean fluorescence intensity) in SG puncta and cytosolic Sec24C). Mean ± s.e.m. n = 50 cells per experiment, N = 3. **(C)** Cells treated as in **(A)** stained with an antibody recognizing the coatomer I (COPI), which does not relocalize to SGs (see also Figure 2—figure supplement 1A-N). **(D)** Representative images of TRAPPC2 localization in Sec23AB-KD and Sec24ABCD-KD cells treated with SA. Cells were fixed and visualized by fluorescence microscopy using anti-TRAPPC2 Ab, anti-G3BP Ab (to label SGs) and DAPI (blue). **(E)** Quantification of TRAPPC2 redistribution to SGs after KD of the indicated Sec23 and Sec24 combinations, calculated as the ratio between TRAPPC2 (mean intensity) in SG puncta and cytosolic TRAPPC2. Mean ± s.e.m., n = 40-60 cells per experiment, N = 3. ns: not significant. **(F)** Representative images of Sec24C

1144 localization at SGs (stained for G3BP) in TRAPPC3-KD and TRAPPC2-KD cells treated
1145 with SA. Depletion of TRAPP or TRAPPC2 reduces Sec24C recruitment. Graph,
1146 quantification of Sec24C at SGs, calculated as in (A). Mean ± s.e.m., n = 40-60 cells
1147 per experiment, N = 3. **** P < 0.0001.
1148 **Figure 2—figure supplement 1.** Sec24C and Sec23, but not components of other
1149 coat complexes or other cytosolic proteins associated with the exocytic and
1150 endocytic pathways, associate with SGs.
1151 **Figure 2—figure supplement 2.** Sec16 does not significantly associate with SGs nor is
1152 it required for the recruitment of COPII to SGs.
1153 **Figure 2—figure supplement 3.** Evaluation of Sec23, Sec24, TRAPPC2 and TRAPPC3
1154 knock down efficiency.

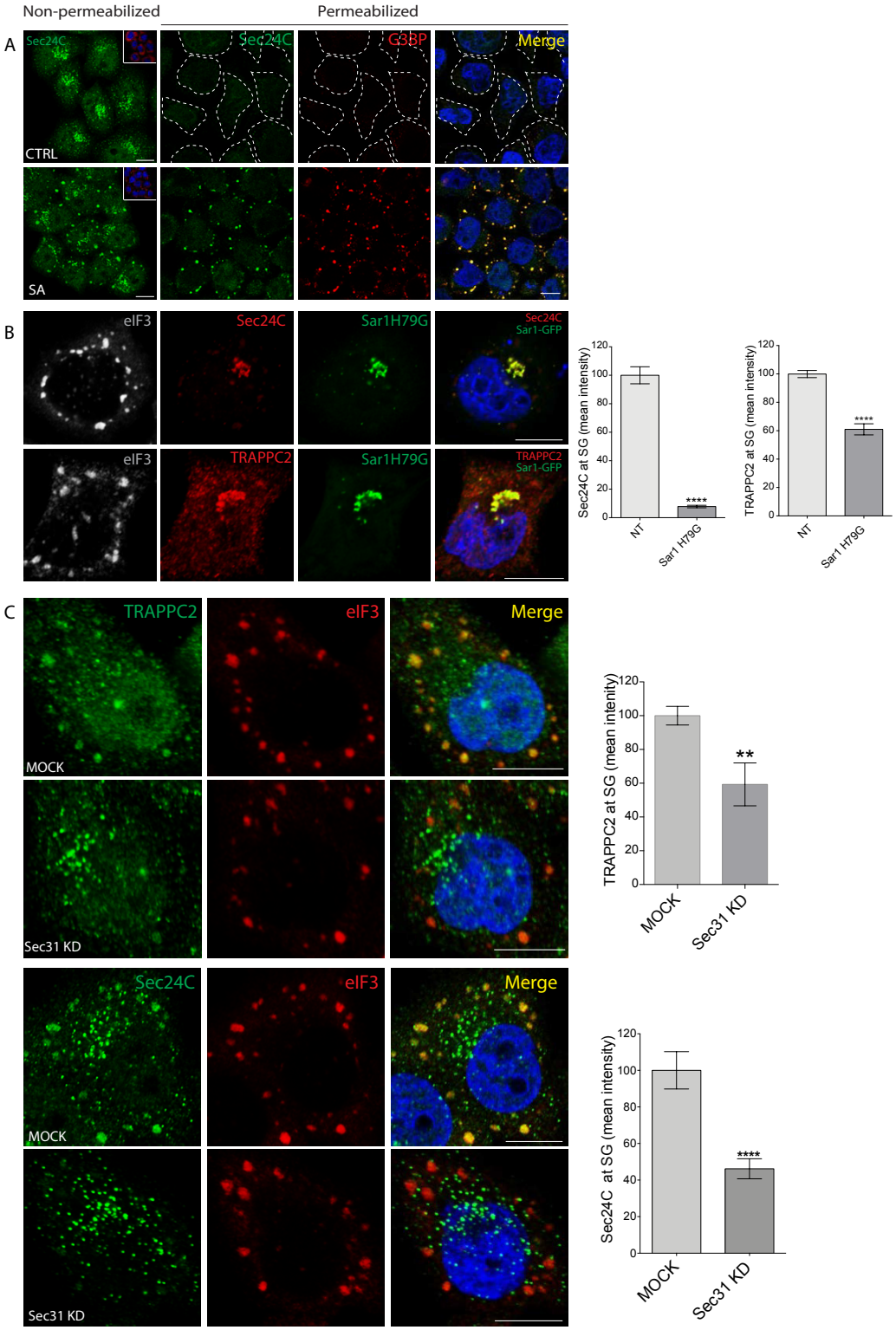

Figure 3. Comparison and relationships between the ERES-associated and the SG-associated pools of TRAPP and COPII. (A) TRAPP and COPII associate more stably with SGs than with ERES. The membrane association of Sec24C was evaluated in non-permeabilized or permeabilized cells with or without SA treatment, as indicated. G3BP was used as an SG marker. Left panel insets, G3BP staining in non-permeabilized cells. Dashed white lines show the outline of permeabilized SA-untreated cells. Blue, DAPI. **(B-C)** Stabilizing TRAPP and COPII at the ERES prevents

1163 their relocalization to SGs. **(B)** HeLa cells overexpressing GFP-Sar1H79G were treated
1164 with SA and immunostained for Sec24C, TRAPPC2, and eIF3, as indicated. Blue, DAPI.
1165 Scale bar 10 µm. Graphs show quantification of Sec24C or TRAPPC2 at SGs in GFP-
1166 Sar1H79G-expressing cells relative to non-transfected cells. Data are the ratio
1167 between Sec24C or TRAPPC2 mean intensity in SG puncta and Sec24C or TRAPPC2
1168 mean intensity at ERES, expressed as a percentage of the non-transfected cells.
1169 Mean ± s.e.m. n = 60-70, three independent experiments ****p<0.0001. **(C)** Effect of
1170 Sec31A depletion on TRAPPC2 and Sec24C recruitment to SGs. Cells were mock-
1171 treated or KD for Sec31, treated with SA (300 µM, 30 min), and then immunostained
1172 for TRAPPC2, Sec24C and eIF3 as indicated. Scale bar, 10 µm. Graph, quantification
1173 of Sec24C and TRAPPC2 at SGs, calculated as in (B). Mean ± s.e.m. of TRAPPC2 and
1174 Sec24C, one representative experiment; n=60-80. ** p<0.001, ****p<0.0001.
1175 **Figure 3—figure supplement 1.** Effect of Sec31 depletion on Sec24C localization at
1176 ERES.

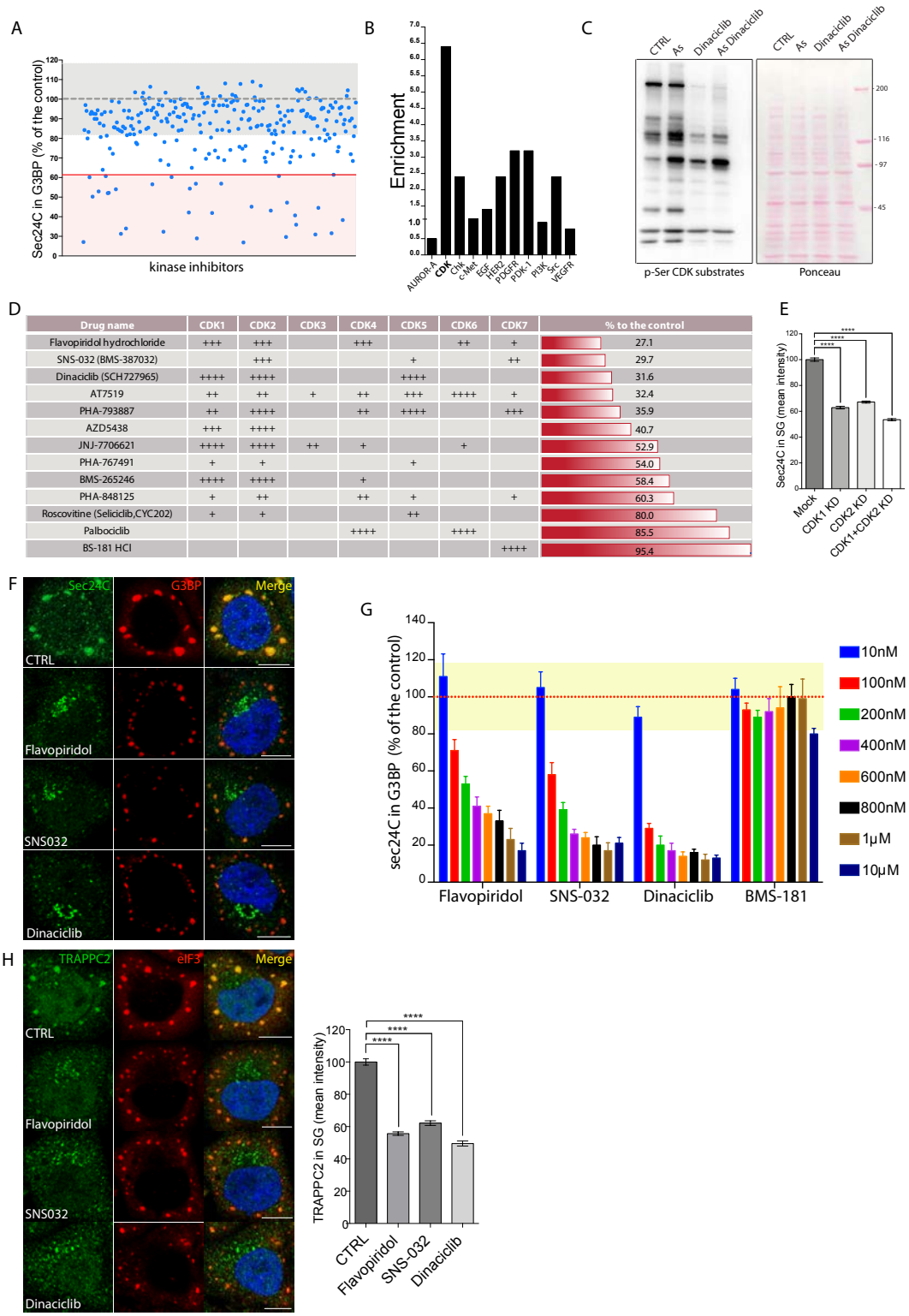

Drug name	CDK1	CDK2	CDK3	CDK4	CDK5	CDK6	CDK7	% to the control
Flavopiridol hydrochloride	+++	+++		+++		++	+	27.1
SNS-032 (BMS-387032)		+++			+		++	29.7
Dinaciclib (SCH727965)	++++	++++			++++			31.6
AT7519	++	++	+	++	+++	++++	+	32.4
PHA-793887	++	++++		++	++++		+++	35.9
AZD5438	+++	++++						40.7
JNJ-7706621	++++	++++	++	+		+		52.9
PHA-767491	+	+			+			54.0
BMS-265246	++++	++++		+				58.4
PHA-848125	+	++		++	+		+	60.3
Roscovitine (Seliciclib,CYC202)	+	+			++			80.0
Palbociclib				++++		++++		85.5
BS-181 HCl							++++	95.4

Figure 4. The association of TRAPP with SGs is under control of CDK1/2. (A) Cells were treated with 273 kinase inhibitors (10 µM) from the Sellekchem library and with SA, and Sec24C localization in G3BP puncta (% of total G3BP area) was calculated (see Materials and methods) and is reported as a percentage of the control (cells treated with SA alone). Gray dashed line, mean of control; gray box, control standard deviation (± 18.2%); dashed red line, threshold of positive hits. **(B)** Enrichment Analysis of the positive hits; for each class of inhibitor, the enrichment

1185 (in percentage) of compounds falling into positive hits and the enrichment (in
1186 percentage) in the total number of compounds was calculated and expressed as a
1187 ratio. **(C)** Evaluation of CDK kinase activity upon SA treatment. Western blot analysis
1188 of phosphoSer-CDK substrates in control, SA (300µM, 30 min), Dinaciclib (10 µM, 180
1189 min) and SA+Dinaciclib (150 min Dinaciclib and 30 minutes SA). CDKs are
1190 hyperactivated upon oxidative stress and this activation is partially prevented upon
1191 CDK inhibition. Left, Western blot, right: Ponceau was used as loading control. Image,
1192 one representative experiments out of 3 independent replicates. **(D)** Drug specificity,
1193 from high (++++) to low (+). for the different CDKs as described by Selleckchem, and
1194 Sec24C recruitment to SGs as a percentage of control. **(E)** Analysis of Sec24C
1195 recruitment to SGs in control (MOCK), CDK1-KD, CDK2-KD and CDK1+2-KD HeLa cells.
1196 Data are expressed as percentage of Sec24C (mean intensity) in SG puncta
1197 normalized for cytosolic signal as a percentage of control conditions. Quantification
1198 of one representative experiment. N>100, mean ± s.e.m. ****p<0.0001. **(F)**
1199 Representative images of HeLa cells treated with the best three hits (Flavopiridol,
1200 SNS-032, Dinaciclib; 1µM 150 min) and then exposed to SA (300 µM, 30 min),
1201 followed by immunostaining for Sec24C and G3BP. Scale bar, 10µm. **(G)** HeLa cells
1202 were treated with Flavopiridol, SNS-032, or Dinaciclib for 150 min at the indicated
1203 concentrations, subsequently treated with SA (300 µM, 30 min), and then
1204 immunostained for Sec24C and G3BP and imaged by OPERA. BS-181, a specific CDK7
1205 inhibitor, was used as negative control. Sec24C localization to SGs is expressed as a
1206 percentage of the control (cells treated with SA alone). Dashed red line, mean of
1207 control; red box, standard deviation of control (± 9.8%). **(H)** Cells were treated as in
1208 (G) and immunostained for TRAPPC2 and eIF3. Scale bar, 10 µm. The graph shows
1209 the quantification of TRAPPC2 localization in SG puncta (mean intensity). Data are
1210 mean ± s.e.m. expressed as a percentage of TRAPPC2 signal in SGs after Flavopiridol,
1211 SNS-032 or Dinaciclib treatment compared to the control (cells treated with SA
1212 alone). N=3, three independent experiments, n=60-80 cells per experiment.
1213 ****p<0.0001.
1214 **Figure 4—figure supplement 1.** Evaluation of CDK1 and CDK2 knock down efficiency.
1215

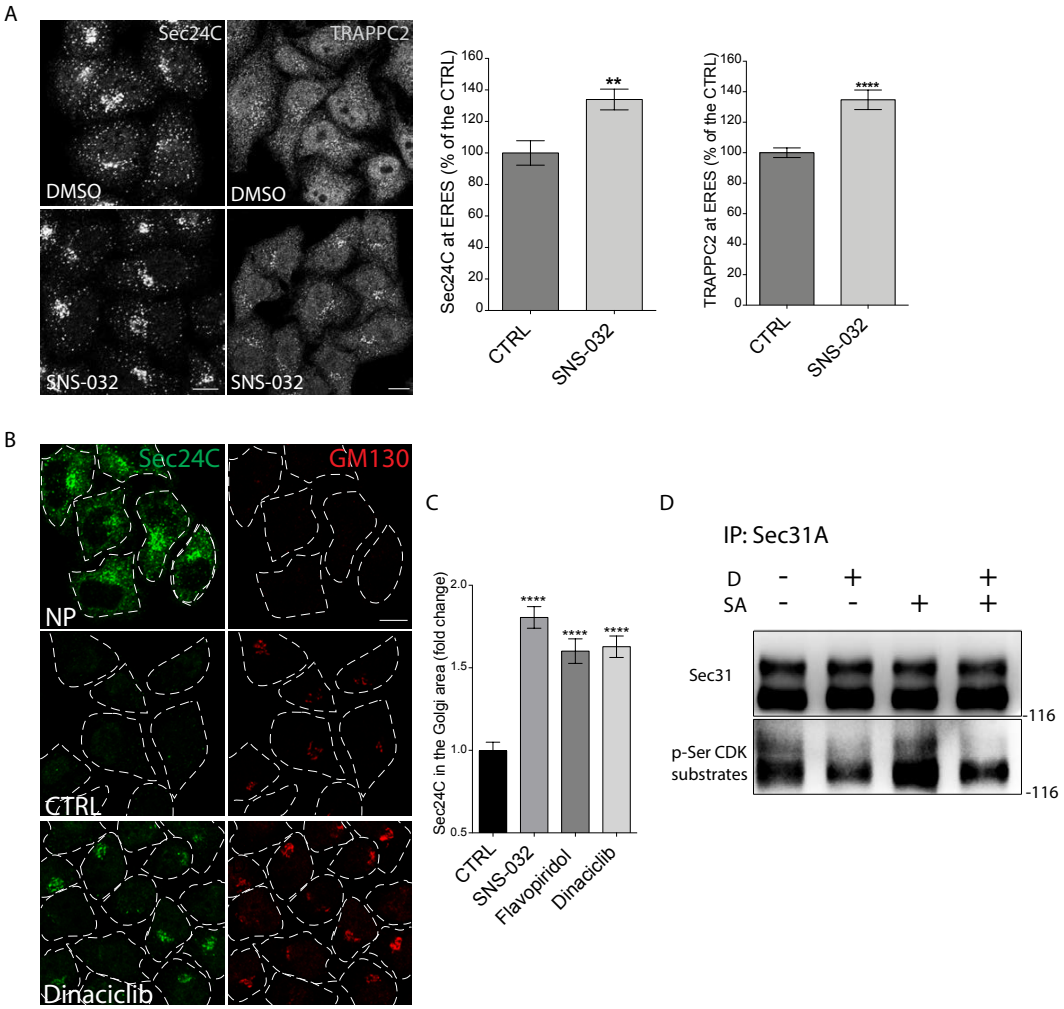

Figure 5. CDK1/2 modulate the COPII cycle at ERES. (A) Immunofluorescence images of Sec24C and TRAPPC2 in vehicle-treated and SNS-032-treated (1 µM, 3 h) cells. Scale bar, 10 µm. Graphs show the quantification of Sec24C and TRAPPC2 in the peri-Golgi area (mean intensity) normalized in SNS-032-treated cells relative to vehicle-treated cells (set as 100%). Mean ± s.e.m. of three independent experiments. **p<0.05****, p<0.0001. **(B)** HeLa cells were treated with Dinaciclib (1 µM, 3 h) and permeabilized or not with digitonin as described in Materials and methods. A GM130 antibody was added to the buffer of living cells to monitor permeabilization efficiency. Upper panels, non-permeabilized (NP) control cells; middle panels, permeabilized control cells; lower panels, permeabilized Dinaciclib-treated cells. Scale bar, 10 µm. **(C)** Quantification of Sec24C membrane association after CDK inhibitor treatment. Digitonin-permeabilized cells treated with vehicle (CTRL) or the indicated CDK inhibitor (1 µM, 3 h) were immunostained for Sec24C. The mean intensity of Sec24C in the perinuclear area normalized for the cytosolic Sec24C signal in drug-treated cells is expressed as fold change compared to the control; n= 60-80; mean ± s.e.m. of three independent experiments ****p<0.0001. **(D)** Cell lysates from HeLa cells treated with SA (300 µM, 10 min), Dinaciclib (10 µM, 180 min), or their combination were immunoprecipitated using a Sec31 Ab. Western blots of the immunoprecipitates probed using the phosphor-Ser-CDK Ab (upper panel) or the anti-Sec31 Ab (lower panel). Note that the anti-Sec31 Ab immunoprecipitates both Sec31 isoforms

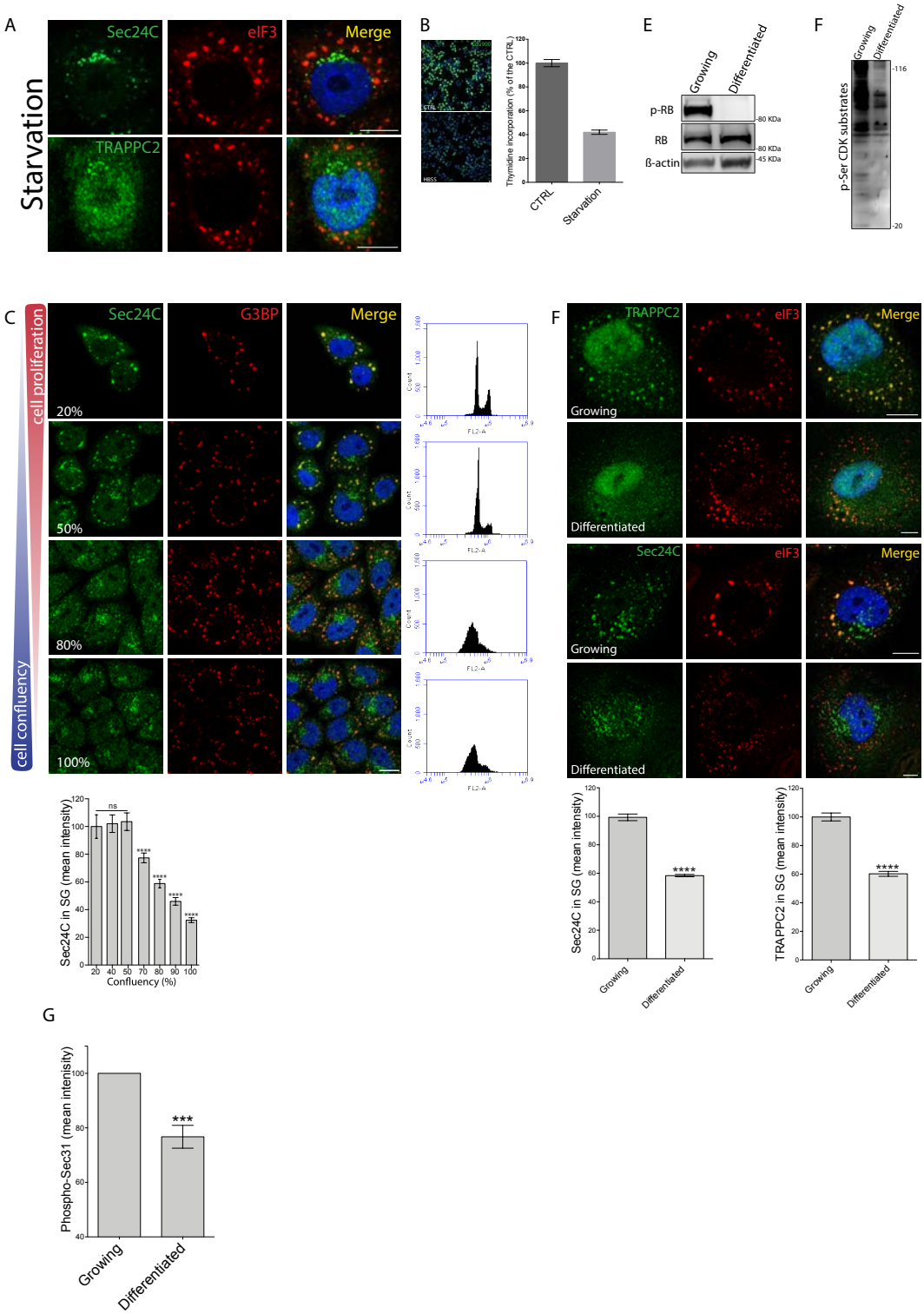

Figure 6. TRAPP and Sec23/24 migration to SGs depends on the proliferation state of cells. (A) HeLa cells were starved for 8 h with HBSS and subsequently exposed to SA (30 min, 300 µM), and immunostained for Sec24C or TRAPPC2 and eIF3. Scale bar 10 µm. **(B)** Analysis of the proliferation status of the cells after 8 h starvation in HBSS. Left, representative images of starved and non-starved cells using EdU incorporation (see Materials and methods) and, right, quantification of EdU incorporation in starved cells as a percentage of incorporation in control fed cells. **(C)** HeLa cells were

1246 seeded at different confluency, treated with SA and stained for Sec24C and G3BP as
1247 an SG marker. Scale bar, 10 µm. Flow cytometry (FACS) analysis (right panels) was
1248 performed to evaluate the distribution of cell cycle phases in HeLa cell populations
1249 seeded at different confluency. The graph shows quantification of Sec24C mean
1250 intensity in SG puncta normalized for the cytosolic Sec24C at the indicated cell
1251 confluency. Mean ± s.e.m. of a representative experiment out of n=5 biological
1252 replicates. n= 50-80. ns, not significant; ****p<0.0001. **(D)** Growing and
1253 differentiated podocytes were treated with SA (300 µM, 30 min) and stained for
1254 TRAPPC2 or Sec24C and eIF3. Scale bar, 10µm. The graphs show quantification of
1255 TRAPPC2 and Sec24C (mean intensity) in SGs. Mean ± s.e.m. of three independents
1256 experiments ****p<0.0001. **(E)** CDK kinase activity in growing and differentiated
1257 podocytes. Western blot using a specific antibody recognizing phosphoSer-CDK
1258 substrates was used on total cell lysates. **(F)** Western blot analysis of phosphorylated
1259 retinoblastoma (p-RB) in growing (non-differentiated) versus differentiated
1260 podocytes. ß-actin was used as loading control. **(G)** Quantification of
1261 immunoprecipitated Sec31 from growing and differentiated podocytes using the
1262 phosphor-Ser-CDK Ab. Mean ± s.e.m. of three independents experiments.
1263 ***p<0.0007.
1264
1265
1266 **Figure 6—figure supplement 1.** Differentiation of podocytes.
1267

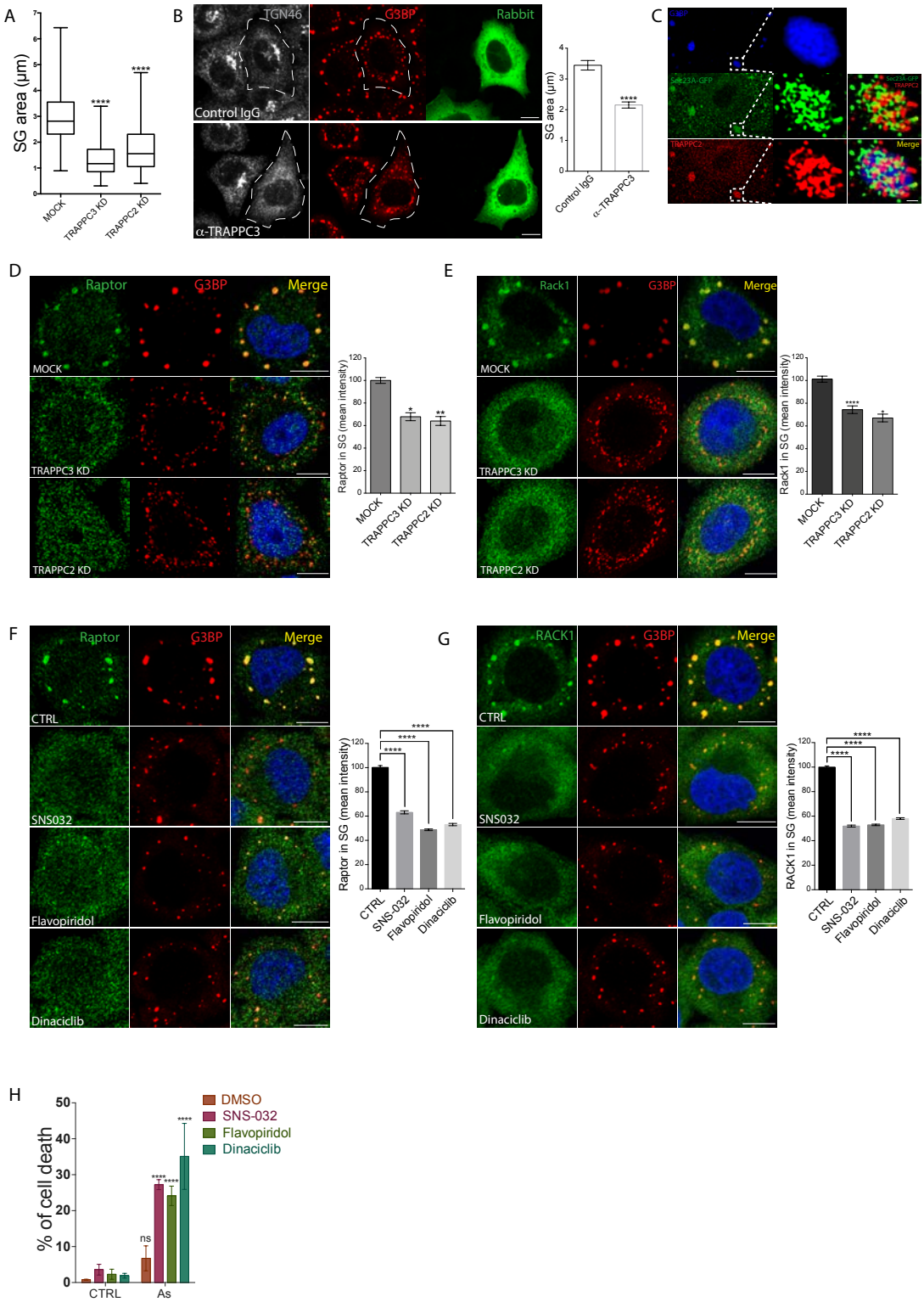

Figure 7. The TRAPP complex controls SG composition and function. (A) Box plot representing SG area (see Materials and methods) in mock, TRAPPC2- and TRAPPC3-depleted cells treated with SA. Distribution of values from three independent experiments. ****p<0.0001. **(B)** HeLa cells microinjected with control preimmune IgG or a TRAPPC3-specific antibody (right panels in green) were treated with SA. The TRAPPC3 Ab disrupts the Golgi (Yu et al., 2006), monitored using an anti-TGN46 Ab. Anti-G3BP was used to stain SGs. The graph shows quantification of the SG area.

1276 Mean ± s.e.m. three independent experiments; n>80. ****p<0.0001. **(C)** Structured
1277 Illumination Microscopy (SIM)-Super resolution (SR) images of endogenous TRAPPC2
1278 and GFP-Sec23 localizing at SGs, stained for G3BP. Right, magnification of boxed area.
1279 **(D,E)** Localization of Raptor **(D)** and RACK1 **(E)** in mock, TRAPPC3-KD and TRAPPC2-
1280 KD HeLa cells treated with SA. G3BP was used to stain SGs. Scale bar, 10 µm. Each
1281 graph shows the quantification (mean intensity) of the respective protein in SG spots
1282 expressed as a percentage of the mock. Mean ± S.D. three independent replicates.
1283 *p<0.02; **p<0.009 in **(D),** *p<0.05; ****p<0.0001 in **(E). (F,G)** Localization of Raptor
1284 **(F)** and RACK1 **(G)** in untreated cells or cells pre-treated with the indicated CDK
1285 inhibitor (1 µM, 150 min) and then with SA (300 µM, 30 min). G3BP was used to stain
1286 SGs. Scale bar, 10 µm. Graphs show quantification of the localization of the
1287 respective protein with SGs, expressed as a percentage of the control. Mean ± s.e.m.
1288 of one representative experiment out of three independent replicates, n=60-80.
1289 ****p<0.0001. **(H)** Analysis of cell death after overnight recovery of HeLa cells
1290 treated or untreated with CDKi (SNS-032; Flavopiridol or Dinaciclib, 1 µM, 150 min)
1291 and then treated with SA (500 µM, 3 h). Images were automatically acquired by
1292 OPERETTA microscopy. Values indicate the percentage of the total number of nuclei
1293 (stained with DAPI) positive for BoBo-3 staining. Mean ± s.d. of one representative
1294 experiment out of three independent replicates. ns, not significant, ****p<0.0001.

1295 **Figure 7—figure supplement 1.** TRAPP depletion does not affect protein translation
1296 inhibition caused by SA treatment.
1297
1298
1299
1300
1301
1302
1303
1304
1305
1306
1307
1308
1309
1310
1311
1312

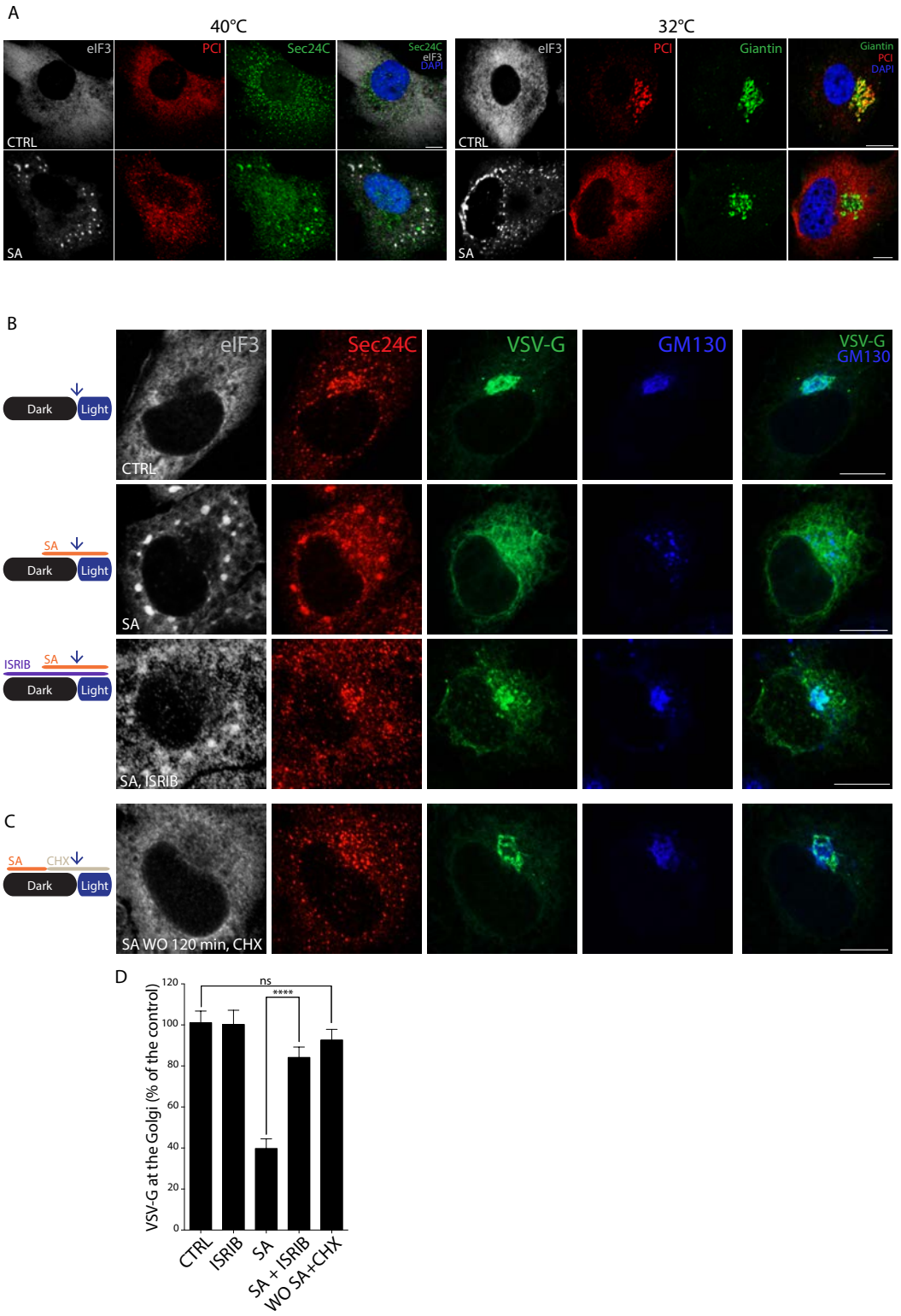

Figure 8. The recruitment of TRAPP and COPII to SGs slows down ER export (A) Left, control or SA-treated (500µM, 120 min) human fibroblasts (HFs) were incubated at 40°C for 180 min and stained for eIF3, PCI, and Sec24C. Right, the cells were imaged 10 min after shifting the temperature from 40°C to 32°C and stained for eIF3, PCI, and Giantin (to label the Golgi). Scale bar, 10 µm. **(B)** HeLa cells expressing VSV-G-UVR8 mEOS were left untreated or treated with SA alone or in combination with ISRIB (1 µM) for the indicated times and then pulsed with blue light. Images were

1321 taken 10 minutes after the UV pulse and processed for staining. **(C)** Cells were
1322 treated with SA for 30 min, the SA was washed out, and cells were left to recover for
1323 180 min in the presence of cycloheximide, followed by a blue light pulse and
1324 processing for staining as described in (B). **(D)** Quantification of VSV-G (mean
1325 intensity) in the Golgi area to the total VSV-G per cell under the conditions described
1326 in (B,C)**.** Data are expressed as percentage of the control. Mean ± s.e.m. of three
1327 independent experiment. ****p<0.0001; ns, not significant.

1328 **Figure 8—figure supplement 1.** ISRIB delays SG nucleation and inhibits Sec24C
1329 relocalization to SGs.

1330

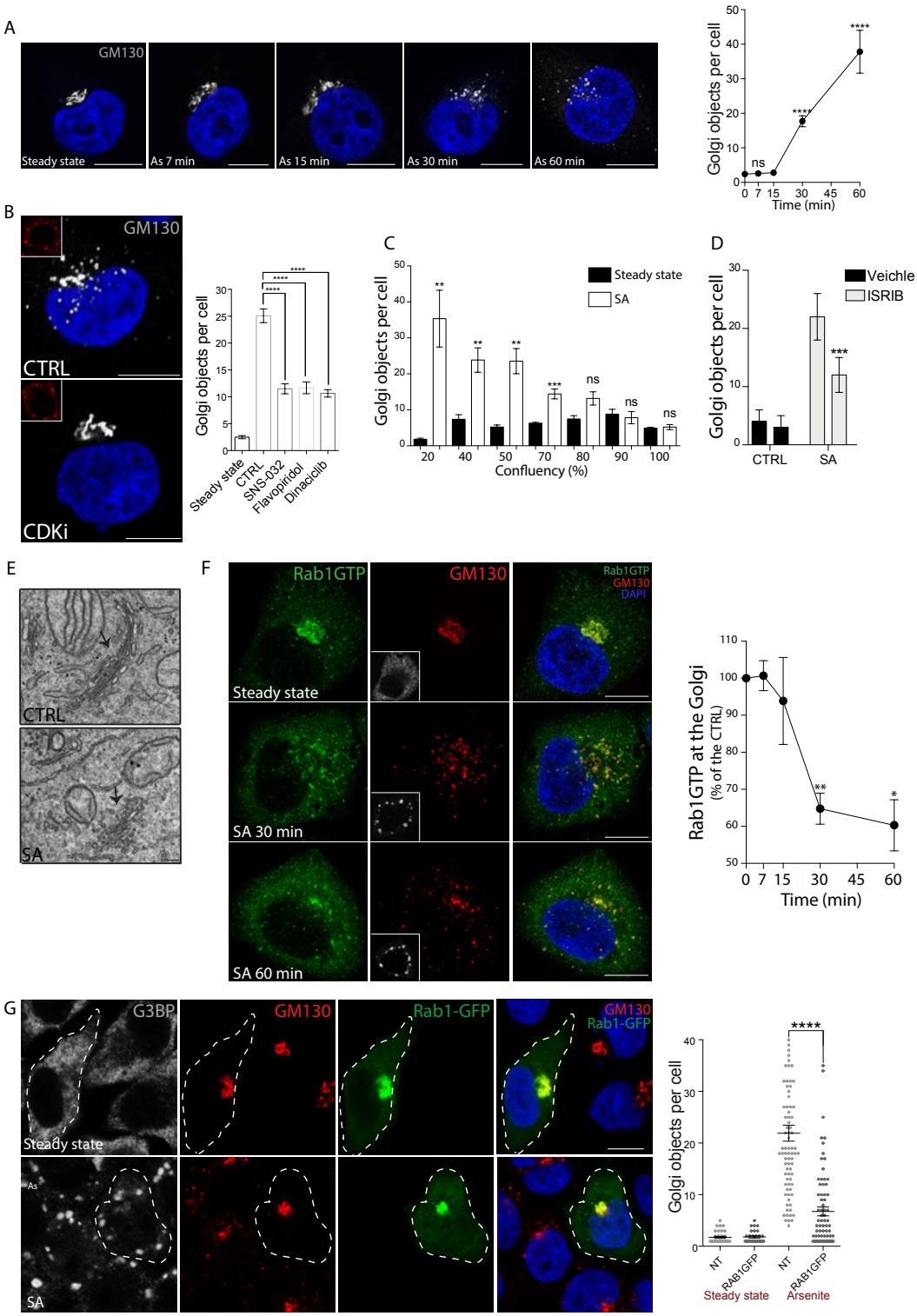

Figure 9. The recruitment of TRAPP induces the fragmentation of the GC in a Rab1-dependent manner. (A) AiryScan images of HeLa cells treated with SA for the indicated times and stained with GM130 (gray). Scale bar, 10 µm. The graph shows quantification of Golgi particles in SA-treated cells. Mean ± s.e.m. of three independent experiments. n=90-100. ****p<0.0001; ns, not significant. **(B)** Control cells and cells treated with Dinaciclib (CDKi) were treated with SA and stained for GM130 (in gray). Insets, eIF3. Blue, nuclear DAPI staining. The graph shows

1339 quantification of Golgi particles in HeLa cells untreated or treated with SNS-032,
1340 Flavopiridol, or Dinaciclib for 150 min and treated with SA (300 µM, 30 min). Mean ±
1341 s.e.m. of three independent experiment. ****p<0.0001. **(C)** Quantification of Golgi
1342 particles in cells plated at different percentage of confluency. Mean ± s.e.m. of three
1343 independent experiment. ** p<0.001; *** p<0.0002; ns: not significant. **(D)**
1344 Quantification of Golgi objects in cells pre-treated with ISRIB (1 µM) for 3 h and
1345 exposed to SA (30 min) in the presence of ISRIB. *** p<0.002. **(E)** Electron
1346 microscopy images of a cell exposed to SA (300 µM, 30 min). GC: Golgi complex.
1347 Scale bar 200 nm. **(F)** AiryScan images of HeLa cells at steady state or exposed to SA
1348 for the indicated times. A Rab1-GTP specific antibody was used to monitor Rab1-GTP
1349 activity and GM130 to stain the Golgi complex. Insets, eIF3. The graph shows
1350 quantification of Rab1-GTP at the Golgi complex expressed as a percentage of the
1351 control. Mean ± s.e.m. of three independent experiments. *p<0.011, **p<0.002. **(G)**
1352 HeLa cells transfected or not with WT GFP-Rab1B were left untreated or treated with
1353 SA and stained for GM130 and G3BP to monitor SGs. Dashed white line, WT GFP-
1354 Rab1B transfected cells. The graph shows quantification of Golgi particles in the
1355 different conditions. NT: non-transfected. Mean ± s.e.m. of three independent
1356 experiment. ****p<0.0001; n=30-50.
1357
1358 **Figure 9—figure supplement 1.** TRAPPC2 migrates to SGs in Rab1 overexpressing
1359 cells.

1360

1361

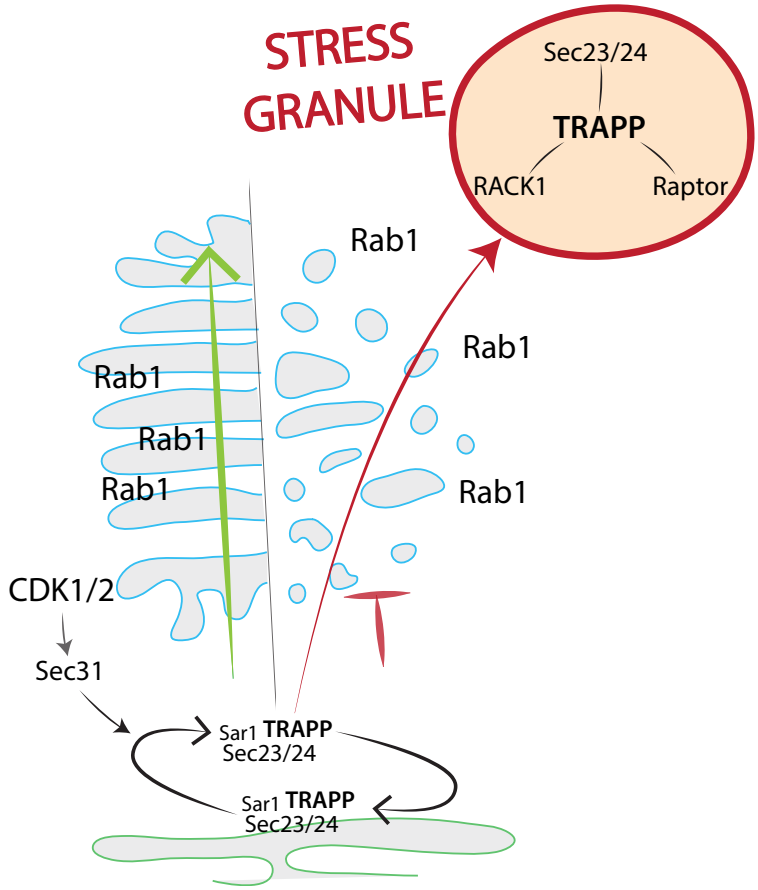

1362

1363 **Figure 10. Proposed model for secretion arrest mediated by TRAPP upon SG**
1364 **assembly in actively proliferating cells.** Upon stress, the TRAPP complex relocalizes
1365 to SGs and drives the sequestering of Sec23/24, RACK1 and Raptor to SGs. This
1366 phenomenon leads to a block in ER-export and contributes to SG maturation.

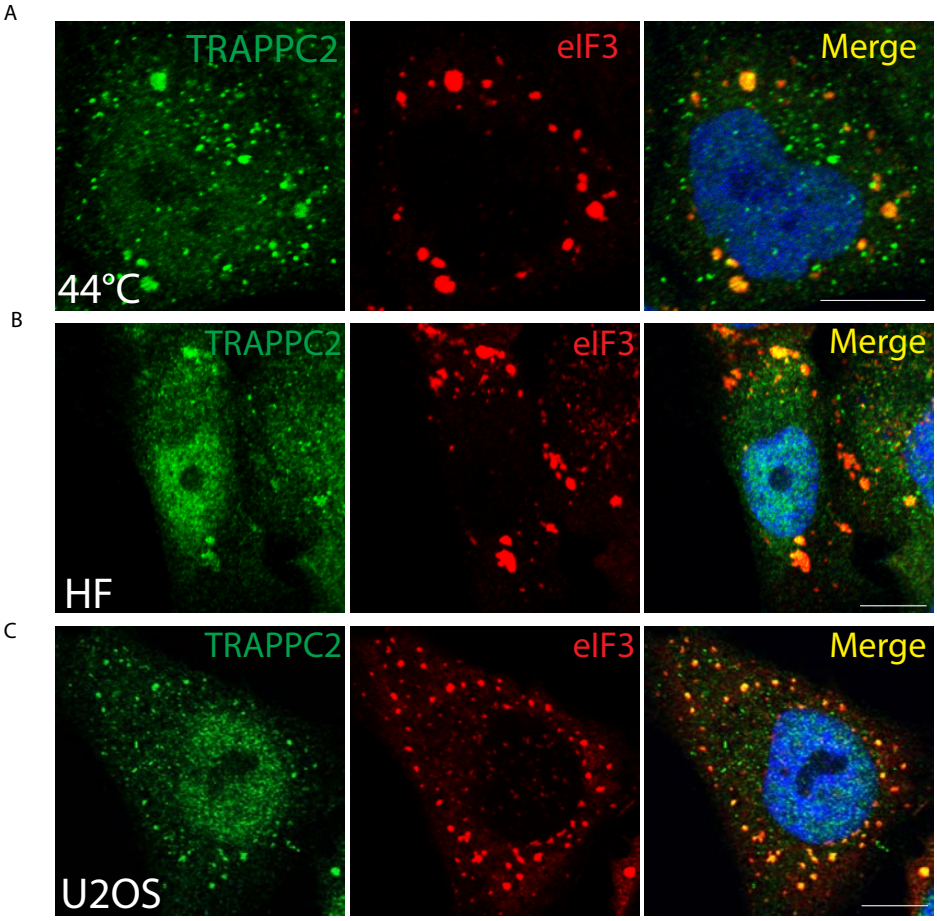

Figure 1—figure supplement 1. Re-localization of TRAPP to SGs is independent of stress stimulus and cell type. (**A**) HeLa cells exposed to heat shock (44°C, 45 min), **(B)** human fibroblasts treated with SA (500 µM, 180 min), **(C)** U2OS cells treated with SA (300 µM, 60 min), stained for eIF3 and TRAPPC2.

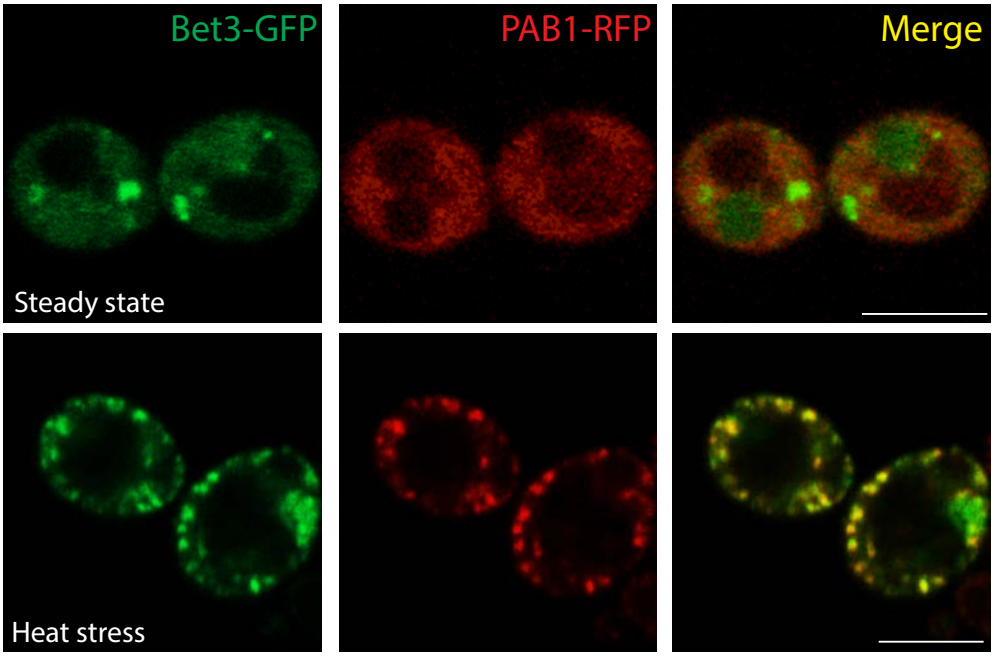

Figure 1—figure supplement 2. Stress-induced localization of Bet3 (TRAPPC3) to SGs in yeast cells. Cells co-expressing Bet3-GFP and the stress granule marker RFP-PAB1 were exposed to heat shock (46°C, 10 min) and imaged.

Figure 1—supplement video 1. Time-lapse fluorescent microscopy of Bet3-GFP (TRAPPC3) and RFP-Pab1 at 30°C in yeast cells. Images were taken every 8 sec for 64 sec.

Figure 1—supplement video 2. Time-lapse fluorescent microscopy of Bet3-GFP (TRAPPC3) and RFP-Pab1 at 46°C in yeast cells. Images were taken every 8 sec for 64 sec.

1383

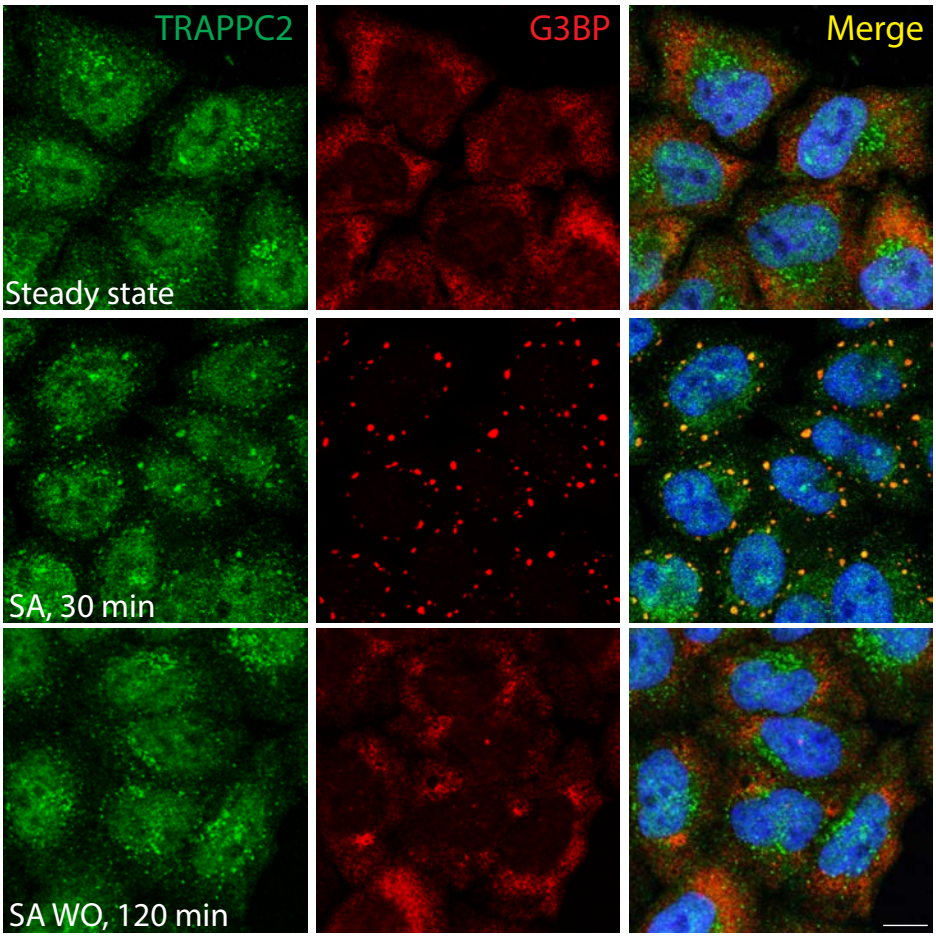

1384
1385 **Figure 1—figure supplement 3.** Association of TRAPP with SGs is reversible after SG
1386 disassembly. Cells were treated with SA for 30 min, the SA was washed out, and cells
1387 were left to recover for 120 min and processing for staining. Scale bar 10 µm.
1388

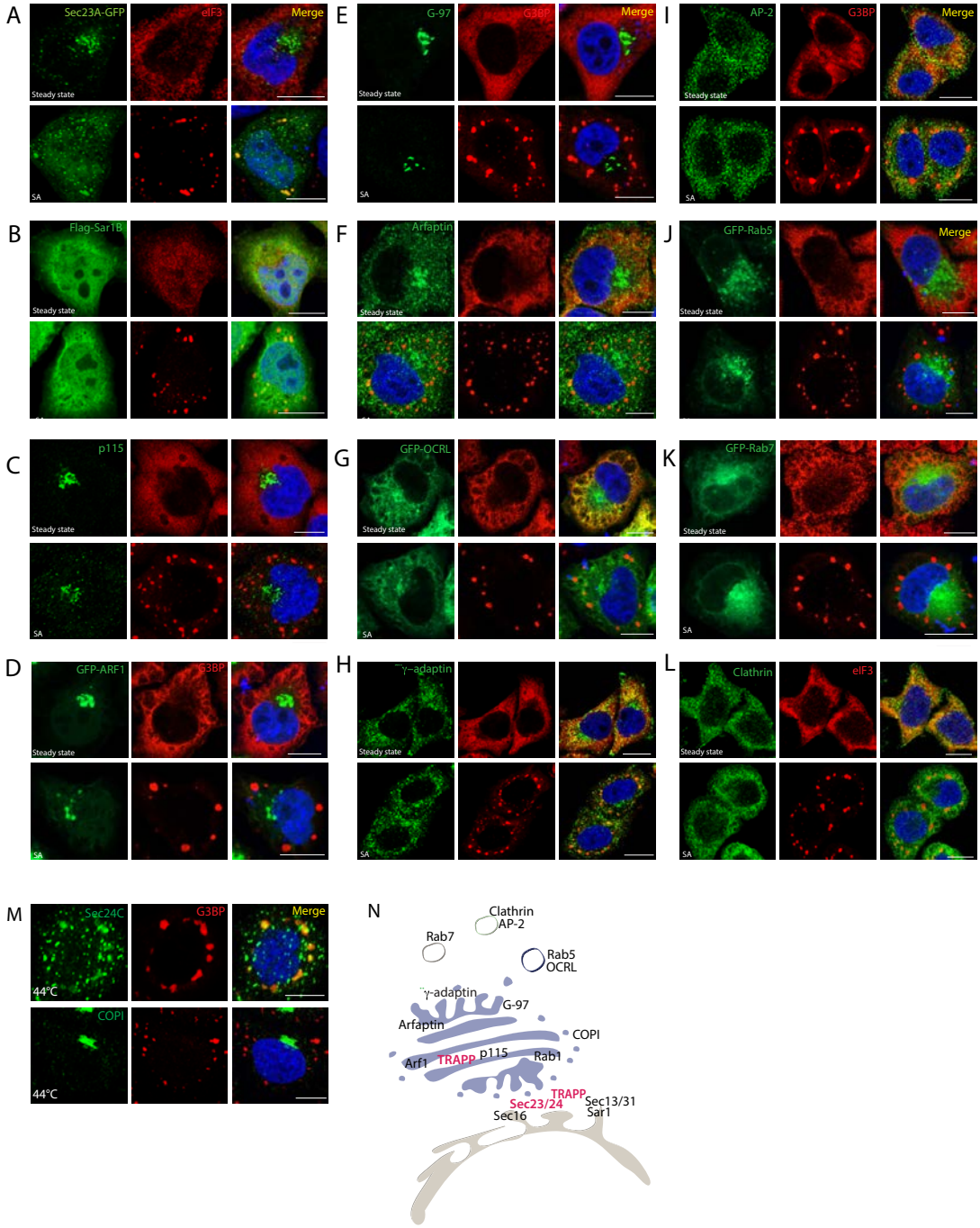

Figure 2—figure supplement 1. Sec24C and Sec23, but not components of other coat complexes or other cytosolic proteins associated with the exocytic and endocytic pathways, associate with SGs. (**A-L**) Cells at steady state or treated with SA were visualized by fluorescence microscopy using antibodies against the endogenous proteins or Flag-tagged proteins, or visualizing transfected GFP-tagged proteins, and co-stained for eIF3 or G3BP, as indicated. (**M**) Cells exposed to heat shock (44°C, 45 min) were stained for Sec24C or COPI, and G3BP. Blue, DAPI. (**N**) Schematic diagram showing the cellular location of the tested proteins that associate (red) or not (black) with SGs.

1401

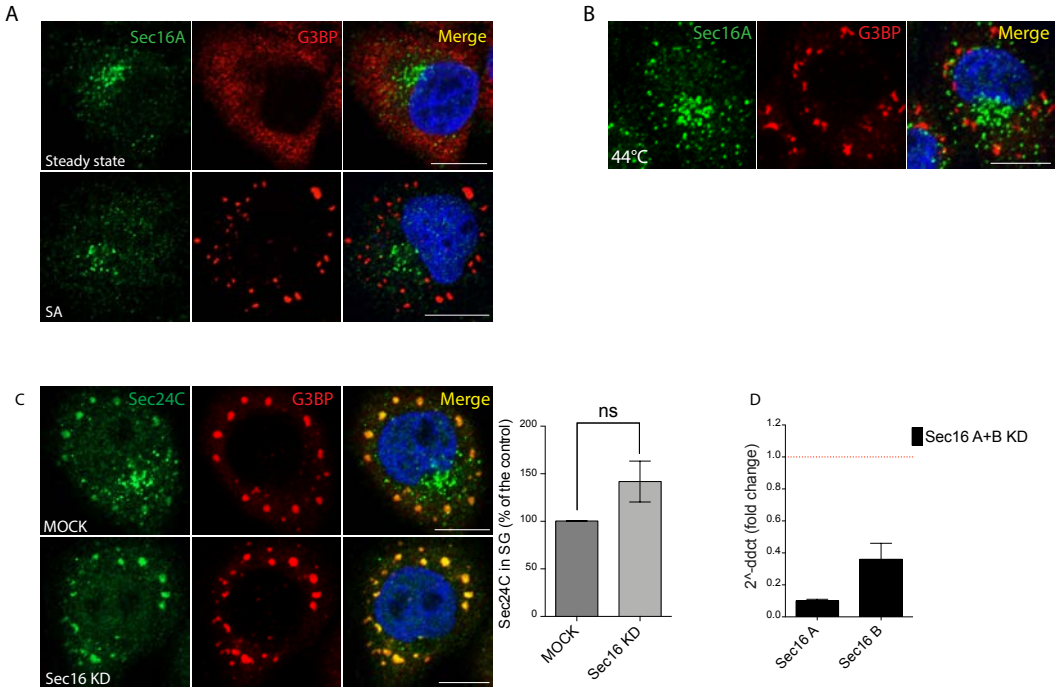

1402
1403 **Figure 2—figure supplement 2.** Sec16 does not significantly associate with SGs nor is
1404 it required for the recruitment of COPII to SGs. **(A)** Cells were treated with SA (300
1405 µM) and co-stained for endogenous Sec16 and G3BP as an SG marker. **(B)** Cells
1406 exposed to heat shock were processed as described in (A). **(C)** Representative images
1407 of Sec24C localization in Sec16-KD cells treated with SA. Cells were fixed and
1408 visualized by fluorescence microscopy using anti-Sec24C Ab, anti-G3BP Ab, and DAPI
1409 (blue). Quantification of TRAPPC2 redistribution to SGs after KD calculated as the
1410 ratio between Sec24C (mean intensity) in SG puncta and cytosolic Sec24C. Mean ±
1411 s.e.m., n = 40-60 cells per experiment, N = 3. ns: not significant. **(D)** Sec16A and B
1412 mRNA levels in Sec16A+B KD cells were evaluated by q-PCR and expressed as fold
1413 change with respect to the MOCK. Dashed red line: MOCK.
1414

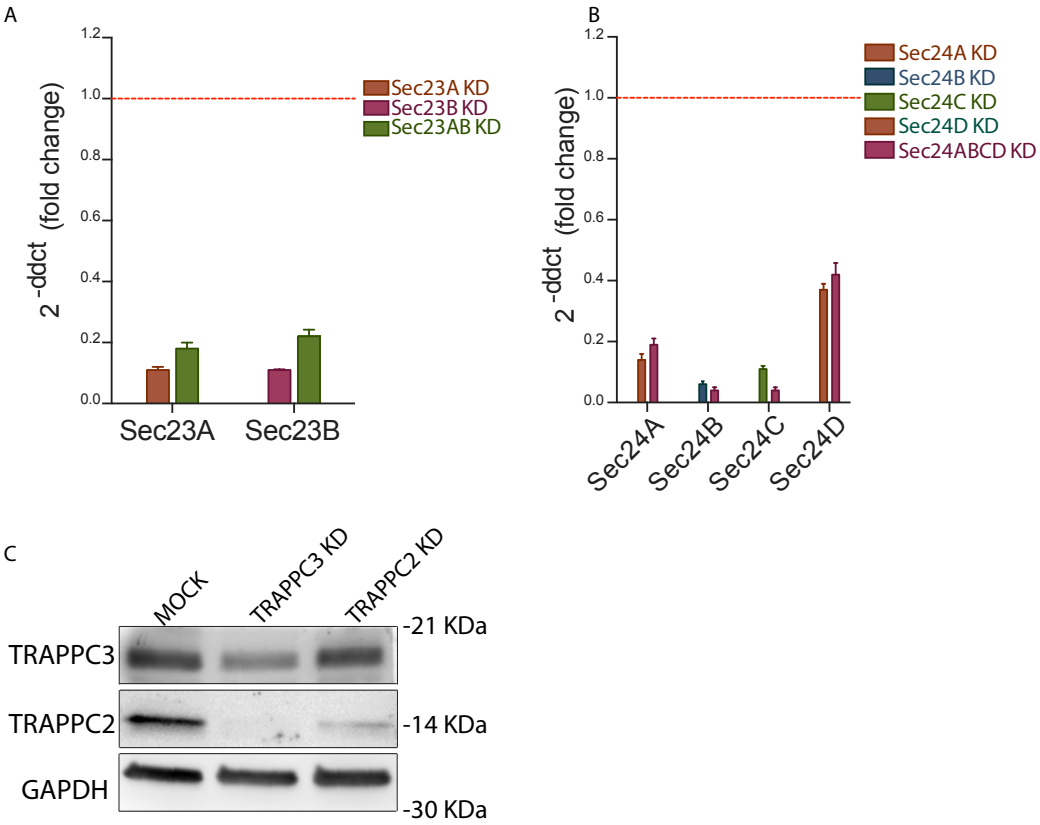

Figure 2—figure supplement 3. Evaluation of Sec23, Sec24, TRAPPC2 and TRAPPC3 knock down efficiencies. (A) Sec23A and Sec23B mRNA levels were evaluated by q-PCR and expressed as fold change with respect to the MOCK. Dashed red line: MOCK. **(B)** Sec24A, B, C and D mRNA levels were evaluated as described in (A). **(C)** Representative Western blot of HeLa cell extracts depleted for TRAPPC2 and TRAPPC3; GAPDH was used as loading control.

1423
1424

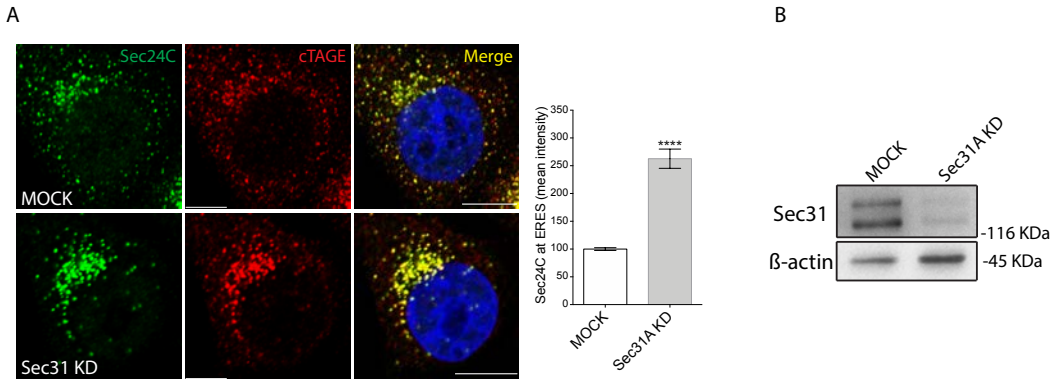

1425
1426 **Figure 3—figure supplement 1. (A)** Effect of Sec31 depletion on Sec24 localization at
1427 ERES. Cells were mock-treated or KD for Sec31 and then immunostained for Sec24C
1428 and cTAGE to stain ERES. Scale bar 10µm. The graph shows the mean intensity of
1429 Sec24C at ERES normalized for cytosolic signal as a percentage of control conditions.
1430 **(A)** Western blot analysis of Sec31A KD cells. ß-actin was used as loading control.
1431

1432

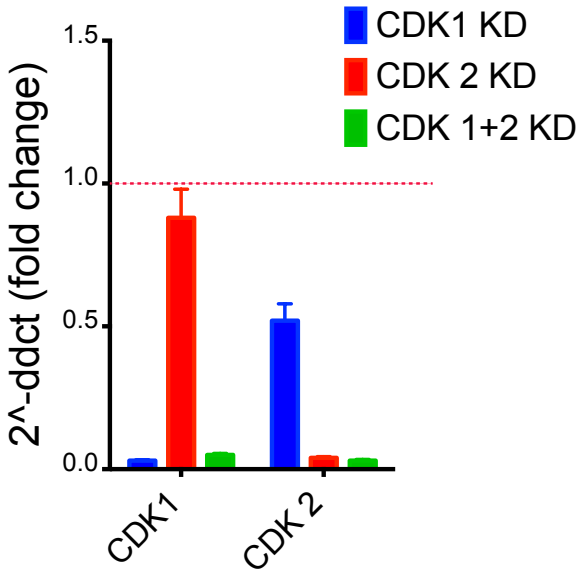

1433
1434 **Figure 4—figure supplement 1 Evaluation of CDK1 and CDK2 knock down efficiency.**
1435 CDK1 and CDK2 mRNA levels were evaluated by q-PCR and expressed as fold change
1436 with respect to the MOCK. Dashed red line: MOCK.
1437

1438
1439

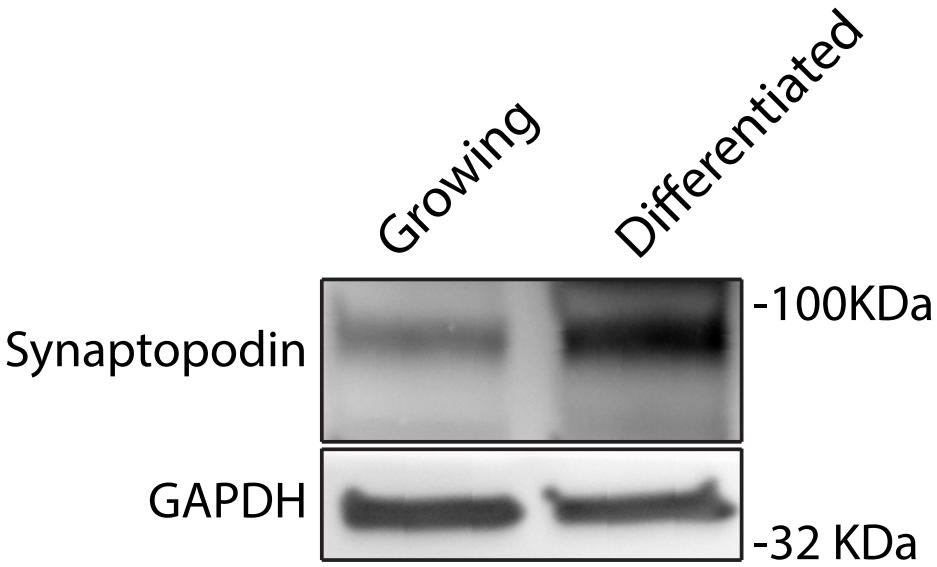

1440
1441 **Figure 6—figure supplement 1.** Differentiation of podocytes. Western blot of
1442 growing and differentiated podocytes. Synaptopodin was used as a differentiation
1443 marker, GAPDH as a loading control.
1444

1445

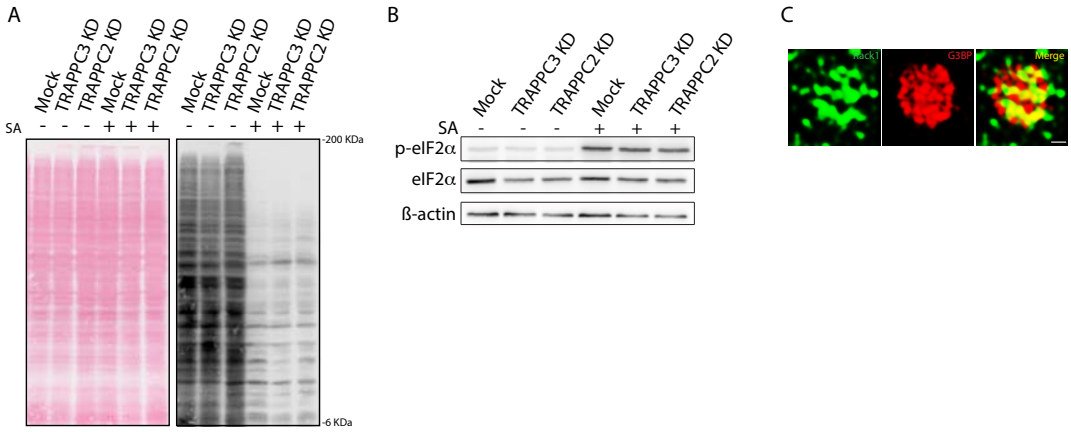

1446

1447 **Figure 7—figure supplement 1.** TRAPP depletion does not affect protein translation
1448 inhibition caused by SA treatment. **(A)** Puromycin assay (see Materials and methods)
1449 of MOCK, TRAPPC3 and TRAPPC2-KD HeLa cells at steady state and upon SA
1450 treatment. **(B)** Evaluation of phosphorylated eIF2a in TRAPPC3 and TRAPPC2
1451 depleted cells exposed to SA. ß-actin was used as a loading control. **(C)** Structured
1452 Illumination Microscopy (SIM)-Super resolution (SR) images of endogenous RACK1
1453 and G3BP. Scale bar 500 nm.

1454

1455
1456

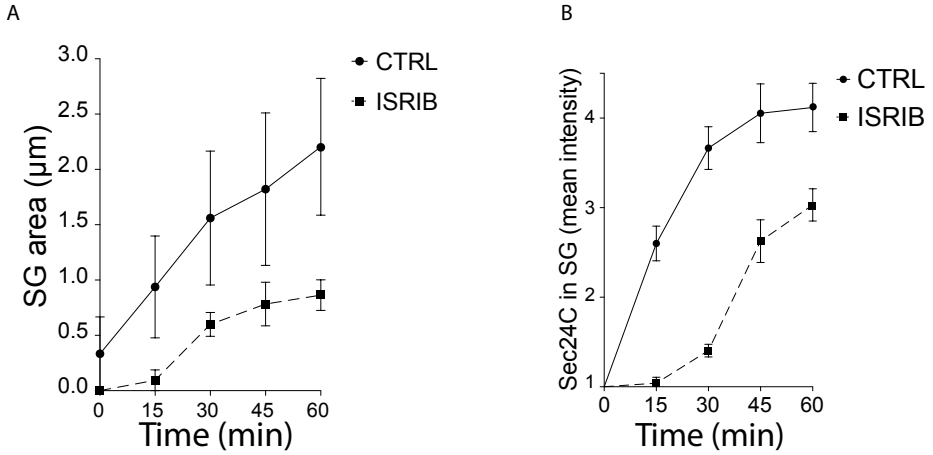

1457
1458 **Figure 8—figure supplement 1.** ISRIB delays SG nucleation and prevents Sec24C
1459 relocalization to SGs. **(A)** HeLa cells were exposed to SA (200 µM) for the indicated
1460 time, alone or in combination with ISRIB and SGs were analyzed. Quantification of SG
1461 area (µm) of three independent experiment Mean ± s.e.m. **(B)** Graph, Quantification
1462 of Sec24C localization at SGs over time (the ratio between Sec24C (mean
1463 fluorescence intensity) in SG puncta and cytosolic) Sec24C. Mean ± SD. n = 60-80
1464 cells per experiment, N = 3.
1465

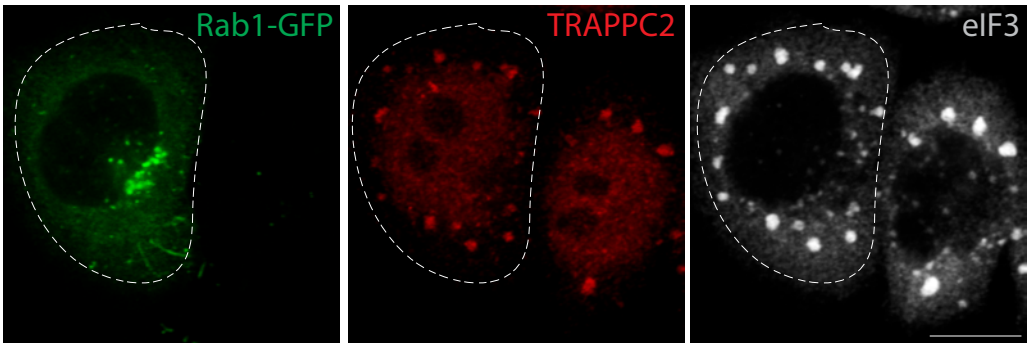

1466
1467 **Figure 9—figure supplement 1.** TRAPPC2 migrates to SGs in Rab1 overexpressing
1468 cells. HeLa cells overexpressing GFP-Rab1B-WT were treated with SA (300 µM 30
1469 min) and stained for TRAPPC2 (in red) and eIF3 (in gray). Dashed white line:
1470 Overexpressing cells.

1471

1472 Table S1 TRAPPC2 interactors.

EEF1B2	P24534	28	24919	2	2	2	2	0.46	Elongation factor 1-beta OS=Homo sapiens GN=EEF1B2 PE=1 SV=3
EEF1D	E9PRY8	346	77150	8	7	7	6	0.44	Elongation factor 1-delta OS=Homo sapiens GN=EEF1D PE=1 SV=1
EEF1E1	H0YAL7	50	15444	2	1	2	1	0.35	Eukaryotic translation elongation factor 1 epsilon-1 (Fragment) OS=Homo sapiens GN=EEF1E1 PE=4 SV=1
EFTUD2	Q15029	84	106286	5	4	5	4	0.19	Isoform 2 of 116 kDa U5 small nuclear ribonucleoprotein component OS=Homo sapiens GN=EFTUD2
EHD2	Q9NZN4	58	46144	3	2	3	2	0.23	Isoform 2 of EH domain-containing protein 2 OS=Homo sapiens GN=EHD2
EIF2S2	P20042	292	38706	13	10	12	9	1.98	Eukaryotic translation initiation factor 2 subunit 2 OS=Homo sapiens GN=EIF2S2 PE=1 SV=2
EIF3G	O75822	446	35874	18	13	13	10	2.71	Eukaryotic translation initiation factor 3 subunit G OS=Homo sapiens GN=EIF3G PE=1 SV=2
EIF3I	O75822	181	29159	5	5	5	5	1.23	Eukaryotic translation initiation factor 3 subunit I OS=Homo sapiens GN=EIF3I PE=1 SV=2
EIF3K	Q9UBQ5	213	25329	9	6	8	5	1.52	Eukaryotic translation initiation factor 3 subunit K OS=Homo sapiens GN=EIF3K PE=1 SV=1
EIF4A2	Q14240	501	46688	12	10	8	7	1.03	Isoform 2 of Eukaryotic initiation factor 4A-II OS=Homo sapiens GN=EIF4A2
EIF4A3	P38919	241	47126	7	6	6	5	0.65	Eukaryotic initiation factor 4A-III OS=Homo sapiens GN=EIF4A3 PE=1 SV=4
EIF5A	I3L397	65	16237	3	2	3	2	0.78	Eukaryotic translation initiation factor 5A-1 (Fragment) OS=Homo sapiens GN=EIF5A PE=1 SV=2
EIF5B	O60841	432	139198	17	14	16	14	0.61	Eukaryotic translation initiation factor 5B OS=Homo sapiens GN=EIF5B PE=1 SV=4
ELMO2	H0YCM7	29	51873	3	1	3	1	0.10	Engulfment and cell motility protein 2 (Fragment) OS=Homo sapiens GN=ELMO2 PE=1 SV=1
EMG1	V9GYP5	115	26809	6	3	5	3	0.69	Uncharacterized protein (Fragment) OS=Homo sapiens PE=1 SV=1
EPRS	P07814	571	172080	20	20	17	17	0.64	Bifunctional glutamate/proline--tRNA ligase OS=Homo sapiens GN=EPRS PE=1 SV=5
ERAL1	J3QRV9	21	31877	1	1	1	1	0.16	GTPase Era, mitochondrial (Fragment) OS=Homo sapiens GN=ERAL1 PE=1 SV=2
ERLIN1	O75477	38	39072	1	1	1	1	0.13	Erlin-1 OS=Homo sapiens GN=ERLIN1 PE=1 SV=1
ESYT1	Q9BSJ8	16	124439	1	1	1	1	0.04	Isoform 2 of Extended synaptotagmin-1 OS=Homo sapiens GN=ESYT1
EWSR1	B0QYK0	267	65174	8	8	5	5	0.54	RNA-binding protein EWS OS=Homo sapiens GN=EWSR1 PE=1 SV=1
EXOC3	D6RB59	15	53607	18	1	2	1	0.09	Exocyst complex component 3 OS=Homo sapiens GN=EXOC3 PE=1 SV=1
EXOSC1	B1AMU7	15	18231	3	1	3	1	0.29	Exosome complex component CSL4 (Fragment) OS=Homo sapiens GN=EXOSC1 PE=1 SV=2
EXOSC10	Q01780	24	98826	3	1	3	1	0.05	Isoform 2 of Exosome component 10 OS=Homo sapiens GN=EXOSC10
EYA3	B1APR7	18	45806	1	1	1	1	0.11	Eyes absent homolog 3 OS=Homo sapiens GN=EYA3 PE=1 SV=1
FABP5	Q01469	33	15497	1	1	1	1	0.35	Fatty acid-binding protein, epidermal OS=Homo sapiens GN=FABP5 PE=1 SV=3
FAM126A	H7C0W7	29	52801	2	1	2	1	0.09	Hypoxia (Fragment) OS=Homo sapiens GN=FAM126A PE=4 SV=1
FAM83B	Q5T0W9	36	115185	3	1	3	1	0.04	Protein FAM83B OS=Homo sapiens GN=FAM83B PE=1 SV=1
FAM98A	Q8NCA5	165	55694	8	6	7	6	0.66	Isoform 2 of Protein FAM98A OS=Homo sapiens GN=FAM98A
FAM98B	Q5ZLI0	49	45918	1	1	1	1	0.11	Isoform 2 of Protein FAM98B OS=Homo sapiens GN=FAM98B
FASN	P49327	48	275877	5	1	5	1	0.02	Fatty acid synthase OS=Homo sapiens GN=FASN PE=1 SV=3
FASTKD2	Q9NYY8	61	75343	1	1	1	1	0.06	Isoform 2 of FAST kinase domain-containing protein 2 OS=Homo sapiens GN=FASTKD2
FAU	E9PR30	42	10898	1	1	1	1	0.53	40S ribosomal protein S30 OS=Homo sapiens GN=FAU PE=1 SV=1
FMC1	Q96HJ9	144	54761	13	6	13	6	0.68	Isoform 2 of UPF0562 protein C7orf55 OS=Homo sapiens GN=C7orf55
FMR1	Q06787	146	67215	5	3	5	3	0.23	Isoform 1 of Fragile X mental retardation protein 1 OS=Homo sapiens GN=FMR1
FOXRED1	Q96CU9	98	30868	2	2	2	2	0.36	Isoform 2 of FAD-dependent oxidoreductase domain-containing protein 1 OS=Homo sapiens GN=FOXRED1
FSCN1	Q16658	37	55123	2	1	2	1	0.09	Fascin OS=Homo sapiens GN=FSCN1 PE=1 SV=3
FTSJ1	Q9UET6	22	36471	1	1	1	1	0.14	Isoform 2 of Putative tRNA (cytidine(32)/guanosine(34)-2'-O)methyltransferase OS=Homo sapiens GN=FTSJ1
FUBP3	Q96I24	48	61944	2	1	2	1	0.08	Far upstream element-binding protein 3 OS=Homo sapiens GN=FUBP3 PE=1 SV=2
FUS	P35637	432	53551	15	14	9	8	1.21	Isoform Short of RNA-binding protein FUS OS=Homo sapiens GN=FUS
FXR2	P51116	197	74520	9	6	9	6	0.46	Fragile X mental retardation syndrome-related protein 2 OS=Homo sapiens GN=FXR2 PE=1 SV=2
GANAB	F5H6X6	41	96441	1	1	1	1	0.05	Neutral alpha-glucosidase AB OS=Homo sapiens GN=GANAB PE=1 SV=1
GART	P22102	26	46631	1	1	1	1	0.11	Isoform Short of Trifunctional purine biosynthetic protein adenosine-3 OS=Homo sapiens GN=GART
GATAD2B	Q8WXI9	19	65562	2	1	2	1	0.07	Transcriptional repressor p66-beta OS=Homo sapiens GN=GATAD2B PE=1 SV=1
GDI2	P50395	63	51087	2	2	2	2	0.20	Rab GDP dissociation inhibitor beta OS=Homo sapiens GN=GDI2 PE=1 SV=2
GEMIN5	Q8TEQ6	48	170821	5	1	5	1	0.03	Gem-associated protein 5 OS=Homo sapiens GN=GEMIN5 PE=1 SV=3
GLUD2	P49448	44	61738	2	1	2	1	0.08	Glutamate dehydrogenase 2, mitochondrial OS=Homo sapiens GN=GLUD2 PE=1 SV=2
GNAS	Q5JWF2	106	110299	3	2	3	2	0.09	Isoform Xlas-2 of Guanine nucleotide-binding protein G(s) subunit alpha isoforms Xlas OS=Homo sapiens GN=GNAS
GNB3	F5H058	34	30024	2	1	2	1	0.17	Guanine nucleotide-binding protein G(I)/G(S)/G(T) subunit beta-3 (Fragment) OS=Homo sapiens GN=GNB3 PE=4 SV=2
GNL3L	Q9NVN8	46	66216	1	1	1	1	0.07	Guanine nucleotide-binding protein-like 3-like protein OS=Homo sapiens GN=GNL3L PE=1 SV=1
GOLGA3	Q08378	110	155987	8	4	7	3	0.10	Isoform 2 of Golgin subfamily A member 3 OS=Homo sapiens GN=GOLGA3
GPATCH4	Q5T3I0	50	51125	3	1	3	1	0.10	Isoform 3 of G-patch domain-containing protein 4 OS=Homo sapiens GN=GPATCH4
GRWD1	M0QX71	98	25632	2	2	2	2	0.44	Glutamate-rich WD repeat-containing protein 1 (Fragment) OS=Homo sapiens GN=GRWD1 PE=1 SV=1
GSTM3	P21266	30	26998	1	1	1	1	0.19	Glutathione S-transferase Mu 3 OS=Homo sapiens GN=GSTM3 PE=1 SV=3
GTPBP1	O00178	28	73035	3	1	3	1	0.07	GTP-binding protein 1 OS=Homo sapiens GN=GTPBP1 PE=1 SV=3
HADHB	B5MD38	31	38128	4	2	3	2	0.28	3-ketoacyl-CoA thiolase OS=Homo sapiens GN=HADHB PE=1 SV=1
HCK	H0Y3C5	20	59986	3	1	3	1	0.08	Tyrosine-protein kinase HCK OS=Homo sapiens GN=HCK PE=1 SV=1
HERC5	Q9UJH4	13	118203	1	1	1	1	0.04	E3 ISG15--protein ligase HERC5 OS=Homo sapiens GN=HERC5 PE=1 SV=2
HIST1H1D	P16402	27	22336	2	1	2	1	0.23	Histone H1.3 OS=Homo sapiens GN=HIST1H1D PE=1 SV=2
HIST1H2BK	O60814	71	13882	5	2	5	2	0.95	Histone H2B type 1-K OS=Homo sapiens GN=HIST1H2BK PE=1 SV=3
HLTF	Q14527	31	100882	2	1	2	1	0.05	Isoform 2 of Helicase-like transcription factor OS=Homo sapiens GN=HLTF
HNRNPA1	P09651	1099	34289	32	30	19	18	16.79	Isoform A1-A of Heterogeneous nuclear ribonucleoprotein A1 OS=Homo sapiens GN=HNRNPA1
HNRNPAB	Q99729	219	36059	6	6	5	5	0.92	Isoform 2 of Heterogeneous nuclear ribonucleoprotein A/B OS=Homo sapiens GN=HNRNPAB
HNRNPDL	O14979	161	33739	8	7	7	6	1.31	Isoform 2 of Heterogeneous nuclear ribonucleoprotein D-like OS=Homo sapiens GN=HNRNPDL
HNRNPF	P52597	308	45985	15	12	10	7	1.05	Heterogeneous nuclear ribonucleoprotein F OS=Homo sapiens GN=HNRNPF PE=1 SV=3
HNRNPK	P61978	2753	48760	82	73	24	23	14.00	Isoform 3 of Heterogeneous nuclear ribonucleoprotein K OS=Homo sapiens GN=HNRNPK
HNRNPUL1	Q9BUJ2	448	84903	19	13	16	11	0.95	Isoform 3 of Heterogeneous nuclear ribonucleoprotein U-like protein 1 OS=Homo sapiens GN=HNRNPUL1
HRNR	Q86YZ3	176	283140	3	3	2	2	0.03	Hornerin OS=Homo sapiens GN=HRNR PE=1 SV=2
HSP90AA1	P07900	345	98670	16	13	14	12	0.86	Isoform 2 of Heat shock protein HSP 90-alpha OS=Homo sapiens GN=HSP90AA1
HSP90AB1	P08238	639	83554	26	23	22	20	2.28	Heat shock protein HSP 90-beta OS=Homo sapiens GN=HSP90AB1 PE=1 SV=4
HSP90B1	P14625	243	92696	6	5	5	4	0.23	Endoplasmin OS=Homo sapiens GN=HSP90B1 PE=1 SV=1
HSPB1	P04792	52	22826	4	4	3	3	0.85	Heat shock protein beta-1 OS=Homo sapiens GN=HSPB1 PE=1 SV=2
HSPD1	P10809	367	61187	10	9	10	9	1.00	60 kDa heat shock protein, mitochondrial OS=Homo sapiens GN=HSPD1 PE=1 SV=2
HTATSF1	Q5H918	57	27898	1	1	1	1	0.18	HIV Tat-specific factor 1 (Fragment) OS=Homo sapiens GN=HTATSF1 PE=1 SV=1
IDH1	O75874	33	46915	1	1	1	1	0.11	Isocitrate dehydrogenase [NADP] cytoplasmic OS=Homo sapiens GN=IDH1 PE=1 SV=2
IGF2BP1	Q9NZI8	468	63783	14	11	12	11	1.26	Insulin-like growth factor 2 mRNA-binding protein 1 OS=Homo sapiens GN=IGF2BP1 PE=1 SV=2
IGF2BP2	Q9Y6M1	219	61918	6	5	6	5	0.46	Isoform 2 of Insulin-like growth factor 2 mRNA-binding protein 2 OS=Homo sapiens GN=IGF2BP2
IGHV4OR15-8	A0A075B7B6	22	13105	1	1	1	1	0.43	Putative V-set and immunoglobulin domain-containing-like protein IGHV4OR15-8 (Fragment) OS=Homo sapiens GN=IGHV4OR15-8 PE=4 SV=1
IGKV2-30	P06310	4080	14811	88	77	3	3	1.57	Ig kappa chain V-II region RPMI 6410 OS=Homo sapiens PE=4 SV=1
IKBIP	Q70UQ0	122	43228	4	3	4	3	0.39	Isoform 4 of Inhibitor of nuclear factor kappa-B kinase-interacting protein OS=Homo sapiens GN=IKBIP
IL17RC	G3V177	34	5031	1	1	1	1	1.45	Interleukin 17 receptor C, isoform CRA_g OS=Homo sapiens GN=IL17RC PE=4 SV=1
ILF2	Q12905	156	43263	7	5	7	5	0.72	Interleukin enhancer-binding factor 2 OS=Homo sapiens GN=ILF2 PE=1 SV=2
ILF3	Q12906	416	76441	17	12	13	10	0.85	Isoform 2 of Interleukin enhancer-binding factor 3 OS=Homo sapiens GN=ILF3
IPO8	O15397	418	120945	11	9	11	9	0.42	Importin-8 OS=Homo sapiens GN=IPO8 PE=1 SV=2
ITPR1	E7EVP7	39	315354	7	1	6	1	0.02	Inositol 1,4,5-trisphosphate receptor type 1 OS=Homo sapiens GN=ITPR1 PE=1 SV=2
JUP	P14923	103	82434	3	2	3	2	0.12	Junction plakoglobin OS=Homo sapiens GN=JUP PE=1 SV=3
KARS	Q15046	192	71908	7	7	7	7	0.58	Isoform Mitochondrial of Lysine--tRNA ligase OS=Homo sapiens GN=KARS
KCTD17	H0Y731	59	20928	1	1	1	1	0.25	BTB/POZ domain-containing protein KCTD17 (Fragment) OS=Homo sapiens GN=KCTD17 PE=4 SV=1
KCTD2	Q14681	323	28794	8	8	5	5	1.66	BTB/POZ domain-containing protein KCTD2 OS=Homo sapiens GN=KCTD2 PE=1 SV=3
KIF2C	Q5JR89	71	32827	1	1	1	1	0.15	Kinesin-like protein KIF2C (Fragment) OS=Homo sapiens GN=KIF2C PE=1 SV=1
KLB	Q86Z14	35	120473	2	1	2	1	0.04	Beta-klotho OS=Homo sapiens GN=KLB PE=1 SV=1
KLHL9	Q9P213	23	70239	1	1	1	1	0.07	Kelch-like protein 9 OS=Homo sapiens GN=KLHL9 PE=1 SV=2
KPNB1	J3QR48	71	16502	2	1	2	1	0.33	Importin subunit beta-1 (Fragment) OS=Homo sapiens GN=KPNB1 PE=1 SV=2
KRAS	G3V4K2	20	4664	1	1	1	1	1.61	GTPase KRas OS=Homo sapiens GN=KRAS PE=4 SV=1
KRI1	Q8N9T8	42	83004	2	1	2	1	0.06	Protein KRI1 homolog OS=Homo sapiens GN=KRI1 PE=1 SV=3
KRT10	P13645	2747	59020	72	65	36	33	16.74	Keratin, type I cytoskeletal 10 OS=Homo sapiens GN=KRT10 PE=1 SV=6
KRT2	P35908	1146	65678	33	31	25	25	5.95	Keratin, type II cytoskeletal 2 epidermal OS=Homo sapiens GN=KRT2 PE=1 SV=2
KRT6A	P02538	644	60293	27	21	21	19	3.79	Keratin, type II cytoskeletal 6A OS=Homo sapiens GN=KRT6A PE=1 SV=3
KRT72	Q14CN4	107	56342	11	5	8	4	0.40	Isoform 2 of Keratin, type II cytoskeletal 72 OS=Homo sapiens GN=KRT72
KRT86	O43790	55	55120	6	3	5	3	0.29	Keratin, type II cuticular Hb6 OS=Homo sapiens GN=KRT86 PE=1 SV=1
KTN1	Q86UP2	108	149804	10	3	9	3	0.10	Isoform 2 of Kinectin OS=Homo sapiens GN=KTN1
LANCL1	F8WD59	26	9334	1	1	1	1	0.64	LanC-like protein 1 OS=Homo sapiens GN=LANCL1 PE=1 SV=1
LAPTM4B	Q86VI4	29	25972	2	2	2	2	0.43	Isoform 2 of Lysosomal-associated transmembrane protein 4B OS=Homo sapiens GN=LAPTM4B
LARP4	Q71RC2	110	81877	5	2	5	2	0.12	Isoform 4 of La-related protein 4 OS=Homo sapiens GN=LARP4
LARP4B	Q92615	27	80902	2	2	2	2	0.12	La-related protein 4B OS=Homo sapiens GN=LARP4B PE=1 SV=3
LARS	B4DER1	140	132410	8	7	8	7	0.28	Leucine--tRNA ligase, cytoplasmic OS=Homo sapiens GN=LARS PE=1 SV=1
LDHB	P07195	226	36900	5	5	5	5	0.89	L-lactate dehydrogenase B chain OS=Homo sapiens GN=LDHB PE=1 SV=2
LGALS3BP	Q08380	29	66202	2	2	2	2	0.15	Galectin-3-binding protein OS=Homo sapiens GN=LGALS3BP PE=1 SV=1
LIFR	P42702	19	125090	1	1	1	1	0.04	Leukemia inhibitory factor receptor OS=Homo sapiens GN=LIFR PE=1 SV=1
LIMA1	Q9UHB6	569	85630	25	19	22	17	1.56	LIM domain and actin-binding protein 1 OS=Homo sapiens GN=LIMA1 PE=1 SV=1
LMNA	P02545	130	65153	5	3	4	3	0.24	Isoform C of Prelamin-A/C OS=Homo sapiens GN=LMNA
LMO7	J3KP06	889	191723	38	32	34	29	1.10	LIM domain only protein 7 OS=Homo sapiens GN=LMO7 PE=1 SV=1
LRMDA	M0R2H0	25	6258	3	1	2	1	1.07	Leucine-rich repeat-containing protein C10orf51 OS=Homo sapiens GN=C10orf51 PE=1 SV=1
LRPPRC	P42704	290	159003	9	6	9	6	0.20	Leucine-rich PPR motif-containing protein, mitochondrial OS=Homo sapiens GN=LRPPRC PE=1 SV=3
LRRK2	Q5S007	14	289568	9	1	9	1	0.02	Leucine-rich repeat serine/threonine-protein kinase 2 OS=Homo sapiens GN=LRRK2 PE=1 SV=2
LSM14A	I3L4Q1	18	11439	1	1	1	1	0.50	Protein LSM14A homolog A OS=Homo sapiens GN=LSM14A PE=1 SV=1
LUC7L	Q9NQ29	80	38781	5	3	5	3	0.44	Isoform 2 of Putative RNA-binding protein Luc7-like 1 OS=Homo sapiens GN=LUC7L
LUC7L3	J3KPP4	81	58698	2	1	2	1	0.08	Cisplatin resistance-associated overexpressed protein, isoform CRA_b OS=Homo sapiens GN=LUC7L3 PE=1 SV=1
MAGED2	Q5H907	71	55932	3	3	3	3	0.29	Melanoma antigen family D, 2, isoform CRA_d OS=Homo sapiens GN=MAGED2 PE=1 SV=1
MAP7	Q14244	39	87014	7	1	7	1	0.06	Isoform 7 of Ensconsin OS=Homo sapiens GN=MAP7
MAT2A	P31153	341	43975	11	10	9	8	1.62	S-adenosylmethionine synthase isoform type-2 OS=Homo sapiens GN=MAT2A PE=1 SV=1
MCAT	Q8N52	32	43390	1	1	1	1	0.11	Malonyl-CoA:acyl carrier protein transacylase, mitochondrial OS=Homo sapiens GN=MCAT PE=1 SV=2
MCRIP2	I3L172	50	7085	2	1	1	1	0.90	Protein FAM195A OS=Homo sapiens GN=FAM195A PE=1 SV=1

1473

Gene name	UNIPROT id	Score	Mass	Num. of matches	Num. of significant matches	Num. of sequences	Num. of significant sequences	emPAI	Description
MARC1	Q5VT66	21	39999	2	1	2	1	0.13	Isoform 2 of Mitochondrial amidoxime-reducing component 1 OS=Homo sapiens GN=MARC1
AAAS	Q9NRG9	130	60392	6	3	6	3	0.26	Aladin OS=Homo sapiens GN=AAAS PE=1 SV=1
ABCF1	Q8NE71	249	92080	11	8	10	8	0.51	Isoform 2 of ATP-binding cassette sub-family F member 1 OS=Homo sapiens GN=ABCF1
AC093512.2	J3KPS3	104	40249	5	4	4	4	0.60	Aldolase A, fructose-bisphosphate, isoform CRA_b OS=Homo sapiens GN=ALDOA PE=1 SV=1
ACADVL	P49748	22	68414	1	1	1	1	0.07	Isoform 2 of Very long-chain specific acyl-CoA dehydrogenase, mitochondrial OS=Homo sapiens GN=ACADVL
ACLY	P53396	102	120608	3	1	3	1	0.04	Isoform 2 of ATP-citrate synthase OS=Homo sapiens GN=ACLY
ACOT9	H7C5Q2	26	30256	1	1	1	1	0.17	Acyl-coenzyme A thioesterase 9, mitochondrial (Fragment) OS=Homo sapiens GN=ACOT9 PE=1 SV=1
ACTBL2	Q562R1	394	42318	18	14	7	5	1.18	Beta-actin-like protein 2 OS=Homo sapiens GN=ACTBL2 PE=1 SV=2
ACTN1	H9KV75	172	95279	7	6	6	5	0.28	Alpha-actinin-1 OS=Homo sapiens GN=ACTN1 PE=1 SV=1
ACTN4	O43707	146	105245	7	7	6	6	0.31	Alpha-actinin-4 OS=Homo sapiens GN=ACTN4 PE=1 SV=2
ACTR1A	P61163	29	42701	3	1	3	1	0.12	Alpha-centractin OS=Homo sapiens GN=ACTR1A PE=1 SV=1
ADAR	H0YCX3	61	133761	3	1	3	1	0.04	Double-stranded RNA-specific adenosine deaminase (Fragment) OS=Homo sapiens GN=ADAR PE=1 SV=1
ADRM1	Q16186	22	42412	1	1	1	1	0.12	Proteasomal ubiquitin receptor ADRM1 OS=Homo sapiens GN=ADRM1 PE=1 SV=2
AGO2	Q9UKV8	96	94758	5	4	5	4	0.22	Isoform 2 of Protein argonaute-2 OS=Homo sapiens GN=AGO2
AHNAK	Q09666	68	629213	10	2	10	2	0.02	Neuroblast differentiation-associated protein AHNAK OS=Homo sapiens GN=AHNAK PE=1 SV=2
AIFM1	O95831	99	66539	10	4	8	4	0.33	Isoform 3 of Apoptosis-inducing factor 1, mitochondrial OS=Homo sapiens GN=AIFM1
AIMP1	Q12904	164	37358	5	5	5	5	0.88	Isoform 2 of Aminoacyl tRNA synthase complex-interacting multifunctional protein 1 OS=Homo sapiens GN=AIMP1
AIMP2	Q13155	57	35668	3	1	3	1	0.14	Aminoacyl tRNA synthase complex-interacting multifunctional protein 2 OS=Homo sapiens GN=AIMP2 PE=1 SV=2
AKAP8L	Q9ULX6	55	72060	2	1	2	1	0.07	A-kinase anchor protein 8-like OS=Homo sapiens GN=AKAP8L PE=1 SV=3
AKAP9	Q99996	19	454989	5	1	5	1	0.01	Isoform 2 of A-kinase anchor protein 9 OS=Homo sapiens GN=AKAP9
ALPG	P10696	344	57626	10	10	8	8	0.93	Alkaline phosphatase, placental-like OS=Homo sapiens GN=ALPPL2 PE=1 SV=4
ANKS6	Q6BDC2	15	92575	2	1	2	1	0.05	Isoform 3 of Ankyrin repeat and SAM domain-containing protein 6 OS=Homo sapiens GN=ANKS6
ANXA1	P04083	33	38918	4	1	4	1	0.13	Annexin A1 OS=Homo sapiens GN=ANXA1 PE=1 SV=2
ANXA2	H0YM50	166	28582	8	6	7	5	1.28	Annexin (Fragment) OS=Homo sapiens GN=ANXA2 PE=1 SV=1
AP2A1	O95782	152	106378	9	5	9	5	0.25	Isoform B of AP-2 complex subunit alpha-1 OS=Homo sapiens GN=AP2A1
AP2B1	P63010	40	106537	5	2	5	2	0.09	Isoform 2 of AP-2 complex subunit beta OS=Homo sapiens GN=AP2B1
AP2M1	E9PFW3	35	52612	2	1	2	1	0.09	AP-2 complex subunit mu OS=Homo sapiens GN=AP2M1 PE=1 SV=1
AP2S1	M0QYZ2	23	19145	3	1	3	1	0.28	AP-2 complex subunit sigma OS=Homo sapiens GN=AP2S1 PE=1 SV=1
AP3S2	H0YLI7	19	23611	1	1	1	1	0.22	AP-3 complex subunit sigma-2 OS=Homo sapiens GN=AP3S2 PE=1 SV=1
ARF5	C9J1Z8	30	17153	2	1	2	1	0.31	ADP-ribosylation factor 5 (Fragment) OS=Homo sapiens GN=ARF5 PE=1 SV=1
ARHGDIA	J3KTF8	20	21561	2	1	2	1	0.24	Rho GDP-dissociation inhibitor 1 (Fragment) OS=Homo sapiens GN=ARHGDIA PE=1 SV=2
ARHGEF2	V9GYM8	103	117025	7	2	7	2	0.08	Rho guanine nucleotide exchange factor 2 OS=Homo sapiens GN=ARHGEF2 PE=1 SV=1
ASF1B	K7ES22	33	16102	1	1	1	1	0.34	Histone chaperone ASF1B OS=Homo sapiens GN=ASF1B PE=1 SV=1
ASPH	Q12797	226	83672	11	8	10	7	0.48	Isoform 10 of Aspartyl/(asparaginyl) beta-hydroxylase OS=Homo sapiens GN=ASPH
ASS1	P00966	39	46786	3	3	3	3	0.35	Argininosuccinate synthase OS=Homo sapiens GN=ASS1 PE=1 SV=2
ATAD3A	Q9NVI7	161	66291	12	9	11	8	0.77	Isoform 2 of ATPase family AAA domain-containing protein 3A OS=Homo sapiens GN=ATAD3A
ATP1A2	B1AKY9	109	112046	4	2	4	2	0.09	Sodium/potassium-transporting ATPase subunit alpha-2 OS=Homo sapiens GN=ATP1A2 PE=1 SV=1
ATP2A2	P16615	61	111103	3	2	3	2	0.09	Isoform 2 of Sarcoplasmic/endoplasmic reticulum calcium ATPase 2 OS=Homo sapiens GN=ATP2A2
ATP2C1	H0Y8X9	16	24342	1	1	1	1	0.21	Calcium-transporting ATPase type 2C member 1 (Fragment) OS=Homo sapiens GN=ATP2C1 PE=1 SV=1
ATP5F1A	P25705	354	59828	12	11	11	10	1.20	ATP synthase subunit alpha, mitochondrial OS=Homo sapiens GN=ATP5A1 PE=1 SV=1
ATP5F1B	P06576	500	56525	18	12	12	9	1.51	ATP synthase subunit beta, mitochondrial OS=Homo sapiens GN=ATP5B PE=1 SV=3
ATP5F1C	P36542	69	33032	3	3	3	3	0.53	ATP synthase subunit gamma, mitochondrial OS=Homo sapiens GN=ATP5C1 PE=1 SV=1
ATP5MD	Q96IX5	28	6510	1	1	1	1	1.00	Up-regulated during skeletal muscle growth protein 5 OS=Homo sapiens GN=USMG5 PE=1 SV=1
ATP5PB	Q5QNZ2	16	22318	1	1	1	1	0.23	ATP synthase F(0) complex subunit B1, mitochondrial OS=Homo sapiens GN=ATP5F1 PE=1 SV=1
ATP5PO	H7C086	112	8242	2	2	2	2	2.05	ATP synthase subunit O, mitochondrial (Fragment) OS=Homo sapiens GN=ATP5O PE=1 SV=1
ATXN2	Q99700	78	106610	4	2	4	2	0.09	Isoform 2 of Ataxin-2 OS=Homo sapiens GN=ATXN2
BASP1	P80723	28	17654	1	1	1	1	0.30	Isoform 2 of Brain acid soluble protein 1 OS=Homo sapiens GN=BASP1
BLM	P54132	29	160611	3	1	3	1	0.03	Bloom syndrome protein OS=Homo sapiens GN=BLM PE=1 SV=1
BRIX1	Q8TDN6	32	41660	2	1	2	1	0.12	Ribosome biogenesis protein BRX1 homolog OS=Homo sapiens GN=BRIX1 PE=1 SV=2
BST2	Q10589	66	18611	1	1	1	1	0.28	Isoform 2 of Bone marrow stromal antigen 2 OS=Homo sapiens GN=BST2
BYSL	Q13895	83	49798	4	2	4	2	0.21	Bystin OS=Homo sapiens GN=BYSL PE=1 SV=3
C1QBP	Q07021	137	31742	4	4	3	3	0.56	Complement component 1 Q subcomponent-binding protein, mitochondrial OS=Homo sapiens GN=C1QBP PE=1 SV=1
C7orf50	H7C0T1	30	18846	1	1	1	1	0.28	Uncharacterized protein C7orf50 (Fragment) OS=Homo sapiens GN=C7orf50 PE=1 SV=1
CALM2	H0Y7A7	123	20863	4	2	3	1	0.25	Calmodulin (Fragment) OS=Homo sapiens GN=CALM2 PE=1 SV=1
CALR	K7EJB9	63	28528	2	2	2	2	0.39	Calreticulin (Fragment) OS=Homo sapiens GN=CALR PE=1 SV=1
CAND1	Q86VP6	26	119182	2	1	2	1	0.04	Isoform 2 of Cullin-associated NEDD8-dissociated protein 1 OS=Homo sapiens GN=CAND1
CAPZB	B1AKB5	37	29703	2	2	2	2	0.37	F-actin-capping protein subunit beta OS=Homo sapiens GN=CAPZB PE=1 SV=1
CAVIN1	Q6NZI2	41	33342	2	2	1	1	0.33	Isoform 2 of Polymerase I and transcript release factor OS=Homo sapiens GN=PTRF
CCAR1	Q8IX12	137	131646	13	7	12	7	0.29	Isoform 2 of Cell division cycle and apoptosis regulator protein 1 OS=Homo sapiens GN=CCAR1
CCDC124	Q96CT7	34	25820	3	1	3	1	0.20	Coiled-coil domain-containing protein 124 OS=Homo sapiens GN=CCDC124 PE=1 SV=1
CCDC137	Q6PK04	31	33268	2	1	2	1	0.15	Coiled-coil domain-containing protein 137 OS=Homo sapiens GN=CCDC137 PE=1 SV=1
CCT5	P48643	247	60089	10	9	9	8	1.03	T-complex protein 1 subunit epsilon OS=Homo sapiens GN=CCT5 PE=1 SV=1
CD55	B1AP13	108	50561	5	5	5	5	0.59	Complement decay-accelerating factor OS=Homo sapiens GN=CD55 PE=1 SV=1
CD59	E9PNW4	19	12604	1	1	1	1	0.44	CD59 glycoprotein OS=Homo sapiens GN=CD59 PE=1 SV=1
CDC5L	Q99459	77	92422	6	2	6	2	0.11	Cell division cycle 5-like protein OS=Homo sapiens GN=CDC5L PE=1 SV=2
CEP164	Q9UPV0	15	163958	5	1	2	1	0.03	Isoform 2 of Centrosomal protein of 164 kDa OS=Homo sapiens GN=CEP164
CHCHD3	F8WJR4	69	27832	2	2	2	2	0.40	Coiled-coil-helix-coiled-coil-helix domain-containing protein 3, mitochondrial OS=Homo sapiens GN=CHCHD3 PE=1 SV=1
CHERP	J3QKB9	225	105324	11	9	9	7	0.43	Calcium homeostasis endoplasmic reticulum protein OS=Homo sapiens GN=CHERP PE=1 SV=1
CKAP5	Q14008	17	220041	2	1	2	1	0.02	Isoform 2 of Cytoskeleton-associated protein 5 OS=Homo sapiens GN=CKAP5
CK8	G3V4N7	64	24272	1	1	1	1	0.21	Creatine kinase B-type (Fragment) OS=Homo sapiens GN=CKB PE=1 SV=1
CKMT1B	F8WCN3	44	33782	1	1	1	1	0.15	Creatine kinase U-type, mitochondrial OS=Homo sapiens GN=CKMT1B PE=1 SV=1
CLIC1	O00299	1590	27248	69	58	13	13	8.42	**Chloride intracellular channel protein 1 OS=Homo sapiens GN=CLIC1 PE=1 SV=4**
CLIC5	Q9NZA1	79	28389	7	3	2	2	0.39	**Isoform 1 of Chloride intracellular channel protein 5 OS=Homo sapiens GN=CLIC5**
CLNS1A	P54105	959	26370	25	23	7	7	6.05	Methylosome subunit pICln OS=Homo sapiens GN=CLNS1A PE=1 SV=1
CLPX	O76031	130	69922	5	5	4	4	0.31	ATP-dependent Clp protease ATP-binding subunit clpX-like, mitochondrial OS=Homo sapiens GN=CLPX PE=1 SV=2
CLTC	Q00610	167	189538	6	4	6	4	0.11	Isoform 2 of Clathrin heavy chain 1 OS=Homo sapiens GN=CLTC
CMAS	Q8NFW8	14	49033	2	1	2	1	0.10	N-acylneuraminate cytidylyltransferase OS=Homo sapiens GN=CMAS PE=1 SV=2
CM8L	Q96DG6	982	28372	36	31	18	18	18.55	Carboxymethylenebutenolidase homolog OS=Homo sapiens GN=CM8L PE=1 SV=1
COPA	**P53621**	**2978**	**140832**	**107**	**99**	**61**	**61**	**9.15**	**Isoform 2 of Coatomer subunit alpha OS=Homo sapiens GN=COPA**
COPB1	**P53618**	**117**	**108214**	**3**	**3**	**2**	**2**	**0.14**	**Coatomer subunit beta OS=Homo sapiens GN=COPB1 PE=1 SV=3**
COPB2	**P35606**	**1727**	**99839**	**50**	**46**	**35**	**32**	**4.50**	**Isoform 2 of Coatomer subunit beta' OS=Homo sapiens GN=COPB2**
COPE	**O14579**	**778**	**34688**	**23**	**22**	**12**	**12**	**8.98**	**Coatomer subunit epsilon OS=Homo sapiens GN=COPE PE=1 SV=3**
COPG1	**Q9Y678**	**66**	**98967**	**3**	**2**	**3**	**2**	**0.10**	**Coatomer subunit gamma-1 OS=Homo sapiens GN=COPG1 PE=1 SV=1**
CPSF6	F8WJN3	249	52409	7	5	6	4	0.43	Cleavage and polyadenylation-specificity factor subunit 6 OS=Homo sapiens GN=CPSF6 PE=1 SV=1
CPSF7	Q8N684	133	51179	7	4	7	4	0.45	Isoform 2 of Cleavage and polyadenylation specificity factor subunit 7 OS=Homo sapiens GN=CPSF7
CPT1A	P50416	123	88995	6	5	6	5	0.30	Carnitine O-palmitoyltransferase 1, liver isoform OS=Homo sapiens GN=CPT1A PE=1 SV=2
CROCC	Q5TZA2	65	228787	16	1	16	1	0.02	Rootletin OS=Homo sapiens GN=CROCC PE=1 SV=1
CSDE1	E9PLT0	49	75164	5	2	4	2	0.13	Cold shock domain-containing protein E1 OS=Homo sapiens GN=CSDE1 PE=1 SV=1
CSNK1A1	P48729	70	37771	3	2	3	2	0.28	Isoform 3 of Casein kinase I isoform alpha OS=Homo sapiens GN=CSNK1A1
CSNK1E	H0Y559	51	12971	2	2	2	2	1.04	Casein kinase I isoform epsilon (Fragment) OS=Homo sapiens GN=CSNK1E PE=1 SV=1
CTAG2	O75638	50	18453	1	1	1	1	0.29	Isoform LAGE-1A of Cancer/testis antigen 2 OS=Homo sapiens GN=CTAG2
CTTN	H7C314	32	25136	1	1	1	1	0.21	Src substrate cortactin (Fragment) OS=Homo sapiens GN=CTTN PE=1 SV=1
CWF19L1	Q69YN2	52	46078	1	1	1	1	0.11	Isoform 3 of CWF19-like protein 1 OS=Homo sapiens GN=CWF19L1
DAP3	P51398	167	41361	7	5	7	5	0.77	Isoform 2 of 28S ribosomal protein S29, mitochondrial OS=Homo sapiens GN=DAP3
DARS	H7BZ35	58	21708	5	4	5	4	1.36	Aspartate--tRNA ligase, cytoplasmic (Fragment) OS=Homo sapiens GN=DARS PE=1 SV=1
DBN1	G10643	76	72068	4	2	4	2	0.14	Isoform 2 of Drebrin OS=Homo sapiens GN=DBN1
DCD	P81605	171	11391	4	4	3	3	2.37	Dermcidin OS=Homo sapiens GN=DCD PE=1 SV=2
DCTN4	Q9UJW0	16	54030	2	1	2	1	0.09	Isoform 3 of Dynactin subunit 4 OS=Homo sapiens GN=DCTN4
DDB1	Q16531	43	128142	4	2	4	2	0.08	DNA damage-binding protein 1 OS=Homo sapiens GN=DDB1 PE=1 SV=1
DDOST	P39656	38	46719	2	1	2	1	0.11	Isoform 2 of Dolichyl-diphosphooligosaccharide--protein glycosyltransferase 48 kDa subunit OS=Homo sapiens GN=DDOST
DDR2	Q16832	21	97586	2	1	2	1	0.05	Discoidin domain-containing receptor 2 OS=Homo sapiens GN=DDR2 PE=1 SV=2
DDX21	Q9NR30	43	80121	4	2	4	2	0.13	Isoform 2 of Nucleolar RNA helicase 2 OS=Homo sapiens GN=DDX21
DDX39B	Q13838	385	51103	13	13	10	10	1.52	Isoform 2 of Spliceosome RNA helicase DDX39B OS=Homo sapiens GN=DDX39B
DDX47	Q9H0S4	50	45312	3	2	2	1	0.11	Isoform 2 of Probable ATP-dependent RNA helicase DDX47 OS=Homo sapiens GN=DDX47
DECR1	E5RJG7	60	19429	2	1	2	1	0.27	2,4-dienoyl-CoA reductase, mitochondrial (Fragment) OS=Homo sapiens GN=DECR1 PE=1 SV=1
DERL1	B4E1G1	16	17079	1	1	1	1	0.31	Derlin-1 OS=Homo sapiens GN=DERL1 PE=1 SV=1
DHCR24	Q15392	57	55456	3	2	3	2	0.19	Isoform 2 of Delta(24)-sterol reductase OS=Homo sapiens GN=DHCR24
DHX30	Q7L2E3	579	137057	22	17	20	15	0.68	Isoform 2 of Putative ATP-dependent RNA helicase DHX30 OS=Homo sapiens GN=DHX30
DHX37	F5H3Y4	17	108432	2	1	2	1	0.04	Probable ATP-dependent RNA helicase DHX37 OS=Homo sapiens GN=DHX37 PE=1 SV=1
DHX9	Q08211	828	142181	26	22	24	20	0.95	ATP-dependent RNA helicase A OS=Homo sapiens GN=DHX9 PE=1 SV=4
DIMT1	D6RCL3	44	17173	3	1	2	1	0.31	Probable dimethyladenosine transferase OS=Homo sapiens GN=DIMT1 PE=1 SV=1
DLD	E9PEX6	24	52182	1	1	1	1	0.09	Dihydrolipoyl dehydrogenase, mitochondrial OS=Homo sapiens GN=DLD PE=1 SV=1
DNAJA1	P31689	161	37762	8	6	5	4	0.65	Isoform 2 of Dnaj homolog subfamily A member 1 OS=Homo sapiens GN=DNAJA1
DNAJA2	O60884	71	46344	3	2	3	2	0.23	Dnaj homolog subfamily A member 2 OS=Homo sapiens GN=DNAJA2 PE=1 SV=1
DNAJB11	H7C2Y5	57	19249	5	1	4	1	0.28	Dnaj homolog subfamily B member 11 (Fragment) OS=Homo sapiens GN=DNAJB11 PE=1 SV=2
DNAJC8	O75937	105	29823	3	3	3	3	0.60	Dnaj homolog subfamily C member 8 OS=Homo sapiens GN=DNAJC8 PE=1 SV=2
DNAJC9	Q8WXX5	29	30062	1	1	1	1	0.17	Dnaj homolog subfamily C member 9 OS=Homo sapiens GN=DNAJC9 PE=1 SV=1
DPM1	H0Y368	47	33537	4	1	4	1	0.15	Dolichol-phosphate mannosyltransferase subunit 1 (Fragment) OS=Homo sapiens GN=DPM1 PE=1 SV=1
DRG1	Q9Y295	106	40802	6	3	5	3	0.41	Developmentally-regulated GTP-binding protein 1 OS=Homo sapiens GN=DRG1 PE=1 SV=1
DYNC1H1	Q14204	31	534809	8	1	8	1	0.01	Cytoplasmic dynein 1 heavy chain 1 OS=Homo sapiens GN=DYNC1H1 PE=1 SV=5
EBNA1BP2	H7C2Q8	49	40830	4	2	3	2	0.26	EBNA1 binding protein 2, isoform CRA_d OS=Homo sapiens GN=EBNA1BP2 PE=1 SV=1

PTBP2	Q9UKA9	90	57725	4	3	4	3	0.28	Isoform 2 of Polypyrimidine tract-binding protein 2 OS=Homo sapiens GN=PTBP2
PTCD3	Q96EY7	32	32128	1	1	1	1	0.16	Isoform 2 of Pentatricopeptide repeat domain-containing protein 3, mitochondrial OS=Homo sapiens GN=PTCD3
PTCHD3	Q3KNS1	17	87842	3	1	2	1	0.06	Patched domain-containing protein 3 OS=Homo sapiens GN=PTCHD3 PE=1 SV=3
PTS	Q03393	163	16489	8	8	5	5	6.19	6-pyruvoyl tetrahydobiopterin synthase OS=Homo sapiens GN=PTS PE=1 SV=1
PUF60	H0YCP8	38	28260	3	1	2	1	0.18	Poly(U)-binding-splicing factor PUF60 (Fragment) OS=Homo sapiens GN=PUF60 PE=1 SV=1
PURA	Q00577	59	35003	3	1	3	1	0.14	Transcriptional activator protein Pur-alpha OS=Homo sapiens GN=PURA PE=1 SV=2
PURB	Q96QR8	30	33392	2	1	2	1	0.15	Transcriptional activator protein Pur-beta OS=Homo sapiens GN=PURB PE=1 SV=3
PWP1	B4DJV5	35	49464	2	1	2	1	0.10	Periodic tryptophan protein 1 homolog OS=Homo sapiens GN=PWP1 PE=1 SV=1
PYM1	Q9BRP8	147	22691	7	6	6	6	2.46	Isoform 2 of Partner of Y14 and mago OS=Homo sapiens GN=WIBG
RAB1A	**P62820**	**76**	**22891**	**5**	**2**	**3**	**2**	**0.51**	**Ras-related protein Rab-1A OS=Homo sapiens GN=RAB1A PE=1 SV=3**
RAB5C	P51148	60	27247	2	1	2	1	0.19	Isoform 2 of Ras-related protein Rab-5C OS=Homo sapiens GN=RAB5C
RAB9A	P51151	27	23108	1	1	1	1	0.22	Ras-related protein Rab-9A OS=Homo sapiens GN=RAB9A PE=1 SV=1
RACK1	P63244	167	35511	7	5	6	5	0.94	Guanine nucleotide-binding protein subunit beta-2-like 1 OS=Homo sapiens GN=GNB2L1 PE=1 SV=3
RANBP9	Q96S59	24	43607	1	1	1	1	0.11	Isoform 2 of Ran-binding protein 9 OS=Homo sapiens GN=RANBP9
RAR5	P54136	222	76129	12	9	12	9	0.75	Arginine--tRNA ligase, cytoplasmic OS=Homo sapiens GN=RARS PE=1 SV=2
RAVER1	K7EKR9	54	10993	1	1	1	1	0.52	Ribonucleoprotein PTB-binding 1 (Fragment) OS=Homo sapiens GN=RAVER1 PE=1 SV=1
RBBP7	Q5JP01	62	31883	4	2	3	2	0.34	Histone-binding protein RBBP7 (Fragment) OS=Homo sapiens GN=RBBP7 PE=1 SV=1
RBM39	H0Y4X3	64	36888	3	3	3	3	0.47	RNA-binding protein 39 (Fragment) OS=Homo sapiens GN=RBM39 PE=1 SV=2
RBM47	A0AV96	39	57340	1	1	1	1	0.09	Isoform 2 of RNA-binding protein 47 OS=Homo sapiens GN=RBM47
RBM6	P78332	98	129192	6	4	6	4	0.16	RNA-binding protein 6 OS=Homo sapiens GN=RBM6 PE=1 SV=5
RCL1	Q9Y2P8	23	41273	1	1	1	1	0.12	RNA 2'-terminal phosphate cyclase-like protein OS=Homo sapiens GN=RCL1 PE=1 SV=3
RFC1	P35251	65	128617	4	2	4	2	0.08	Isoform 2 of Replication factor C subunit 1 OS=Homo sapiens GN=RFC1
RFC2	P35250	40	39588	2	1	2	1	0.13	Replication factor C subunit 2 OS=Homo sapiens GN=RFC2 PE=1 SV=3
RFC3	P40938	51	35589	3	1	3	1	0.14	Isoform 2 of Replication factor C subunit 3 OS=Homo sapiens GN=RFC3
RFC4	P35249	78	40170	4	3	4	3	0.42	Replication factor C subunit 4 OS=Homo sapiens GN=RFC4 PE=1 SV=2
RFC5	P40937	32	36367	3	1	2	1	0.14	Isoform 2 of Replication factor C subunit 5 OS=Homo sapiens GN=RFC5
RHOC	Q5JR08	34	21794	1	1	1	1	0.24	Rho-related GTP-binding protein RhoC (Fragment) OS=Homo sapiens GN=RHOC PE=1 SV=2
ROCK1	Q13464	140	159102	13	7	12	7	0.23	Rho-associated protein kinase 1 OS=Homo sapiens GN=ROCK1 PE=1 SV=1
RPA1	I3L4R8	39	35378	2	1	2	1	0.14	Replication protein A 70 kDa DNA-binding subunit (Fragment) OS=Homo sapiens GN=RPA1 PE=1 SV=1
RPL10	X1WI28	540	23416	20	17	13	10	12.46	60S ribosomal protein L10 (Fragment) OS=Homo sapiens GN=RPL10 PE=1 SV=1
RPL15	P61313	191	24245	9	8	8	7	2.88	60S ribosomal protein L15 OS=Homo sapiens GN=RPL15 PE=1 SV=2
RPL23A	K7EJV9	260	19354	7	7	7	7	4.44	60S ribosomal protein L23a (Fragment) OS=Homo sapiens GN=RPL23A PE=1 SV=1
RPL26	J3KT18	159	11491	9	7	6	6	15.54	60S ribosomal protein L26 (Fragment) OS=Homo sapiens GN=RPL26 PE=1 SV=2
RPL32	D3YTB1	19	15721	1	1	1	1	0.34	60S ribosomal protein L32 (Fragment) OS=Homo sapiens GN=RPL32 PE=1 SV=1
RPL34	P49207	121	13513	5	5	5	5	4.55	60S ribosomal protein L34 OS=Homo sapiens GN=RPL34 PE=1 SV=3
RPL36A	J3KQN4	41	16653	4	1	4	1	0.32	60S ribosomal protein L36a OS=Homo sapiens GN=RPL36A PE=3 SV=1
RPL37A	C9J4Z3	99	7847	6	4	4	2	2.19	60S ribosomal protein L37a OS=Homo sapiens GN=RPL37A PE=1 SV=1
RPL6	Q02878	501	32765	13	13	11	11	3.85	60S ribosomal protein L6 OS=Homo sapiens GN=RPL6 PE=1 SV=3
RPL8	P62917	302	28235	12	10	10	8	3.47	60S ribosomal protein L8 OS=Homo sapiens GN=RPL8 PE=1 SV=2
RPLP2	P05387	134	11658	4	4	4	4	3.90	60S acidic ribosomal protein P2 OS=Homo sapiens GN=RPLP2 PE=1 SV=1
RPN2	Q5JYR7	90	37200	3	2	3	2	0.29	Dolichyl-diphosphooligosaccharide--protein glycosyltransferase subunit 2 (Fragment) OS=Homo sapiens GN=RPN2 PE=1 SV=2
RPS16	M0R210	279	14524	11	10	8	8	11.91	40S ribosomal protein S16 OS=Homo sapiens GN=RPS16 PE=1 SV=1
RPS27	Q5T4L4	201	7523	7	7	4	4	19.62	40S ribosomal protein S27 OS=Homo sapiens GN=RPS27 PE=1 SV=1
RPS27A	P62979	302	18296	17	14	7	6	4.95	Ubiquitin-40S ribosomal protein S27a OS=Homo sapiens GN=RPS27A PE=1 SV=2
RPS27L	Q71UM5	90	9813	4	3	2	2	3.12	40S ribosomal protein S27-like OS=Homo sapiens GN=RPS27L PE=1 SV=3
RPS8	P62241	318	24475	12	10	8	8	3.64	40S ribosomal protein S8 OS=Homo sapiens GN=RPS8 PE=1 SV=2
RPUSD3	Q6P087	34	37264	2	1	2	1	0.13	Isoform 2 of RNA pseudouridylate synthase domain-containing protein 3 OS=Homo sapiens GN=RPUSD3
RRBP1	F8W755	75	84674	7	2	6	2	0.12	Ribosome-binding protein 1 OS=Homo sapiens GN=RRBP1 PE=1 SV=1
RRP1B	Q14684	60	82467	1	1	1	1	0.06	Isoform 2 of Ribosomal RNA processing protein 1 homolog B OS=Homo sapiens GN=RRP1B
RTRAF	Q9Y224	268	28165	7	7	5	5	1.30	UPF0568 protein C14orf166 OS=Homo sapiens GN=C14orf166 PE=1 SV=1
RUVBL1	Q9Y265	60	42499	2	2	2	2	0.25	Isoform 2 of RuvB-like 1 OS=Homo sapiens GN=RUVBL1
RUVBL2	M0R0Y3	131	38845	5	5	5	5	0.83	RuvB-like 2 OS=Homo sapiens GN=RUVBL2 PE=1 SV=1
SAFB2	Q14151	70	107921	5	2	5	2	0.09	Scaffold attachment factor B2 OS=Homo sapiens GN=SAFB2 PE=1 SV=1
SAMM50	Q9Y512	41	52342	2	1	2	1	0.09	Sorting and assembly machinery component 50 homolog OS=Homo sapiens GN=SAMM50 PE=1 SV=3
SAR1A	**Q9NR31**	**20**	**17603**	**3**	**1**	**2**	**1**	**0.30**	**Isoform 2 of GTP-binding protein SAR1a OS=Homo sapiens GN=SAR1A**
SAR1B	**Q9Y6B6**	**37**	**22510**	**3**	**1**	**2**	**1**	**0.23**	**GTP-binding protein SAR1b OS=Homo sapiens GN=SAR1B PE=1 SV=1**
SART1	O43290	77	90371	3	2	3	2	0.11	U4/U6.U5 tri-snRNP-associated protein 1 OS=Homo sapiens GN=SART1 PE=1 SV=1
SCYL2	Q6P3W7	98	104327	3	3	2	2	0.09	SCY1-like protein 2 OS=Homo sapiens GN=SCYL2 PE=1 SV=1
SERPINH1	E9PPV6	94	35758	4	3	4	3	0.48	Serpin H1 OS=Homo sapiens GN=SERPINH1 PE=1 SV=1
SF1	Q15637	44	68817	1	1	1	1	0.07	Isoform 2 of Splicing factor 1 OS=Homo sapiens GN=SF1
SF3A1	Q15459	452	88888	23	19	19	17	1.60	Splicing factor 3A subunit 1 OS=Homo sapiens GN=SF3A1 PE=1 SV=1
SF3A2	Q15428	79	49338	4	3	4	3	0.33	Splicing factor 3A subunit 2 OS=Homo sapiens GN=SF3A2 PE=1 SV=2
SF3A3	Q12874	304	59154	11	9	9	7	0.75	Splicing factor 3A subunit 3 OS=Homo sapiens GN=SF3A3 PE=1 SV=1
SF3B1	O75533	1022	146479	41	34	32	27	1.55	Splicing factor 3B subunit 1 OS=Homo sapiens GN=SF3B1 PE=1 SV=2
SF3B4	Q5SZ64	106	20733	2	2	2	2	0.57	Splicing factor 3B subunit 4 (Fragment) OS=Homo sapiens GN=SF3B4 PE=1 SV=1
SKP1	E5RJR5	65	18879	1	1	1	1	0.28	S-phase kinase-associated protein 1 OS=Homo sapiens GN=SKP1 PE=1 SV=1
SLC1A3	P43003	90	55284	2	1	2	1	0.09	Isoform 2 of Excitatory amino acid transporter 1 OS=Homo sapiens GN=SLC1A3
SLC25A1	B4DP62	54	23423	1	1	1	1	0.22	Solute carrier family 25 (Mitochondrial carrier citrate transporter), member 1, isoform CRA_b OS=Homo sapiens GN=SLC25A1 PE=1 SV=1
SLC25A13	Q9UJS0	18	74656	2	1	2	1	0.07	Isoform 2 of Calcium-binding mitochondrial carrier protein Aralar2 OS=Homo sapiens GN=SLC25A13
SLC25A5	P05141	88	33059	3	3	3	3	0.53	ADP/ATP translocase 2 OS=Homo sapiens GN=SLC25A5 PE=1 SV=7
SLC3A2	J3KPF3	171	68230	6	3	6	3	0.23	4F2 cell-surface antigen heavy chain OS=Homo sapiens GN=SLC3A2 PE=1 SV=1
SLC7A5	Q01650	66	55659	1	1	1	1	0.09	Large neutral amino acids transporter small subunit 1 OS=Homo sapiens GN=SLC7A5 PE=1 SV=2
SLIRP	Q96DT3	18	12171	1	1	1	1	0.46	Isoform 2 of SRA stem-loop-interacting RNA-binding protein, mitochondrial OS=Homo sapiens GN=SLIRP
SND1	Q7KZF4	163	102618	12	6	11	6	0.32	Staphylococcal nuclease domain-containing protein 1 OS=Homo sapiens GN=SND1 PE=1 SV=1
SNRNP200	O75643	135	246006	17	4	13	4	0.08	U5 small nuclear ribonucleoprotein 200 kDa helicase OS=Homo sapiens GN=SNRNP200 PE=1 SV=2
SNRNP40	Q96DI7	18	45001	1	1	1	1	0.11	Isoform 2 of U5 small nuclear ribonucleoprotein 40 kDa protein OS=Homo sapiens GN=SNRNP40
SNRNP70	P08621	43	51583	4	2	4	2	0.20	U1 small nuclear ribonucleoprotein 70 kDa OS=Homo sapiens GN=SNRNP70 PE=1 SV=2
SNRPA1	P09661	288	28512	9	8	8	7	2.16	U2 small nuclear ribonucleoprotein A' OS=Homo sapiens GN=SNRPA1 PE=1 SV=2
SNRPB2	P08579	44	25470	2	1	2	1	0.20	U2 small nuclear ribonucleoprotein B'' OS=Homo sapiens GN=SNRPB2 PE=1 SV=1
SNRPD1	P62314	113	13273	3	3	2	2	1.01	Small nuclear ribonucleoprotein Sm D1 OS=Homo sapiens GN=SNRPD1 PE=1 SV=1
SNRPD2	P62316	169	13632	7	7	6	6	9.82	Small nuclear ribonucleoprotein Sm D2 OS=Homo sapiens GN=SNRPD2 PE=1 SV=1
SNRPG15	A8MWD9	90	8595	6	3	4	2	4.01	Putative small nuclear ribonucleoprotein G-like protein 15 OS=Homo sapiens GN=SNRPG15 PE=5 SV=2
SNRPN	J3QLE5	488	17706	15	15	7	7	9.64	Small nuclear ribonucleoprotein-associated protein N (Fragment) OS=Homo sapiens GN=SNRPN PE=4 SV=1
SORBS2	O94875	21	135708	2	1	2	1	0.04	Isoform 11 of Sorbin and SH3 domain-containing protein 2 OS=Homo sapiens GN=SORBS2
SPDEF	O95238	20	35920	2	1	2	1	0.14	Isoform 2 of SAM pointed domain-containing Ets transcription factor OS=Homo sapiens GN=SPDEF
SPINDOC	Q9BUA3	73	41297	7	3	6	3	0.41	Uncharacterized protein C11orf84 OS=Homo sapiens GN=C11orf84 PE=1 SV=3
SPTAN1	Q13813	2509	282906	83	74	71	63	1.92	Isoform 3 of Spectrin alpha chain, non-erythrocytic 1 OS=Homo sapiens GN=SPTAN1
SPTLC1	O15269	121	53281	2	2	2	2	0.19	Serine palmitoyltransferase 1 OS=Homo sapiens GN=SPTLC1 PE=1 SV=1
SPTLC3	H0Y733	18	13620	2	2	1	1	0.41	Serine palmitoyltransferase 3 (Fragment) OS=Homo sapiens GN=SPTLC3 PE=4 SV=1
SRP68	Q9UHB9	75	67775	2	1	2	1	0.07	Isoform 2 of Signal recognition particle subunit SRP68 OS=Homo sapiens GN=SRP68
SRPK2	H7C5L6	30	33605	2	1	2	1	0.15	SRSF protein kinase 2 (Fragment) OS=Homo sapiens GN=SRPK2 PE=1 SV=1
SRPRB	Q9Y5M8	98	29912	5	4	5	4	0.88	Signal recognition particle receptor subunit beta OS=Homo sapiens GN=SRPRB PE=1 SV=3
SRRT	H7C3A1	68	57154	1	1	1	1	0.09	Serrate RNA effector molecule homolog (Fragment) OS=Homo sapiens GN=SRRT PE=1 SV=1
SRSF1	J3KTL2	322	28426	9	9	7	7	2.18	Serine/arginine-rich splicing factor 1 OS=Homo sapiens GN=SRSF1 PE=1 SV=1
SRSF3	P84103	104	14422	5	4	4	4	2.63	Isoform 2 of Serine/arginine-rich splicing factor 3 OS=Homo sapiens GN=SRSF3
SRSF4	Q08170	69	56759	4	3	4	3	0.28	Serine/arginine-rich splicing factor 4 OS=Homo sapiens GN=SRSF4 PE=1 SV=2
SRSF7	C9JA82	133	27140	6	6	4	4	1.37	Serine/arginine-rich splicing factor 7 OS=Homo sapiens GN=SRSF7 PE=1 SV=1
SSR1	C9JZQ1	119	33866	2	2	1	1	0.15	Translocon-associated protein subunit alpha OS=Homo sapiens GN=SSR1 PE=1 SV=1
SSR4	P51571	125	19158	3	3	3	3	1.07	Translocon-associated protein subunit delta OS=Homo sapiens GN=SSR4 PE=1 SV=1
STAU2	Q9NUL3	37	43397	4	2	4	2	0.24	Isoform 6 of Double-stranded RNA-binding protein Staufen homolog 2 OS=Homo sapiens GN=STAU2
STOM	P27105	445	31882	13	10	11	9	3.37	Erythrocyte band 7 integral membrane protein OS=Homo sapiens GN=STOM PE=1 SV=3
STRAP	B4DN36	37	40095	3	2	3	2	0.26	Serine-threonine kinase receptor-associated protein OS=Homo sapiens GN=STRAP PE=1 SV=1
STX6	O43752	13	17480	2	1	2	1	0.31	Isoform 2 of Syntaxin-6 OS=Homo sapiens GN=STX6
SUB1	P53999	43	14386	1	1	1	1	0.38	Activated RNA polymerase II transcriptional coactivator p15 OS=Homo sapiens GN=SUB1 PE=1 SV=3
SVIL	O95425	39	202262	2	1	2	1	0.02	Isoform 2 of Supervillin OS=Homo sapiens GN=SVIL
SYTL2	Q9HCH5	28	84884	2	1	2	1	0.06	Isoform 12 of Synaptotagmin-like protein 2 OS=Homo sapiens GN=SYTL2
TAB2	Q9NYJ8	77	58323	3	2	3	2	0.18	Isoform 2 of TGF-beta-activated kinase 1 and MAP3K7-binding protein 2 OS=Homo sapiens GN=TAB2
TCP1	P17987	174	60819	10	6	9	5	0.59	T-complex protein 1 subunit alpha OS=Homo sapiens GN=TCP1 PE=1 SV=1
TECR	Q9NZ01	40	36410	2	1	2	1	0.14	Very-long-chain enoyl-CoA reductase OS=Homo sapiens GN=TECR PE=1 SV=1
TFRC	G3V0E5	80	76259	3	3	3	3	0.20	Transferrin receptor (P90, CD71), isoform CRA_c OS=Homo sapiens GN=TFRC PE=1 SV=1
TGFBR1	B4DY26	29	49642	3	1	2	1	0.10	TGF-beta receptor type-1 OS=Homo sapiens GN=TGFBR1 PE=1 SV=1
TIMM50	M0R003	76	28432	3	1	3	1	0.18	Mitochondrial import inner membrane translocase subunit TIM50 (Fragment) OS=Homo sapiens GN=TIMM50 PE=1 SV=1
TJP2	Q9UDY2	68	131516	4	3	4	3	0.11	Isoform C1 of Tight junction protein ZO-2 OS=Homo sapiens GN=TJP2
TKT	B4E022	146	63410	7	5	6	4	0.35	Transketolase OS=Homo sapiens GN=TKT PE=1 SV=1
TMED10	G3V2K7	65	17008	1	1	1	1	0.32	Transmembrane emp24 domain-containing protein 10 OS=Homo sapiens GN=TMED10 PE=1 SV=1
TMED2	F5GX39	36	13679	1	1	1	1	0.41	Transmembrane emp24 domain-containing protein 2 OS=Homo sapiens GN=TMED2 PE=1 SV=1
TMEM214	H7BZ10	68	15615	2	1	2	1	0.35	Transmembrane protein 214 (Fragment) OS=Homo sapiens GN=TMEM214 PE=1 SV=1
TMEM59	Q9BXS4	85	36884	4	2	3	2	0.29	Transmembrane protein 59 OS=Homo sapiens GN=TMEM59 PE=1 SV=1
TMEM9	B1ALM5	16	21458	2	1	2	1	0.24	Transmembrane protein 9 OS=Homo sapiens GN=TMEM9 PE=1 SV=1
TMOD3	Q9NVL9	85	39741	3	3	3	3	0.43	Tropomodulin-3 OS=Homo sapiens GN=TMOD3 PE=1 SV=1
TNFRSF1A	F5H061	27	47081	2	1	2	1	0.11	Tumor necrosis factor receptor superfamily member 1A OS=Homo sapiens GN=TNFRSF1A PE=4 SV=1
TPI1	P60174	139	26938	6	6	6	6	1.84	Isoform 2 of Triosephosphate isomerase OS=Homo sapiens GN=TPI1

1475

MCU	S4R468	60	19186	1	1	1	1	0.28	Calcium uniporter protein, mitochondrial (Fragment) OS=Homo sapiens GN=MCU PE=4 SV=1
MDH2	G3XAL0	58	24921	1	1	1	1	0.21	Malate dehydrogenase OS=Homo sapiens GN=MDH2 PE=1 SV=1
MGST2	Q99735	62	8524	1	1	1	1	0.71	Isoform 2 of Microsomal glutathione S-transferase 2 OS=Homo sapiens GN=MGST2
MGST3	Q5VV87	93	14427	1	1	1	1	0.38	Microsomal glutathione S-transferase 3 OS=Homo sapiens GN=MGST3 PE=1 SV=1
MISP	Q8IVT2	45	75482	4	1	2	1	0.06	Mitotic interactor and substrate of PLK1 OS=Homo sapiens GN=MISP PE=1 SV=1
MLEC	H0YG07	41	19893	2	1	2	1	0.27	Malectin (Fragment) OS=Homo sapiens GN=MLEC PE=1 SV=1
MOB1B	Q7L9L4	50	25654	1	1	1	1	0.20	Isoform 2 of MOB kinase activator 1B OS=Homo sapiens GN=MOB1B
MOGS	Q13724	111	92032	3	2	3	2	0.11	Mannosyl-oligosaccharide glucosidase OS=Homo sapiens GN=MOGS PE=1 SV=5
MORF4L2	Q15014	43	32345	2	1	2	1	0.16	Mortality factor 4-like protein 2 OS=Homo sapiens GN=MORF4L2 PE=1 SV=1
MRPL11	Q9Y3B7	58	20727	3	2	3	2	0.57	39S ribosomal protein L11, mitochondrial OS=Homo sapiens GN=MRPL11 PE=1 SV=1
MRPL14	Q6P1L8	38	16165	2	1	2	1	0.33	39S ribosomal protein L14, mitochondrial OS=Homo sapiens GN=MRPL14 PE=1 SV=1
MRPL22	J3KQY1	105	26686	4	4	4	4	1.02	39S ribosomal protein L22, mitochondrial OS=Homo sapiens GN=MRPL22 PE=1 SV=1
MRPL24	Q96A35	40	25013	1	1	1	1	0.21	39S ribosomal protein L24, mitochondrial OS=Homo sapiens GN=MRPL24 PE=1 SV=1
MRPL3	H0Y9G6	57	40898	5	2	5	2	0.26	39S ribosomal protein L3, mitochondrial (Fragment) OS=Homo sapiens GN=MRPL3 PE=1 SV=1
MRPL30	Q8TCC3	15	21939	1	1	1	1	0.24	Isoform 2 of 39S ribosomal protein L30, mitochondrial OS=Homo sapiens GN=MRPL30
MRPL37	S4R369	60	55659	4	1	4	1	0.09	39S ribosomal protein L37, mitochondrial OS=Homo sapiens GN=MRPL37 PE=1 SV=1
MRPL38	Q96DV4	65	44968	2	2	2	2	0.23	39S ribosomal protein L38, mitochondrial OS=Homo sapiens GN=MRPL38 PE=1 SV=2
MRPL4	K7ES61	151	33771	6	4	5	3	0.52	39S ribosomal protein L4, mitochondrial (Fragment) OS=Homo sapiens GN=MRPL4 PE=1 SV=1
MRPL40	Q9NQ50	15	24475	1	1	1	1	0.21	39S ribosomal protein L40, mitochondrial OS=Homo sapiens GN=MRPL40 PE=1 SV=1
MRPL44	Q9H9J2	127	37854	7	4	6	4	0.64	39S ribosomal protein L44, mitochondrial OS=Homo sapiens GN=MRPL44 PE=1 SV=1
MRPL45	Q9BRJ2	78	35613	3	2	3	2	0.30	39S ribosomal protein L45, mitochondrial OS=Homo sapiens GN=MRPL45 PE=1 SV=2
MRPL48	F5H8D0	45	13699	2	1	2	1	0.41	39S ribosomal protein L48, mitochondrial OS=Homo sapiens GN=MRPL48 PE=1 SV=1
MRPL49	H0YDP7	68	14731	3	1	3	1	0.37	39S ribosomal protein L49, mitochondrial (Fragment) OS=Homo sapiens GN=MRPL49 PE=1 SV=1
MRPL9	Q9BVD2	37	30395	2	1	2	1	0.17	39S ribosomal protein L9, mitochondrial OS=Homo sapiens GN=MRPL9 PE=1 SV=2
MRPS2	Q5T8A0	44	30745	1	1	1	1	0.17	28S ribosomal protein S2, mitochondrial (Fragment) OS=Homo sapiens GN=MRPS2 PE=1 SV=1
MRPS23	J3QLR8	56	17563	1	1	1	1	0.30	28S ribosomal protein S23, mitochondrial OS=Homo sapiens GN=MRPS23 PE=1 SV=1
MRPS27	G5EA06	37	41588	3	3	3	3	0.40	28S ribosomal protein S27, mitochondrial OS=Homo sapiens GN=MRPS27 PE=1 SV=1
MRPS28	H0YAT2	46	16063	2	1	2	1	0.34	28S ribosomal protein S28, mitochondrial (Fragment) OS=Homo sapiens GN=MRPS28 PE=1 SV=1
MRPS30	Q9NP92	23	50960	1	1	1	1	0.10	28S ribosomal protein S30, mitochondrial OS=Homo sapiens GN=MRPS30 PE=1 SV=2
MRPS34	C9JI19	44	26373	2	1	2	1	0.19	28S ribosomal protein S34, mitochondrial OS=Homo sapiens GN=MRPS34 PE=1 SV=2
MRPS7	J3QKW2	70	20882	3	3	2	2	0.57	28S ribosomal protein S7, mitochondrial OS=Homo sapiens GN=MRPS7 PE=1 SV=1
MRPS9	P82933	131	46034	6	4	6	4	0.51	28S ribosomal protein S9, mitochondrial OS=Homo sapiens GN=MRPS9 PE=1 SV=2
MSI2	J3KTC1	62	15507	1	1	1	1	0.35	Protein turtle homolog B (Fragment) OS=Homo sapiens GN=GSF3B PE=1 SV=2
MSN	P26038	23	67892	2	1	2	1	0.07	Moesin OS=Homo sapiens GN=MSN PE=1 SV=3
MTDH	Q86UE4	254	63856	12	9	10	9	0.95	Protein LYRIC OS=Homo sapiens GN=MTDH PE=1 SV=2
MTERF3	Q96E29	29	48055	2	1	2	1	0.10	Transcription termination factor 3, mitochondrial OS=Homo sapiens GN=MTERF3 PE=1 SV=2
MTHFD1	F5H2F4	44	111342	3	1	3	1	0.04	C-1-tetrahydrofolate synthase, cytoplasmic OS=Homo sapiens GN=MTHFD1 PE=1 SV=1
MUM1	Q2TAK8	14	71715	2	1	1	1	0.07	Isoform 2 of PWWP domain-containing protein MUM1 OS=Homo sapiens GN=MUM1
MYBBP1A	I3L1L3	64	141124	3	2	3	2	0.07	Myb-binding protein 1A (Fragment) OS=Homo sapiens GN=MYBBP1A PE=1 SV=1
MYO1E	Q12965	62	127552	3	1	3	1	0.04	Unconventional myosin-Ie OS=Homo sapiens GN=MYO1E PE=1 SV=2
MYO5B	Q9ULV0	65	215135	4	2	4	2	0.04	Unconventional myosin-Vb OS=Homo sapiens GN=MYO5B PE=1 SV=3
NACA	E9PAV3	62	205979	3	1	2	1	0.02	Nascent polypeptide-associated complex subunit alpha, muscle-specific form OS=Homo sapiens GN=NACA PE=1 SV=1
NAP1L1	H0YH88	120	21179	5	5	4	4	2.01	Nucleosome assembly protein 1-like 1 (Fragment) OS=Homo sapiens GN=NAP1L1 PE=1 SV=1
NAT10	Q9H0A0	85	108084	3	1	3	1	0.04	Isoform 2 of N-acetyltransferase 10 OS=Homo sapiens GN=NAT10
NCBP1	Q09161	61	92864	3	2	3	2	0.11	Nuclear cap-binding protein subunit 1 OS=Homo sapiens GN=NCBP1 PE=1 SV=1
NCOA5	Q9HCD5	75	65725	5	2	5	2	0.15	Nuclear receptor coactivator 5 OS=Homo sapiens GN=NCOA5 PE=1 SV=2
NDC1	Q9BTX1	61	61768	4	2	4	2	0.17	Isoform 4 of Nucleoporin NDC1 OS=Homo sapiens GN=NDC1
NDUFA9	Q16795	56	42654	3	1	3	1	0.12	NADH dehydrogenase [ubiquinone] 1 alpha subcomplex subunit 9, mitochondrial OS=Homo sapiens GN=NDUFA9 PE=1 SV=2
NELFE	E9PD43	25	30046	3	1	3	1	0.17	Negative elongation factor E (Fragment) OS=Homo sapiens GN=NELFE PE=1 SV=1
NEMF	O60524	41	121085	3	1	3	1	0.04	Isoform 3 of Nuclear export mediator factor NEMF OS=Homo sapiens GN=NEMF
NES	P48681	105	177788	6	3	6	3	0.08	Nestin OS=Homo sapiens GN=NES PE=1 SV=2
NFATC4	Q14934	20	91153	4	1	3	1	0.05	Isoform 11 of Nuclear factor of activated T cells, cytoplasmic 4 OS=Homo sapiens GN=NFATC4
NGRN	Q9NPE2	39	32502	2	1	2	1	0.16	Neugrin OS=Homo sapiens GN=NGRN PE=1 SV=2
NIPSNAP1	Q9BPW8	51	33460	2	2	2	2	0.32	Protein NipSnap homolog 1 OS=Homo sapiens GN=NIPSNAP1 PE=1 SV=1
NKRF	O15226	47	80130	3	1	3	1	0.06	Isoform 2 of NF-kappa-B-repressing factor OS=Homo sapiens GN=NKRF
NME1	P15531	118	19869	4	4	3	3	1.56	Isoform 2 of Nucleoside diphosphate kinase A OS=Homo sapiens GN=NME1
NME2P1	O60361	111	15690	5	4	4	3	2.29	Putative nucleoside diphosphate kinase OS=Homo sapiens GN=NME2P1 PE=5 SV=1
NOTCH2	Q04721	78	279082	4	3	4	3	0.05	Neurogenic locus notch homolog protein 2 OS=Homo sapiens GN=NOTCH2 PE=1 SV=3
NSMCE1	H3BR31	13	8492	2	1	1	1	0.71	Non-structural maintenance of chromosomes element 1 homolog OS=Homo sapiens GN=NSMCE1 PE=4 SV=1
NSUN5	Q96P11	24	51120	2	1	2	1	0.10	Isoform 2 of Probable 28S rRNA (cytosine-C(5))-methyltransferase OS=Homo sapiens GN=NSUN5
NTSC2	P49902	69	61858	2	2	2	2	0.16	Isoform 2 of Cytosolic purine 5'-nucleotidase OS=Homo sapiens GN=NTSC2
NUBP2	H3BNF0	36	26764	1	1	1	1	0.19	Cytosolic Fe-S cluster assembly factor NUBP2 OS=Homo sapiens GN=NUBP2 PE=1 SV=1
OCIAD1	D6RBN5	19	24409	2	1	2	1	0.21	OCIA domain-containing protein 1 OS=Homo sapiens GN=OCIAD1 PE=1 SV=1
OGT	O15294	60	116887	5	5	5	5	0.22	Isoform 1 of UDP-N-acetylglucosamine--peptide N-acetylglucosaminyltransferase 110 kDa subunit OS=Homo sapiens GN=OGT
P4HB	P07237	99	57480	6	4	5	4	0.39	Protein disulfide-isomerase OS=Homo sapiens GN=P4HB PE=1 SV=3
PABPC1	E7EQV3	1430	65878	45	39	30	28	8.92	Polyadenylate-binding protein 1 OS=Homo sapiens GN=PABPC1 PE=1 SV=1
PACSIN3	Q9UKS6	71	48799	3	1	3	1	0.10	Protein kinase C and casein kinase substrate in neurons protein 3 OS=Homo sapiens GN=PACSIN3 PE=1 SV=2
PAIP1	D6RE84	86	40225	2	2	2	2	0.26	Uncharacterized protein OS=Homo sapiens GN=PAIP1 PE=1 SV=1
PCBP2	F8VZX2	409	34121	13	12	9	8	2.46	Poly(rC)-binding protein 2 OS=Homo sapiens GN=PCBP2 PE=1 SV=1
PCNA	P12004	53	29092	3	1	3	1	0.18	Proliferating cell nuclear antigen OS=Homo sapiens GN=PCNA PE=1 SV=1
PDCD6	H0Y9X3	37	12277	2	1	2	1	0.46	Programmed cell death protein 6 (Fragment) OS=Homo sapiens GN=PDCD6 PE=1 SV=1
PDE4D	Q08499	24	24584	2	1	1	1	0.21	Isoform 12 of cAMP-specific 3',5'-cyclic phosphodiesterase 4D OS=Homo sapiens GN=PDE4D
PDIA3	P30101	53	57146	1	1	1	1	0.09	Protein disulfide-isomerase A3 OS=Homo sapiens GN=PDIA3 PE=1 SV=4
PDIA6	Q15084	33	54380	1	1	1	1	0.09	Isoform 2 of Protein disulfide-isomerase A6 OS=Homo sapiens GN=PDIA6
PEG10	Q86TG7	85	80692	3	2	3	2	0.12	Retrotransposon-derived protein PEG10 OS=Homo sapiens GN=PEG10 PE=1 SV=2
PFKFB2	B0FLL2	61	55199	4	2	4	2	0.19	6-phosphofructo-2-kinase/fructose-2, 6-bisphosphatase 2 transcript variant 3 OS=Homo sapiens GN=PFKFB2 PE=1 SV=1
PFN1	P07737	140	15216	4	4	4	4	2.40	Profilin-1 OS=Homo sapiens GN=PFN1 PE=1 SV=2
PGAM4	Q8N0Y7	29	28930	2	1	2	1	0.18	Probable phosphoglycerate mutase 4 OS=Homo sapiens GN=PGAM4 PE=2 SV=1
PHF5A	Q7RTV0	75	13138	3	2	3	2	1.03	PHD finger-like domain-containing protein 5A OS=Homo sapiens GN=PHF5A PE=1 SV=1
PI4KA	J3KN10	19	239244	4	1	4	1	0.02	Phosphatidylinositol 4-kinase alpha OS=Homo sapiens GN=PI4KA PE=1 SV=1
PKM	P14618	333	58470	12	9	11	9	1.07	Pyruvate kinase PKM OS=Homo sapiens GN=PKM PE=1 SV=4
PKP2	Q99959	59	97868	2	1	2	1	0.05	Plakophilin-2 OS=Homo sapiens GN=PKP2 PE=1 SV=2
PLEC	Q15149	#######	533462	317	290	228	210	6.25	Plectin OS=Homo sapiens GN=PLEC PE=1 SV=1
PLIN4	Q96Q06	115	135204	6	5	6	5	0.19	Perilipin-4 OS=Homo sapiens GN=PLIN4 PE=2 SV=2
PLP2	Q04941	23	17022	1	1	1	1	0.32	Proteolipid protein 2 OS=Homo sapiens GN=PLP2 PE=1 SV=1
POLDIP3	Q9BY77	18	43096	2	1	2	1	0.12	Isoform 2 of Polymerase delta-interacting protein 3 OS=Homo sapiens GN=POLDIP3
POP1	Q99575	48	116346	7	4	7	4	0.18	Ribonucleases P/MRP protein subunit POP1 OS=Homo sapiens GN=POP1 PE=1 SV=2
PPFIBP1	Q86W92	23	97303	3	1	3	1	0.05	Isoform 3 of Liprin-beta-1 OS=Homo sapiens GN=PPFIBP1
PPIA	P62937	320	18229	10	10	8	8	9.05	Peptidyl-prolyl cis-trans isomerase A OS=Homo sapiens GN=PPIA PE=1 SV=2
PPIB	P23284	43	23785	2	1	2	1	0.22	Peptidyl-prolyl cis-trans isomerase B OS=Homo sapiens GN=PPIB PE=1 SV=2
PPP1CC	F8VYE8	26	35669	2	2	2	2	0.30	Serine/threonine-protein phosphatase OS=Homo sapiens GN=PPP1CC PE=1 SV=1
PPP2R1A	P30153	69	66065	7	2	7	2	0.15	Serine/threonine-protein phosphatase 2A 65 kDa regulatory subunit A alpha isoform OS=Homo sapiens GN=PPP2R1A PE=1 SV=4
PPP2R2A	E5RFR9	64	23448	2	2	2	2	0.49	Serine/threonine-protein phosphatase 2A 55 kDa regulatory subunit B alpha isoform (Fragment) OS=Homo sapiens GN=PPP2R2A PE=1 SV=1
PRDX2	P32119	103	22049	5	4	5	4	1.33	Peroxiredoxin-2 OS=Homo sapiens GN=PRDX2 PE=1 SV=5
PRDX4	A6NJJ0	65	21403	3	1	2	1	0.24	Peroxiredoxin-4 (Fragment) OS=Homo sapiens GN=PRDX4 PE=1 SV=1
PRKACA	P17612	21	40042	3	1	3	1	0.12	Isoform 2 of cAMP-dependent protein kinase catalytic subunit alpha OS=Homo sapiens GN=PRKACA
PRKAR1A	X6RAV4	23	15032	2	1	2	1	0.36	cAMP-dependent protein kinase type I-alpha regulatory subunit OS=Homo sapiens GN=PRKAR1A PE=1 SV=1
PRKDC	E7EUY0	499	470050	26	16	25	15	0.16	DNA-dependent protein kinase catalytic subunit OS=Homo sapiens GN=PRKDC PE=1 SV=1
PRKRA	O75569	17	33672	2	1	2	1	0.15	Isoform 2 of Interferon-inducible double-stranded RNA-dependent protein kinase activator A OS=Homo sapiens GN=PRKRA
PRMT1	H7C2I1	59	43061	5	3	5	3	0.39	Protein arginine N-methyltransferase 1 OS=Homo sapiens GN=PRMT1 PE=1 SV=1
PRPF19	Q9UMS4	130	55603	7	5	7	5	0.53	Pre-mRNA-processing factor 19 OS=Homo sapiens GN=PRPF19 PE=1 SV=1
PRPF31	Q8WWY3	300	55649	18	12	9	8	0.97	U4/U6 small nuclear ribonucleoprotein Prp31 OS=Homo sapiens GN=PRPF31 PE=1 SV=2
PRPF4	O43172	81	58969	2	1	2	1	0.08	Isoform 2 of U4/U6 small nuclear ribonucleoprotein Prp4 OS=Homo sapiens GN=PRPF4
PRPF8	Q6P2Q9	63	274738	6	2	4	2	0.04	Pre-mRNA-processing-splicing factor 8 OS=Homo sapiens GN=PRPF8 PE=1 SV=2
PRPS2	P11908	585	35431	15	12	9	7	1.53	Isoform 2 of Ribose-phosphate pyrophosphokinase 2 OS=Homo sapiens GN=PRPS2
PRPSAP1	B4DP31	632	31474	17	15	8	8	3.44	Phosphoribosyl pyrophosphate synthase-associated protein 1 OS=Homo sapiens GN=PRPSAP1 PE=1 SV=1
PRPSAP2	O60256	602	41299	18	16	10	9	2.51	Phosphoribosyl pyrophosphate synthase-associated protein 2 OS=Homo sapiens GN=PRPSAP2 PE=1 SV=1
PRRC2C	E7EPN9	127	309159	13	6	12	6	0.10	Protein PRRC2C OS=Homo sapiens GN=PRRC2C PE=1 SV=1
PRSS56	P0CW18	48	65583	1	1	1	1	0.07	Serine protease 56 OS=Homo sapiens GN=PRSS56 PE=1 SV=1
PSMA1	F5GX11	26	26774	1	1	1	1	0.19	Proteasome subunit alpha type-1 OS=Homo sapiens GN=PSMA1 PE=1 SV=1
PSMB2	P49721	42	22993	1	1	1	1	0.23	Proteasome subunit beta type-2 OS=Homo sapiens GN=PSMB2 PE=1 SV=1
PSMB5	H0YJN8	48	13021	1	1	1	1	0.43	Proteasome subunit beta type-5 (Fragment) OS=Homo sapiens GN=PSMB5 PE=1 SV=1
PSMC3	R4GNH3	27	47608	3	1	2	1	0.10	26S proteasome regulatory subunit 6A OS=Homo sapiens GN=PSMC3 PE=1 SV=1
PSMC4	P43686	41	43595	4	1	4	1	0.11	Isoform 2 of 26S proteasome regulatory subunit 6B OS=Homo sapiens GN=PSMC4
PSMC5	P62195	147	44927	6	4	6	4	0.52	Isoform 2 of 26S proteasome regulatory subunit 8 OS=Homo sapiens GN=PSMC5
PSMC6	H0YJC0	30	29919	2	1	2	1	0.17	26S proteasome regulatory subunit 10B (Fragment) OS=Homo sapiens GN=PSMC6 PE=1 SV=1
PSMD11	O00231	46	47790	3	2	3	2	0.22	Isoform 2 of 26S proteasome non-ATPase regulatory subunit 11 OS=Homo sapiens GN=PSMD11
PSMD13	J3KNQ3	16	40090	1	1	1	1	0.12	26S proteasome non-ATPase regulatory subunit 13 OS=Homo sapiens GN=PSMD13 PE=1 SV=1
PSMD14	O00487	33	34726	1	1	1	1	0.14	26S proteasome non-ATPase regulatory subunit 14 OS=Homo sapiens GN=PSMD14 PE=1 SV=1
PSMD2	Q13200	105	82825	3	2	3	2	0.12	Isoform 2 of 26S proteasome non-ATPase regulatory subunit 2 OS=Homo sapiens GN=PSMD2
PSMD6	C9J7B7	16	16725	1	1	1	1	0.32	26S proteasome non-ATPase regulatory subunit 6 (Fragment) OS=Homo sapiens GN=PSMD6 PE=1 SV=1
PSMD7	P51665	41	37060	2	2	2	2	0.29	26S proteasome non-ATPase regulatory subunit 7 OS=Homo sapiens GN=PSMD7 PE=1 SV=2

1476

TPM1	**B7Z596**	19	31904	2	1	2	1	0.16	Tropomyosin alpha-1 chain OS=Homo sapiens GN=TPM1 PE=1 SV=1
TRA2B	**P62995**	105	22036	5	5	4	4	1.33	Isoform 3 of Transformer-2 protein homolog beta OS=Homo sapiens GN=TRA2B
TRAPPC1	**I3L1R8**	40	5018	1	1	1	1	1.45	Trafficking protein particle complex subunit 1 OS=Homo sapiens GN=TRAPPC1 PE=1 SV=1
TRAPPC11	**Q7Z392**	**97**	**125008**	**4**	**3**	**3**	**3**	**0.12**	**Isoform 3 of Trafficking protein particle complex subunit 11 OS=Homo sapiens GN=TRAPPC11**
TRAPPC12	**Q8WVT3**	**100**	**79781**	**4**	**3**	**4**	**3**	**0.19**	**Trafficking protein particle complex subunit 12 OS=Homo sapiens GN=TRAPPC12 PE=1 SV=3**
TRAPPC13	**A5PLN9**	**89**	**46589**	**3**	**3**	**2**	**2**	**0.22**	**Isoform 2 of Trafficking protein particle complex subunit 13 OS=Homo sapiens GN=TRAPPC13**
TRAPPC2	**P0DI81**	547	20418	20	17	7	6	6.85	Isoform 3 of Trafficking protein particle complex subunit 2 OS=Homo sapiens GN=TRAPPC2
TRAPPC2L	**H3BUK6**	63	12667	4	2	3	2	1.08	Trafficking protein particle complex subunit 2-like protein OS=Homo sapiens GN=TRAPPC2L PE=1 SV=1
TRAPPC3	**O43617**	**645**	**20432**	**16**	**16**	**10**	**10**	**14.60**	**Trafficking protein particle complex subunit 3 OS=Homo sapiens GN=TRAPPC3 PE=1 SV=1**
TRAPPC4	**E9PN70**	62	29313	3	2	3	2	0.38	Trafficking protein particle complex subunit 4 OS=Homo sapiens GN=TRAPPC4 PE=1 SV=1
TRAPPC5	**Q8IUR0**	**235**	**20884**	**10**	**9**	**8**	**7**	**3.80**	**Trafficking protein particle complex subunit 5 OS=Homo sapiens GN=TRAPPC5 PE=1 SV=1**
TRAPPC8	**J3QQJ5**	175	156369	10	7	8	6	0.20	Trafficking protein particle complex subunit 8 OS=Homo sapiens GN=TRAPPC8 PE=1 SV=1
TRAPPC9	**Q96Q05**	**139**	**140775**	**12**	**6**	**12**	**6**	**0.22**	**Isoform 2 of Trafficking protein particle complex subunit 9 OS=Homo sapiens GN=TRAPPC9**
TRIM25	**Q14258**	196	72581	5	5	4	4	0.30	E3 ubiquitin/ISG15 ligase TRIM25 OS=Homo sapiens GN=TRIM25 PE=1 SV=2
TRIM28	**M0R0K9**	34	49031	1	1	1	1	0.10	Transcription intermediary factor 1-beta (Fragment) OS=Homo sapiens GN=TRIM28 PE=1 SV=1
TRIM29	**Q14134**	20	64488	1	1	1	1	0.08	Isoform Beta of Tripartite motif-containing protein 29 OS=Homo sapiens GN=TRIM29
TRMT1L	**Q7Z2T5**	14	82893	3	1	3	1	0.06	TRMT1-like protein OS=Homo sapiens GN=TRMT1L PE=1 SV=2
TROVE2	**P10155**	46	59129	1	1	1	1	0.08	Isoform 3 of 60 kDa SS-A/Ro ribonucleoprotein OS=Homo sapiens GN=TROVE2
TSR1	**Q2NL82**	48	92151	3	1	3	1	0.05	Pre-rRNA-processing protein TSR1 homolog OS=Homo sapiens GN=TSR1 PE=1 SV=1
TUBA1C	**F5H5D3**	1002	58606	29	28	21	21	4.42	Tubulin alpha-1C chain OS=Homo sapiens GN=TUBA1C PE=1 SV=1
TUBA4A	**P68366**	655	48982	24	23	18	18	4.66	Isoform 2 of Tubulin alpha-4A chain OS=Homo sapiens GN=TUBA4A
TUFM	**P49411**	111	49852	3	3	3	3	0.33	Elongation factor Tu, mitochondrial OS=Homo sapiens GN=TUFM PE=1 SV=2
TXN	**P10599**	42	9674	1	1	1	1	0.61	Isoform 2 of Thioredoxin OS=Homo sapiens GN=TXN
U2AF1	**Q01081**	42	28378	1	1	1	1	0.18	Isoform 2 of Splicing factor U2AF 35 kDa subunit OS=Homo sapiens GN=U2AF1
U2SURP	**H7C4P4**	50	10874	1	1	1	1	0.53	U2 snRNP-associated SURP motif-containing protein (Fragment) OS=Homo sapiens GN=U2SURP PE=1 SV=1
U2SURP	**O15042**	343	118618	18	12	15	10	0.49	Isoform 2 of U2 snRNP-associated SURP motif-containing protein OS=Homo sapiens GN=U2SURP
U3KQJ1	**U3KQJ1**	56	42136	2	1	2	1	0.12	Polymerase delta-interacting protein 2 OS=Homo sapiens GN=POLDIP2 PE=1 SV=1
UBTF	**E9PKP7**	27	87722	4	2	4	2	0.11	Nucleolar transcription factor 1 OS=Homo sapiens GN=UBTF PE=1 SV=1
UPF2	**Q9HAU5**	21	148972	3	1	3	1	0.03	Regulator of nonsense transcripts 2 OS=Homo sapiens GN=UPF2 PE=1 SV=1
USP10	**Q14694**	59	93281	2	1	2	1	0.05	Isoform 2 of Ubiquitin carboxyl-terminal hydrolase 10 OS=Homo sapiens GN=USP10
USP15	**Q9Y4E8**	109	110482	3	3	3	3	0.14	Isoform 2 of Ubiquitin carboxyl-terminal hydrolase 15 OS=Homo sapiens GN=USP15
VCP	**P55072**	546	89950	20	16	18	15	1.20	Transitional endoplasmic reticulum ATPase OS=Homo sapiens GN=VCP PE=1 SV=4
VDAC1	**P21796**	275	30868	7	7	7	7	1.90	Voltage-dependent anion-selective channel protein 1 OS=Homo sapiens GN=VDAC1 PE=1 SV=2
WDR1	**D6RD66**	42	27066	3	1	3	1	0.19	WD repeat-containing protein 1 (Fragment) OS=Homo sapiens GN=WDR1 PE=1 SV=1
WDR13	**Q9H1Z4**	13	43637	2	1	2	1	0.11	Isoform 2 of WD repeat-containing protein 13 OS=Homo sapiens GN=WDR13
WDR26	**Q9H7D7**	37	71385	5	2	4	2	0.14	Isoform 2 of WD repeat-containing protein 26 OS=Homo sapiens GN=WDR26
WDR77	**H0Y711**	1820	31706	47	37	10	9	2.79	Methyltransferase protein 50 (Fragment) OS=Homo sapiens GN=WDR77 PE=1 SV=1
WLS	**H0YCG9**	31	23225	1	1	1	1	0.22	Protein wntless homolog (Fragment) OS=Homo sapiens GN=WLS PE=1 SV=1
WWP1	**Q9H0M0**	41	92174	4	2	3	2	0.11	Isoform 3 of NEDD4-like E3 ubiquitin-protein ligase WWP1 OS=Homo sapiens GN=WWP1
XPC	**Q01831**	23	102639	2	1	2	1	0.05	Isoform 2 of DNA repair protein complementing XP-C cells OS=Homo sapiens GN=XPC
YBX3	**P16989**	301	31928	9	9	6	6	1.42	Isoform 2 of Y-box-binding protein 3 OS=Homo sapiens GN=YBX3
YES1	**J3QRU1**	30	61861	4	1	3	1	0.08	Tyrosine-protein kinase Yes OS=Homo sapiens GN=YES1 PE=1 SV=1
YME1L1	**Q96TA2**	79	80011	4	1	4	1	0.06	Isoform 2 of ATP-dependent zinc metalloprotease YME1L1 OS=Homo sapiens GN=YME1L1
YTHDC2	**D6RST8**	28	15543	1	1	1	1	0.35	Probable ATP-dependent RNA helicase YTHDC2 (Fragment) OS=Homo sapiens GN=YTHDC2 PE=4 SV=1
YTHDF3	**R4GN55**	38	63772	1	1	1	1	0.08	YTH domain-containing family protein 3 OS=Homo sapiens GN=YTHDF3 PE=1 SV=1
YWHAB	**P31946**	114	27947	7	4	4	4	0.96	Isoform Short of 14-3-3 protein beta/alpha OS=Homo sapiens GN=YWHAB
YWHAE	**P62258**	161	26658	6	5	5	5	1.41	Isoform SV of 14-3-3 protein epsilon OS=Homo sapiens GN=YWHAE
YWHAG	**P61981**	82	28456	5	4	4	4	0.94	14-3-3 protein gamma OS=Homo sapiens GN=YWHAG PE=1 SV=2
YWHAZ	**E7EX29**	233	28190	10	6	7	6	1.71	14-3-3 protein zeta/delta (Fragment) OS=Homo sapiens GN=YWHAZ PE=1 SV=1
ZBTB42	**B2RXF5**	31	47602	1	1	1	1	0.10	Zinc finger and BTB domain-containing protein 42 OS=Homo sapiens GN=ZBTB42 PE=1 SV=2
ZRANB2	**O95218**	251	36753	8	7	8	7	1.45	Isoform 2 of Zinc finger Ran-binding domain-containing protein 2 OS=Homo sapiens GN=ZRANB2
ZYX	**H0YZY8**	79	58804	3	2	3	2	0.17	Zyxin (Fragment) OS=Homo sapiens GN=ZYX PE=1 SV=1

* TRAPP interactors are highlighted in bold

1480 **Table S2. Small interfering RNA oligonucleotides used in the study.**

Gene name		siRNA sequence
TRAPPC2	#1	GGGCAUAUGAGGUUUAUUA
	#2	GAGCUUCUACUUUGUAAUU
	#3	ACAUGUGGCUAUCGAACAA
	#4	CAUAAGACAAGAAGAUGGA
TRAPPC3		GGGCAUCACUCCAAGCAUU
Sec23A	#1	GUUAUGCUGGUAUAUCUGA
	#2	GCAUAAUGCUCCAAUUCCU
Sec23B	#1	CACGUUACAUCAACACGGA
	#2	CACUAUGAGAUGCUUGCUA
Sec24A		GAGUCAGUGAGCCAAGGAU
Sec24B		GCCGAUCCUGUCGAACGUAUA
Sec24C		GGCUGCUGUGUAGAUCUCU
Sec24D		CUGUCUUACCCAGGAGGCU
Sec31A		GCUUCUCUUCCACUCAAUA
Sec16A		GGGCGCAAAGUGAGCUGCCAGAUUU
Sec16B		CCCUGCCUAGUUUCCAGGUGUUUAA
CDK1	#1	GAACUUCGUCAUCCAAAUA
	#2	GGUUAUAUCUCAUCUUUGA
	#3	GAAUCUUUACAGGACUAUA
CDK2	#1	CGGAGCUUGUUAUCGCAAA
	#2	GAGUCCCUGUUCGUACUUA
	#3	CAAGAUCUCAAGAAAUUCA

1481

1482 **Table S3. Primers for real time PCR used in this study**

Gene name		Primer sequence
Sec23A	(+)	CCAGATTTCCAATGCCAAGATAC
Sec23A	(-)	TGAGTCTGTGAAGGGTTGAC
Sec23B	(+)	GAATGTGAAAGGACCGTGTG
Sec23B	(-)	AGATGCCAAGTGTAGATGTAGG
Sec24A	(+)	GTTTATGGAGAACCTCACAGAAG
Sec24A	(-)	ACAAAGAGATACACTGGAGGC
Sec24B	(+)	GGGCTCCTGTACCTAACTTG
Sec24B	(-)	AGTAAAGCCTGTGTCTGTGG
Sec24C	(+)	CATCAAACCGCTGGCAAG
Sec24C	(-)	GGGACACATGTATGCTTTGC
Sec24D	(+)	GAGGACAAGTTTATGCCACC
Sec24D	(-)	TGTACAACGGATGAATCGAGG
Sec16A	(+)	AACCAACGAAGCAATCCAG
Sec16A	(-)	GCGGCAGGAGTAGATGAAC
Sec16B	(+)	GGTTTTAGAAAGACGCAGTGG
Sec16B	(-)	TGAGCGAGTAGGATGAGGAT
HPRT	(+)	TGCTGACCTGCTGGATTACA
HPRT	(-)	CCTGACCAAGGAAAGCAAAG
CDK1	(+)	AAGGAACAATTAAACTGGCTGAT
CDK1	(-)	TGACCCCAGCAATACTTCTG
CDK2	(+)	GCATTCCTCTTCCCCTCATC
CDK2	(-)	AGGTTTAAGGTCTCGGTGG

1483